Optimal Reaction Route for Hydroformylation of Long-Chain Olefins in Thermomorphic Solvent Systems

Dissertation

zur Erlangung des akademischen Grades

Doktoringenieur

(Dr.-Ing.)

von: Dipl.-Ing. Benjamin Hentschel

geb. am: 07. April 1985

in: Löbau

genehmigt durch die Fakultät für Verfahrens- und Systemtechnik
der Otto-von-Guericke-Universität Magdeburg

Gutachter: Prof. Dr.-Ing. Kai Sundmacher

              Prof. Dr.-Ing. Hannsjörg Freund

              Prof. Dr.-Ing. Robert Güttel

eingereicht am 04. Juli 2017

Promotionskolloquium am 25. Oktober 2017

Abstract

The chemical reactor is the most important part of a chemical process. Its performance defines the effort, hence the costs of the downstream product separation. Besides unwanted side-products, which directly reduce the efficiency of the chemical conversion, also unconverted reactants have to be recovered in the downstream process. These unconverted reactants can be recycled to the reactor, which yields a feedback system of reactor and downstream process. Due to this central role of the reactor, its design should be performed as integrated system.

Especially in solvent-based reaction systems which also involve solvent regeneration, such an integrated design is promising. The work presented in this thesis was part of the DFG-funded collaborative research cluster SFB-TR 63, "Integrated Processes in Liquid Multiphase Systems". Based on a representative reaction system, hydroformylation of long-chain olefins in thermomorphic solvent systems, this thesis provides a "best practice" example for the integrated design of reactor and process. The work flow can be transferred to other reaction systems, especially those involving strong feedback of reactor and process.

The backbone of the design procedure is a mathematical model of reactor and process, comprising balance equations, thermodynamics, constitutive equations, and connectivity equations. The predictability of the model however, depends highly on the kinetic parameters, which should be obtained at a representative operating point, e.g. account for possible recycling conditions. Hence, in the first part of the thesis it is shown how mathematical optimization can be used to define process relevant working points for parameter estimation yielding a predictive kinetic model applicable for dynamic optimization.

Using the predictive model optimal reaction routes with respect to different objective functions, which represent chemical engineering performance measures, are calculated for the stand-alone reactor. It can be shown that these objectives are mostly contradictory and that weighting factors need to be known in order to find an objective that represents a suitable measure of process-wide optimality. On the stage of the stand-alone reactor the ideal recycle composition can already be calculated, which

gives a guideline for the downstream process. It is shown that, due to the presence of reversible reactions, recycling of reactants and intermediates will affect the reaction kinetics yielding a different reactor design than without recycle. Hence, recycling should always be considered.

The two problems arising in case of the stand-alone reactor, unknown weighting factors for the multi-objective problem and unknown realistic recycle composition, are finally tackled with a simultaneous optimization of process and reaction route. Here the multi-objective problem is condensed to a single economic objective, representing total production costs, including capital investment, raw material and operational costs.

Zusammenfassung

Da der chemische Reaktor durch seine Effizienz den Aufwand und damit auch die Kosten der anschließenden Produkttrennung bestimmt kann er als das wichtigste Element eines jeden chemischen Prozesses betrachtet werden. Neben möglichen Nebenprodukten, welche die Effizienz der chemischen Umwandlung reduzieren, müssen in der Produkttrennung auch unverbrauchte Einsatzstoffe abgetrennt werden. Diese zurückgewonnenen Einsatzstoffe werden üblicherweise dem Reaktor wieder zugeführt um den Gesamtumsatz des Prozesses und damit seine Effizienz zu erhöhen. Eine solche Rückführung von Einsatzstoffen führt dazu, dass der chemische Prozess ein rückgekoppeltes System darstellt, wo die Reaktoreffizienz sich indirekt auf die Anfangsbedingungen des im Reaktor ablaufenden dynamischen Reaktionsprozesses auswirkt. In Bezug auf die Optimierung chemischer Produktionsprozesse verlangt die Eigenschaft der Rückkopplung nach einem integrierten Ansatz welcher Reaktor und Prozess nicht separat betrachtet, sondern als zusammengehöriges System.

Besonders im Falle lösungsmittelbasierter Reaktionssysteme, welche eine Regeneration des Lösungsmittels verlangen ist ein solch integrierter Optimierungsansatz von Vorteil. Die in dieser Dissertation dargestellten Ergebnisse sind im Rahmen des DFG-geförderten transregionalen Kooperationsprojektes SFB-TR 63, "Integrierte chemische Prozesse in flüssigen Mehrphasensystemen", ausgearbeitet worden. Auf dem representativen Reaktionssystem der Hydroformylierung langkettiger Alkene basierend, liefert diese Arbeit ein "Best-Practice-Beispiel" für die Auslegung und Optimierung des chemischen Reaktors und des entsprechenden Downstreamprozesses als integrierte Einheit.

Der vorgestellte theoretisch-experimentelle Ansatz beruht auf einem mathematischen Modell von Reaktor und Prozess, welches sich aus den systembeschreibenden Bilanzgleichungen, thermodynamischen Ansätzen und konstitutiven Gleichungen zusammensetzt. Die Vorhersagekraft des Modells hängt maßgeblich von der Qualität der Modellparameter ab. Die experimentelle Bestimmung dieser Parameter sollte daher an einem representativen Arbeitspunkt erfolgen, welcher auch den Einfluß möglicher Rückführströme berücksichtigt. Demzufolge wird im ersten Teil dieser Arbeit vorgestellt, wie mit Hilfe mathematischer Optimierung Arbeitspunkte

für die experimentelle Bestimmung der reaktionskinetischen Modellparameter bestimmt werden können. Da die experimentellen Arbeitspunkte bereits prozessrelevante Bedingungen representieren geht aus den experimentell bestimmten Parametern ein Modell mit hoher Vorhersagekraft hervor, welches sich für die anschließende Optimierung der Reaktor-Prozess-Einheit sehr gut eignet.

Auf Grundlage des parametrierten Modells des Reaktionssystems werden im Folgenden optimale Reaktionsrouten bezüglich reaktionstechnischer Kenngrößen berechnet. Es zeigt sich, dass diese unterschiedlichen Zielfunktionale nicht gleichermaßen optimiert werden können, sondern, dass eine Verbesserung eines Zielfunktionals vielmehr mit einer Verschlechterung eines anderen einhergeht. Eine geeignete Zielfunktion zur Beschreibung des Prozessoptimums ist also ein Kompromiss unterschiedlicher Zielfunktionale, welche auch als unterschiedliche Gewichtung reaktionstechnischer Kenngrößen verstanden werden kann.

Auf der Ebene des Stand-alone-Reaktors kann mit Hilfe dynamischer Optimierung basierend auf den experimentell bestimmten Parametern eine optimale Zusammensetzung des Recyclestroms bestimmt werden welche wiederum Anforderungen an den Downstreamprozess vorgibt. Durch die Anwesenheit reversibler Reaktionen wirkt sich die Rückführung nichtumgesetzter chemischer Komponenten auf die Reaktionskinetiken aus und kann zu Reaktionsführungen führen die sich von Systemen ohne Rückführung unterscheiden und damit auch zu einer anderen Reaktorauslegung führen würden. Aus diesem Grund sollte eine mögliche Rüchführung einzelner Komponenten immer Berücksichtigt werden, was durch den beschriebenen Ansatz gewährleistet ist.

Die zwei Probleme des Stand-alone-Reaktors, unbekannte Gewichtung der reaktionstechnischen Zielfunktionale und unbekannte realistische Recyclezusammensetzung, werden in einem weiteren Schritt durch eine simultane Optimierung des Reaktor-Prozess-Verbundes gelöst. Anstatt der Optimierung mehrerer Zielfunktionale werden die Produktionskosten des Prozesses als globale Zielfunktion in einem simultanen Ansatz unter Variation dynamischer Steuergrößenprofile in der Reaktionsstufe und Betriebsparametern der Apparate der Trennsequenz minimiert.

Preface

This thesis is the result of research conducted at the chair of Process Systems Engineering at the Otto-von-Guericke University Magdeburg and the Process Systems Engineering group of the Max Planck Institute for Dynamics of Complex Technical Systems in Magdeburg conducted from 2010 to 2014. The work was part of the collaborative research cluster SFB-TR 63, "Integrated Processes in Liquid Multiphase Systems", funded by the DFG which is hereby gratefully acknowledged.

My special thanks goes to Prof. Dr.-Ing. Kai Sundmacher (Max Planck Institute for Dynamics of Complex Technical Systems and Otto-von-Guericke University Magdeburg) for the interesting and challenging topic as well as for the excellent supervision and support. I also want to express my gratitude to Prof. Dr.-Ing. Hannsjörg Freund (Friedrich-Alexander University Erlangen-Nuremberg) for the supervision and valuable advice. Additional thanks I owe to Prof. Dr.-Ing. Robert Güttel (Ulm University) for reviewing and evaluating my thesis as external referee.

I want to express my thanks to all my colleagues and friends at the Max Planck Institute and the Otto-von-Guericke University Magdeburg for their support, inspiring discussions, and funny conversations. Special thanks to my office mates Dr.-Ing. Andreas Peschel, Dr.-Ing. Rayees Ahamed, Dr.-Ing. Kevin McBride, and Dr.-Ing. Teng Zhou for your valuable scientific input, critical questioning, coffee sessions and Chinese lessons. I further acknowledge Dipl.-Ing. Nicolas Kaiser, M. Sc. Ali elSibai, M. Sc. Marcus Wenzel, Bianka Stein, Dr. rer. nat. Andreas Voigt, Dr.-Ing. Melanie Fachet, Dipl.-Ing. Florian Karst and many others.

Additionally, many thanks to my dear friends in Magdeburg for our off-work activities, especially Dr.-Ing. André Franz, Dr.-Ing. Robert Dürr, Dr.-Ing. Astrid Bensmann, and Dr.-Ing. Boris Bensmann.

Zu guter Letzt danke ich meinen Eltern, Harald und Annett Hentschel, sowie meinen Brüdern Christian und Georg für die ständige Unterstützung auf meinem Lebensweg.

Hai you feichang ganxie wo laopo he erzi jianchi zhichi wo!

Contents

Notation

Latin Symbols

Symbol	Description	Units
A_hex	Heat exchanger area	(m^2)
c_p	Heat capacity	$\left(\frac{W}{kmol \cdot K}\right)$
C	Concentration	$\left(\frac{kmol}{m^3}\right)$
	Total production costs	$\left(\frac{\$}{kmol}\right)$
C^*	Equilibrium concentration	$\left(\frac{kmol}{m^3}\right)$
C_invest	Investment costs	$(\$)$
C_util	Utility costs	$\left(\frac{\$}{min}\right)$
C_rawmat	Raw material costs	$\left(\frac{\$}{min}\right)$
C_sb	Flooding parameter	$\left(\frac{m}{s}\right)$
D	Diameter	(m)
E_A	Activation energy	$\left(\frac{kJ}{mol}\right)$
F_fl	Flooding flow factor	$(-)$
H	Henry's constant	$\left(\frac{MPa \cdot m^3}{kmol}\right)$
	Height	(m)
h	Molar enthalpy	$\left(\frac{kJ}{kmol}\right)$
j_i	Component dosing flux	$\left(\frac{kmol}{min}\right)$
j_q	Heat flux	$\left(\frac{kJ}{min}\right)$
k_LLE	Distribution coefficient for LLE	$(-)$
k_j	Rate constant	various units
k_0	Frequency factor	various units
K	Constant in reaction kinetics	$\left(\frac{m^3}{kmol}\right)$
K_p	Equilibrium constant	$(-)$
L	Length	(m)
$\dot{m}$	Mass flow rate	$\left(\frac{kg}{min}\right)$
M	Molar mass	$\left(\frac{kg}{kmol}\right)$
N	Number of equilibrium stages	$(\#)$

N_CPS	Number of compressor stages	$(\#)$
$\dot{n}$	Molar flow rate	$\left(\frac{kmol}{min}\right)$
n_i	Amount of substance	$(kmol)$
p_i	Partial pressure	(MPa)
P	Total pressure	(MPa)
p^vap	Vapor pressure	(MPa)
$\dot{Q}$	Heat flux	$\left(\frac{kJ}{min}\right)$
r_j	Reaction rate	$\left(\frac{kmol}{kg \cdot min}\right)$
R	Gas constant	$\left(\frac{kJ}{mol \cdot K}\right)$
	Reflux ratio	$(-)$
S	Selectivity	$(-)$
	Dimension variable in BC	various units
t	Reaction time of fluid element	(min)
T	Temperature	(K)
u_fl	Flooding velocity	$\left(\frac{m}{s}\right)$
U	Set of control variables	various units
	Heat transfer coefficient	$\frac{W}{m^2 \cdot K}$
v	Stoichiometry factor	$(-)$
V	Volume	(m^3)
x	Molar fraction	$(-)$
X	Conversion	$(-)$

Greek Symbols

α	Relative volatility	$(-)$
$\bar{\alpha}$	Mean relative volatility	$(-)$
ΔG	Gibbs energy	$\left(\frac{kJ}{mol}\right)$
Δp	Pressure drop	(MPa)
ϵ_m	Motor efficiency	$(-)$
ϵ_p	Pump efficiency	$(-)$
ϵ_c	Compression efficiency	$(-)$
ϵ_vap	Vapor efficiency	$(-)$
η_N	Tray efficiency	$(-)$
η_{fl}	Flooding efficiency	$(-)$
Θ	Underwood factor	$(-)$
ξ	Recovery ratio	$(-)$

ρ	Density	$\left(\frac{kg}{m^3}\right)$
σ	Surface tension	$\left(\frac{mN}{m}\right)$
τ	Residence time	(min)
Ψ	Price	$\left(\frac{\$}{kmol}\right)$ or $\left(\frac{\$}{kJ}\right)$ or $\left(\frac{\$}{kg}\right)$
ω	Mass fraction	$(-)$

Superscripts

base	Base value
c	Low temperature stream
cw	Cooling water
i, j	Component index
j	Reaction index
f	Formation, final
s	Stream index
0	Standard value, initial value
bub	Bubble point
B	Bottom stream (C1: 403, C2: 503)
dew	Dewpoint
D	Distillate stream (C1: 405, C2: 504)
el	Electricity
V	Gas phase or vapor phase
in	Inlet
liq	Liquid phase
lm	Log mean
LK	Light key component (C1: iC12en, C2: iC13al)
HK	Heavy key component (C1: iC13al, C2: nC13al)
h	High temperature stream
max	Maximum value, upper bound, maximize
min	Minimum value, lower bound, minimize
ref	Reference value
rel	Relative value
cat	Catalyst
col	Column
con	Condenser
th	Theoretical
reb	Reboiler

u	Unit index
vap	Vapor, Vaporization

Sets

COM	Set of components (DMF, C10an, nC12an, nC12en, iC12en, nC13al, iC13al, H_2, CO)
COMP	Set of compressors (CP307)
GAS	Set of gaseous components (H_2, CO)
HEX	Set of heat exchangers (H101, H201, H301, H305, H403, H405, H503, H504)
PUMP	Set of pumps (P104, P303, P401, P403)
RCT	Set of reactions (1, 2, 3, 4, 5, 6)

Abbreviations

BMC	Bare module costs
BC	Bare costs
C1	Solvent/aldehyde column
C2	n/iso column
CE	Chemical engineering index
CP	Compressor
CSTR	Continuously stirred tank reactor
D	Decanter
DAE	Differential algebraic equation
EPF	Elementary process function
H	Heat exchanger
LLE	Liquid-liquid equilibrium
MINLP	Mixed integer nonlinear program
MF	Module factor
MPF	Material and pressure factor
OP	Optimization problem
P	Pump
PC-SAFT	Perturbed chain statistically associating fluid theory
R	Reactor
RRP	Ruhrchemie-Rhône-Poulenc process
TMS	Thermomorphic multicomponent solvent system

UF	Update factor

Components

C10an	Decane
CO	Carbonmonoxide
DMF	Dimethylformamide
H_2	Hydrogen
nC12an	n-Dodecane
nC12en	1-Dodecene
iC12en	Internal dodecane
nC13al	n-Tridecanal
iC13al	Isomeric aldehyde

1. Introduction

The modern chemical industries is mainly based on the utilization of fossil resources, such as crude oil, natural gas, and coal. The abundance of these feedstocks provided enough time for the establishment of a complex chemical production network since around 1850 [1, 2]. Within the past 150 years (petro)chemical industries experienced a rapid development due to the persisting need for new chemicals. This demand was driven by innovations, such as automotive industry, aircraft industry, military, information technology, and others. The growing portfolio of chemicals was connected to an increasing size and complexity of the chemical production network. The global competition between chemical companies led to the improvement of chemical processes and yielded interconnections between different production pathways.

Today, as the world is aware of the limitation of the fossil feedstock and as sustainability becomes more and more important, it is desired to change the fossil basis into a renewable one. In order to use the existing highly developed technology and production chains of chemical industries, such renewable feedstocks should ideally substitute platform chemicals. Platform chemicals are chemical intermediates which are a branch point of many subsequent production pathways (refer to Fig. 1.1). An example for such platform chemicals are long chain aldehydes. These aldehydes could be further converted using the established production networks. Products of aldehyde conversion are alcohols as intermediates and finally plasticizers, detergents, and lubricants. A promising link between aldehydes and renewables is the functionalization of C-C double bonds, as they occur in olefins and fatty acid esters which can be supplied from biological sources.

The transformation of long chain olefins into valuable platform chemicals and products mostly requires the addition of oxygen or nitrogen groups. The long carbon chain of the olefin inherently constitutes a nonpolar molecule. In order to provide the necessarily high reaction rates homogeneous catalysis is required for the conversion of long chain olefins. Moreover, only rather expensive transition metal catalysts provide the catalytic activity which is required for the economic viability of those processes. However, besides the advantages of homogeneous catalysis, such as high activity and

**Consumer goods and
specialized products: about 30.000**

Fuels, polymers, drugs, pigments, solvents,
fertilizers, fibers, dispersions, cosmetics, ...

Intermediates & precursors: about 300

Long chain aldehydes, methanol, vinyl chloride, styrene, urea, formaldehyde,
ethylene oxide, acetic acid, acrylonitrile, cyclohexane, acrylic acid, ...

Base chemicals: about 20

Ethylene, propene, butadiene, benzene, syngas, acetylene,
ammonia, sulfuric acid, sodium hydroxide, chlorine, ...

Raw materials: about 10

Crude oil, natural gas, coal, biomass,
rock salt/sodium chloride, phosphate, sulfur, air, water

Figure 1.1.: Chemistree: Hierarchy of chemical products.

selectivity compared to heterogeneous catalysts, the main drawback is the inconvenient catalyst separation from the products. This thesis represents an attempt to investigate the problems in process and reactor design which immanently occur in production systems dealing with the functionalization of long chained hydrocarbons, such as homogeneously catalyzed reactions of gaseous and liquid reactants. As example for this class of reaction systems the rhodium catalyzed hydroformylation of long chain olefins was chosen. Due to the extremely high costs of rhodium catalyst loss into the product has to be minimized down to ppb level.

Within the collaborative research cluster SFB/TR 63, where the work of this thesis is part of, it is desired to use liquid-liquid multiphase systems to recover the homogeneous catalyst by phase separation. Depending on the polarity of the ligands the catalyst molecule preferentially dissolves in the non-product phase. However, while the catalyst can be easily separated using this concept, it also has to be in close contact with the reactant during the reaction step. The necessary exchange area for mass transfer between catalytic and reactant phase cannot entirely be achieved by intensive mixing, hence, no economically viable hydroformylation process of this kind has been commercialized so far. Recently, innovative solvent systems or tunable solvents are investigated which are able to incorporate homogeneous reaction and phase separation with a single solvent system. The phase behavior of these solvents can be switched by changing temperature or pressure. Thus, it is possible to provide homogeneous reaction conditions in the reactor while enabling a phase split in the separator using a single solvent system. In this kind of liquid multiphase systems the chemical reactor is of special importance. Besides the catalytic reactions, also solvent recycles have to be considered in the reactor design. Further, the operation parameters have to be chosen to provide homogeneous reaction conditions while the reactor outlet composition needs to provide advantageous separation conditions.

It has to be kept in mind that the chemical conversion is a dynamic process where the optimal reaction conditions change over reaction time as the composition changes. Assuming a fluid element on its way through the reactor, there exists at any time point an optimal value for material and energy fluxes to keep its thermodynamic state on an optimal trajectory. Accordingly, an optimal reactor can be defined as a reaction vessel which, at any time, provides optimal material and energy fluxes into a fluid element which is moving from the inlet to the outlet. This approach does not only apply for chemical reactors, but for any other process unit and the concept was published by Freund and Sundmacher as elementary process function (EPF) concept [3].

Peschel et al. [4] demonstrated that by solving the reverse problem, beginning at

the optimal profiles of control fluxes over reaction time for a given reaction system, followed by the technical approximation of these control profiles it is possible to design tailor-made reactors for a specific reaction system instead of screening a catalog of existing reactors which will hardly contain a truly optimal type. Prerequisite for such a rigorous dynamic model approach is a reliable and predictive mathematical model.

The **scope of this thesis** is the identification of the optimal reaction route of a complex hydroformylation reaction system by means of mathematical optimization according to the EPF concept. This work shows a best practice workflow from identification of reasonable reaction conditions for parameter estimation, experimental validation of the kinetic model and the theoretically predicted optimal reaction route, and finally identification of the process wide optimal reaction route.

In the following the **structure of this thesis** is outlined. Chapter 2 gives an introduction on the background of liquid multiphase systems, homogeneous catalysis, and hydroformylation concepts. Further, the basic modeling framework, namely the elementary process function concept is reviewed. In Chapter 3 the methodological approach and workflow for the identification of the optimal reaction route within integrated processes is presented. Afterwards, the design approach is exemplified on the rhodium catalyzed hydroformylation of 1-dodecene in a thermomorphic solvent system (TMS) in Chapter 4. The practical example contains the experimental validation and refinement of the underlying mathematical model for the reaction kinetics, the experimental validation of the optimal reaction route in a semibatch reactor, and the derivation of a process-wide cost optimal reaction route. Finally, the results are summarized and conclusions are drawn in Chapter 5.

2. Background

2.1. Liquid Multiphase Systems

The term liquid multiphase systems describes a solvent mixture which, under certain physical conditions, consists of more than one liquid phase. A simple example of a system of multiple liquid phases is a mixture of water and oil. Due to the different polarity of the liquids the associative forces between similar components lead to the formation of oil and water-rich phases with a phase boundary in between. Due to the physical equilibrium of the phases each component is present in both phases, but with different amount. While thermodynamics determine the equilibrium composition of each phase, transport kinetics determine the time until equilibrium is reached.

The different preferences of chemicals to distribute within multiple liquid phases are industrially used in form of liquid-liquid extraction processes [5]. The performance of the extraction process is determined by the solubility of the target component in the extractive phase and the interphase mass transfer. While the equilibrium composition depends on the chosen solvent, the interface mass transfer can be enhanced by increasing the exchange area between the phases. Established industrial liquid-liquid extraction processes use countercurrent columns, centrifugal extractors, and mixer-settlers to provide the necessary mass transfer interface. The basic principle is the dispersion of one of the two liquids into the other in order to enlarge the contact area for mass transfer and/or to influence drop generation by energy input such as mixing or pulsing [5].

As stripping, liquid-liquid extraction enables a separation without additional supply of heat, which is suitable for the treatment of temperature sensible components, such as homogeneous catalysts or products which tend to thermal degeneration, such as enzymes. In conventional extraction processes the extraction solvent is circulated within a separate solvent loop inside the process consisting of absorption and regeneration step. This additional demand for an extraction solvent (loop) and a downstream process for the recovery of this solvent is a significant cost factor. A more elegant

way would be to integrate the extraction solvent into the solvent used for the reaction step. In this way, the additional extraction unit would be unnecessary since the mixing and phase transfer is performed inside the reactor. The new solvent would be a multi-component solvent system whose chemical and physical properties must be suitable for the reaction and separation step. Moreover, in the reaction step mass transfer limitation between the two liquid phases should be avoided. So to say, the solvent system should behave like a homogeneous solvent during the reaction while enabling an efficient phase separation in the separation step. Such solvent systems are currently under investigation in academia and the most important concepts are further discussed later in this chapter.

In the context of this work the concept of liquid multiphase systems is applied on the recovery of homogeneous catalysts on the example of the hydroformylation of long chain olefins. Due to the high costs of the homogeneous transition metal catalysts the catalyst recovery is of special economic importance. Although the application of the concept of liquid multiphase systems seems straight forward, the technical realization is still challenging due to nonideal phase behavior and only a limited number of industrial processes has been established so far, such as the Ruhrchemie/Rhone-Poulenc process and the UCC Low Pressure Oxo process.

Another important field where liquid multiphase systems occur are systems which use water as solvent. Since many industrially used solvents are toxic or environmentally harmful, the use of water as solvent is a considerable step towards sustainable processes. The high polarity of water leads to the formation of organic and aqueous phases if nonpolar reactants and products are involved. State-of-the-art synthesis methods enable the design of homogeneous catalysts with defined phase behavior. By adding polar ligands to the central atom of the catalyst it can be made hydrophilic and thereby immobilized within the aqueous phase.

2.1.1. Homogeneous Catalysis

The use of catalysts for the enhancement of chemical reactions is the most important step in process intensification due to the fact that on the molecular level the potential for process improvement is the largest [3]. Although the catalyst does not affect the thermodynamic equilibrium, but by selective enhancement of the speed of reaction it can improve selectivity and conversion which would otherwise be kinetically hindered. Selectivity, conversion, and also the catalyst specific product spectrum ultimately determine the product separation task.

6

Since homogeneous catalysts enable the use of a wide spectrum of analytic methods, such as GC, IR, NMR spectroscopy, the catalytic mechanism can be investigated very reliably. In contrast, the phenomena which occur on the surface of heterogeneous catalysts can hardly be analyzed quantitatively and the reaction network usually consists of hundreds of reactions. Further, the electronic structure of the catalyst depends on the orientation of the crystal shape (especially local geometry, such as corners, edges, defects), hence the same catalytic element can have different performance depending on its geometrical structure. Hence, the reaction mechanism of homogeneous catalysts is generally more simple and better understood than that of heterogeneous catalysts. This knowledge enables a more rational catalyst design and ultimately leads to more active and selective catalysts. Due to the limitation of heterogeneous catalysts to react only on a surface, their activity is usually lower compared to homogeneous catalysts which act everywhere in the volume.

However, the homogeneity which enables the understanding, control and tuning of the catalytic mechanism is also the major drawback of homogeneous catalysis, since it inherently complicates the recovery of the catalyst from the product mixture.

Liquid multiphase systems enable an efficient and gentle catalyst separation and subsequent recycling to the chemical reactor. However, the solvent design is challenging.

2.2. Hydroformylation of Long Chain Olefins

2.2.1. General

Table 2.1.: Reactants of the hydroformylation and their industrial importance [6].

C atoms of olefin	2	3	4-12	≥ 13
Market share	2	70	20	8
End product	solvents diluents intermediates	solvents diluents intermediates	plasticizers	detergents surfactants

The hydroformylation is the addition of hydrogen (H_2) and carbon monoxide (CO) to the double bond of an alkene or other unsaturated hydrocarbons [7]. The hydro-

formylation of linear olefins always yields a mixture of branched and linear aldehydes. Due to its similar physical properties, the separation of the aldehyde mixture is energetically demanding, thus a high n/iso aldehyde ratio is an important performance measure of the used catalyst. In case of short chain olefins (less than 6 carbon atoms, < C6) the reactant is a gas ($T_{b,1-penten} = 30^oC$), whereas it is a liquid in case of long chain olefins (> C5, $T_{b,1-hexen} = 63.48^oC$) under atmospheris conditions, respectively. The aldehyde product is always a liquid (> C3, $T_{b,n-propanal} = 48^oC$) at atmospheric pressure. The hydroformylation is one of the most important homogeneously catalyzed chemical reactions in industry with an annual production capacity of about 9.2 million tons in 2002 [6]. Depending on the chain length of the olefin different aldehyde products can be produced, where n-butanal is the most important product with over 70% market share [6] (refer to Tab. 2.1). n-Butanal is ultimately processed to Bis(2-ethylhexyl)phthalat, an important softener for polyvinylchloride, or to n-butanol, which is used as solvent in esterification. Aldehydes of intermediate chain length (C6-C12) are used to synthesize plasticizers. Higher aldehydes (C13-C18) are mostly converted into anionic surfactants.

Despite the typical drawbacks, such as challenging catalyst separation from product and solvent, the hydroformylation is technically realized as homogeneously catalyzed reaction, so far. Although a lot of research has been done regarding the immobilization of the catalyst on solid surfaces, a commercial application seems not feasible due to leaching and reduced activity compared to the homogeneous option [8]. The advantage of homogeneous catalysis over heterogeneous catalysis is the much higher activity which requires less severe reaction conditions.

2.2.2. Catalyst Systems

Transition metals

In general all transition metals are possible catalysts for the hydroformylation as long as the central atom is able to form carbonyl complexes, such as $HM(CO)_X L_Y$ where M is the transition metal and L a ligand. The number of attached CO molecules and ligands is variable and affects the selectivity of the catalyst. The possible transition metals differ in their catalytic activity and price as shown in Tab. 2.2 [6]. Practically relevant catalysts are rhodium and cobalt catalysts, whereas other transition metals are mainly investigated in academia [8]. As can be seen from the much higher costs of Rhodium compared to Cobalt, a quantitative catalyst recovery is much more important in a rhodium based process.

Table 2.2.: Transition metals used in hydroformylation and their relative activity with respect to Cobalt [6]. Prices are spot market prices from January 2006 [9]

Transition metal	Rh	Co	Ir	Ru	Os	Pt	Pd	Fe	Ni
Rel. activity	10^3	1	10^{-2}	10^{-3}	10^{-4}	10^{-6}	-	-	-
Price (01/2006) $\frac{\$}{mol}$	12151	2.36	1465	305	2877	6960	1068	0.4	0.86

(a) Metal price per gram

(b) Metal price per mole
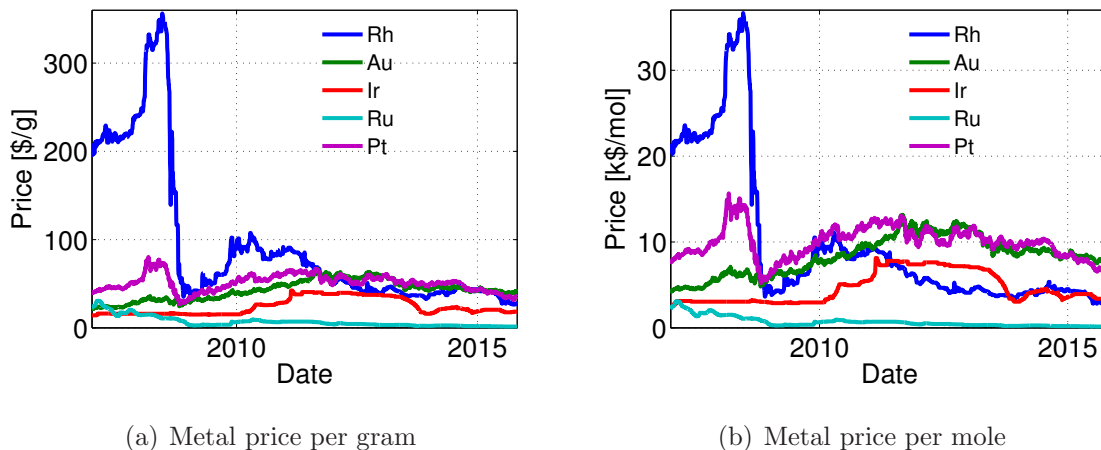
Figure 2.1.: Prices of precious metals from January 1st 2007 to October 29th 2015 [9].

Table 2.3.: Ligands used in hydroformylation and their costs.

Ligand	TPP	Xanphos	BIPHEP
Costs $\frac{€}{g}$	0.11	61.40	135.00

The price for catalyst metals is highly uncertain (refer to Fig. 2.1), since it is subject to various factors, such as purity, manufacturer, amount, market condition. Since catalyst metals are very rare materials with a annual supply rate of 200 to 240 ta^{-1} for Palladium [10] their price is heavily affected by world wide industrial demand.

Ligands

While the transition metal determines mainly the catalytic activity of the catalyst, it needs a ligand to adjust the selectivity. Without ligand most transition metals

produce a bunch of different products. The efficiency of ligands depends on their steric and electronic properties. Steric properties represent size and orientation of the ligand, which forces reactant and product into a favorable position for the reaction. The electronic structure of the ligand affects the electron density on the transition metal core, which leads to a selective attachment of reactants. The book of Van Leeuven [7] gives a broad overview on this topic.

Besides activity and selectivity, also the phase behavior of the catalyst complex is determined by the ligand. In case of the RCH-RP process the TPPTS ligand contains hydrophilic sulfon groups which keep the catalyst complex within the aqueous phase and enable a convenient catalyst separation from the hydrophobic product phase. Depending on its complexity and performance of the ligand its price reaches from quite low (TPP) up into the same range as rhodium (BIPHEPH) (refer to Tab. 2.3). In addition, the ligand is always used in excess to the transition metal which could lead to even higher makeup costs for the ligand than for the metal. However, high performance ligands, such as Biphephos, are still special chemicals with a small or even without market share. In contrast to precious metals, such as rhodium, the ligand price would actually decrease once a process will be commercialized due to initiation of large scale production.

Reaction mechanism

The generally accepted mechanism of the catalytic cycle was developed in the 1960th by Heck and Breslow [11, 12] for the hydroformylation using unmodified Co catalyst. This mechanism is also accepted for the rhodium catalyzed hydroformylation and was adapted by Wilkinson [11, 12] for the rhodium/triphenyphosphine (TPP) catalyst complex (refer to Fig. 2.2). It contains the following catalytic steps:

1. Alkene association

2. Alkyl complex formation

3. CO association

4. CO insertion

5. Oxidative addition of H_2

6. Reductive elimination of the aldehyde

The n/iso aldehyde ratio is determined by the probability of association of a lin-
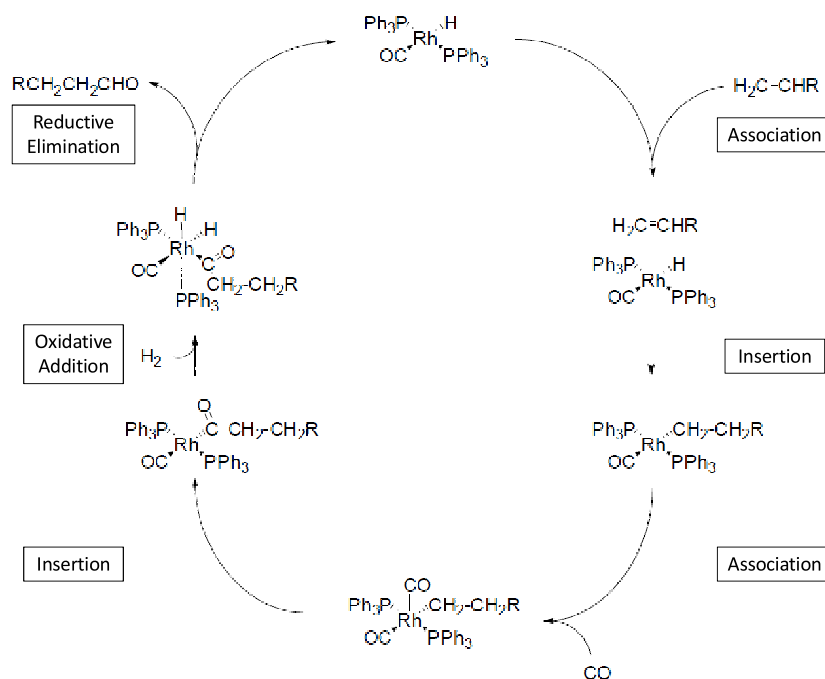
Figure 2.2.: Catalytic cycle of the rhodium based hydroformylation proposed by Wilkinson [11, 12]

ear alkene and the subsequent formation of the alkyl complex. This probability is depending on the ligand as discussed before. Different catalytic mechanisms have been proposed which try to describe the formation of linear and branched aldehyde products separately. However, mostly both products originate from the same active catalyst species, hence no difference in the catalyst equilibrium can be found. The resulting n/iso ratio of the catalyst is merely a probabilistic phenomenon. Otherwise it would be possible to formulate mechanistic equations which describe the separate formation of n and iso aldehyde, which have not been published so far. Rather do mostly both reaction kinetics depend on the same mechanism but with different rate constants.

Kiedorf et al. [13] extended the Wilkinson cycle for the ligand Biphephos by making two proposals. First, the active catalyst is in equilibrium with inactive catalyst species, depending on the amount of ligand, hydrogen, and carbon monoxide. They show that the active catalyst species is actually only a very small proportion of the total amount of catalyst. Second, the catalytic cycle of the hydroformylation also involves the hydrogenation and isomerization within the same cycle. Hydroformylation, hydrogenation, and isomerization are competing for the same catalyst.

Co-Based Catalysts

While in case of short chain olefins cobalt is almost completely substituted by rhodium, up to now it is still the established catalyst for the hydroformylation of long chain olefins. Although activity and selectivity of cobalt are much lower than in case of rhodium, but due to the low price of cobalt higher catalyst losses and higher costs for product purification are acceptable (see Tab. 2.2). However, the catalyst recovery and regeneration contributes still a major part to the investment costs. So it is common practice to destroy the cobalt catalyst, e.g. via precipitation or distillation, to remove it from the product phase. The destroyed catalyst complex is then regenerated and recycled to the reactor which causes remarkable operating and investment costs for the regeneration equipment [14]. In order to compensate the low activity of cobalt and to prevent catalyst decomposition due to low CO partial pressure the hydroformylation reaction usually requires severe pressure and temperature conditions (refer to Tab. 2.4). These extreme reaction conditions also support the production of undesired side products, which lowers the efficiency and complicate the downstream processing.

Rh-Based Catalysts

Rhodium based hydroformylation catalysts are about 1000 times more active than cobalt catalysts and yield much higher selectivities. Moreover, the catalyst complex is more stable and does not require high CO partial pressures as in case of rhodium. Thus, a much lower catalyst concentration and milder reaction conditions are required. However, due to the high price of rhodium the economy of the process depends highly on the efficiency of the catalyst separation. This is not an issue for short chain olefins, since the low boiling point and high volatility of the olefin and the product aldehyde enable an efficient and nondestructive catalyst separation. Hence, up to now, rhodium catalyzed hydroformylation is commercially established only for short chain olefins. However, the catalyst separation problem is still the only reason that prevents the commercial application of homogeneous rhodium catalysis in case of long chain olefins. Due to the high boiling point and low volatility of the olefins and product aldehydes the catalyst cannot be efficiently removed from the products by distillation. For that purpose highly sophisticated ligands and innovative solvent systems are under investigation in order to utilize liquid multiphase systems to selectively remove the catalyst from the products. Although lots of research is done in this field, but no commercial process using rhodium for the hydroformylation of long chain olefins is established so far. Until now the RCH-RP process for C3 olefins and the LPO process for C2-C4 are the only established industrial hydroformylation pro-

Table 2.4.: Comparison of processes for propene hydroformylation [15, 8].

Process	BASF	Shell	UCC (LPO)	RCH-RP
Catalyst	Co	Co/TPP	Rh/TPP	Rh/TPPTS
Olefin feed	C6-C12	C7-C14	C2-C4	C3
Temperature [^oC]	120-180	150-190	85-95	110-130
Pressure [bar]	270-300	40-80	15-18	40-60
Cat. conc. [mol%]	0.1-1	0.6	0.01-0.1	0.001-0.01
Products	Aldehyde	Alcohol	Aldehyde	Aldehyde
n/iso ratio	80:20	88:12	92:8	95:5
Cat. recycle	precipitation	thermal	thermal stripping	LL-separation

cesses which efficiently use rhodium as catalyst. More information on these processes are provided in the following section.

2.2.3. Process Concepts for Short Chain Olefins

Due to their low boiling point and high solubility in polar solvents, short chain olefins enable efficient hydroformylation processes. After the homogeneous reaction in the reactor the products and remaining reactants can be separated from the high boiling solvent, which contains the catalyst, via stripping with syngas ("gas recycle process") or distillation ("liquid recycle process").

BASF Oxo Process

In the BASF Oxo process the Co-catalyst is precipitated after the reaction by addition of acid and oxygen and subsequently separated into an aqueous phase. The destroyed catalyst is then reconverted into the active species by addition of syngas and fresh cobalt and recycled to the reactor. The unmodified cobalt catalyst requires reaction pressures of 300 bar and temperatures of 150 to 170 ^oC. The process is mostly used for long chain olefins. Advantages of the process which are claimed by BASF are an easy recovery of high boiling components and the applicability of the catalyst to all types of olefins [6]. Disadvantages are the severe reaction conditions which lead to high formation of high boilers and alkanes.
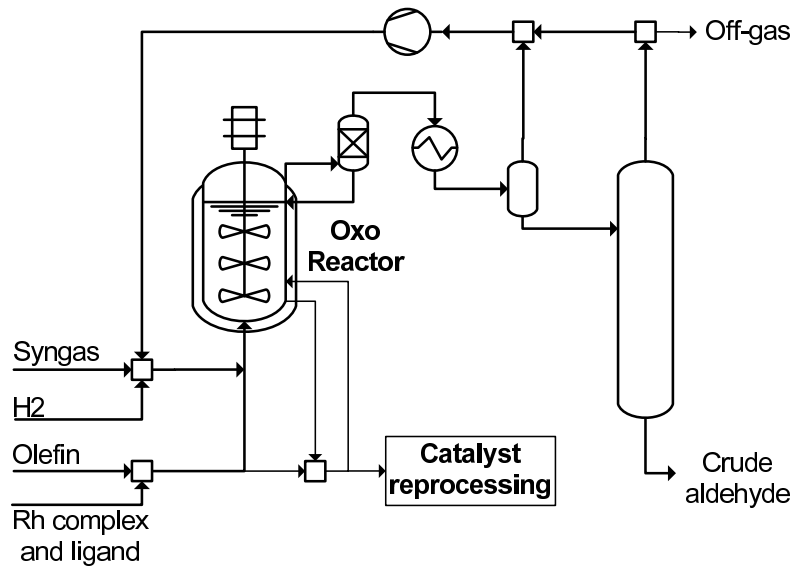
Figure 2.3.: LPO Process with gas recycle. Adapted from [16].

Exxon/Kuhlmann Process

The Exxon process is used for the hydroformylation of C6 to C12 olefins. The organic product phase is mixed with caustic then the catalyst is extracted with fresh olefin and neutralized with sulfuric acid. At elevated CO pressure the metal carbonyl is reformulated. The catalyst is then stripped with syngas and recycled to the reactor. The used unmodified cobalt catalyst requires reaction pressures of 300 bar (to stabilize the cobalt-carbonyl complex) and 160 to 180 ^oC.

Shell Process

The Shell process is used for C7 to C14 olefins and uses a phosphine modified cobalt catalyst. Aldehyde is subsequently hydrogenated to fatty alcohols in a one pot reaction. Product and catalyst are separated by distillation where the catalyst is contained in the bottom stream of the column and can be recycled to the reactor. The reactor operates at 40 to 80 bar and 150 to 190 ^oC.
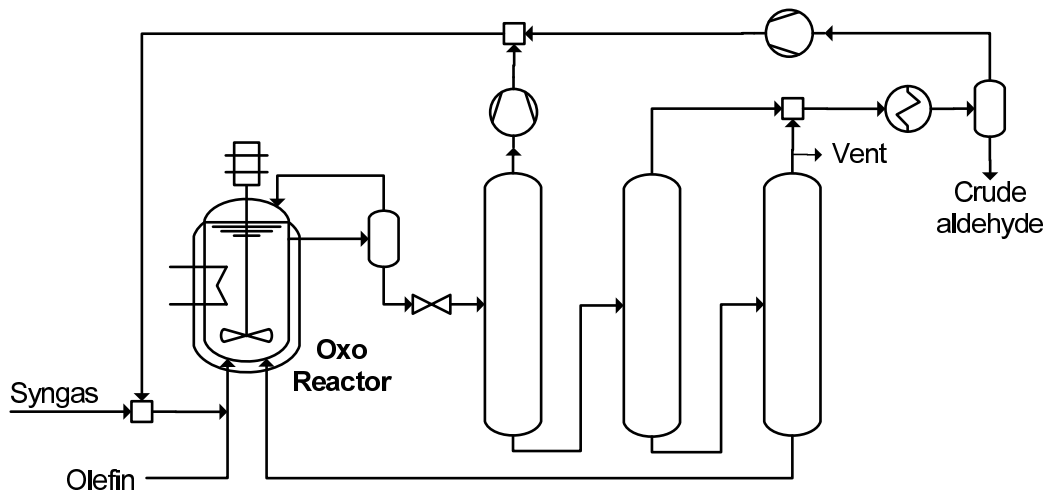
Figure 2.4.: LPO Process with liquid recycle. Adapted from [6].
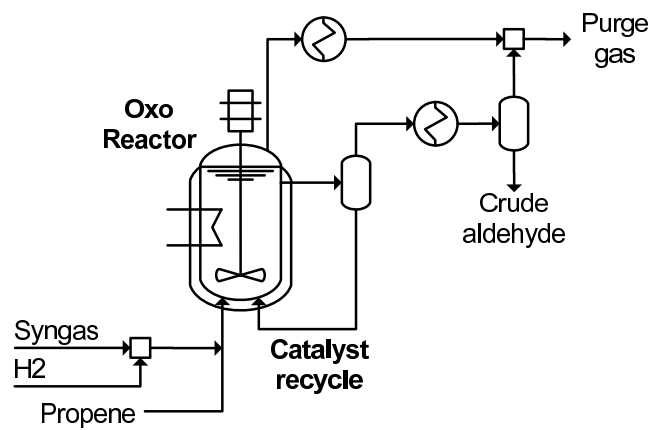
Figure 2.5.: Mk4 Process applying rhodium/bisphosphite catalysts. Adapted from [6].

Low Pressure Oxo Process

In the Low Pressure Oxo (LPO) process which was jointly developed by Union Carbide, Davy McKee, and Johnson Matthey the catalyst, a rhodium triphenyl phosphine complex ($HRh(CO)(PPh_3)_3$), is dissolved in a high boiling organic solvent, which consists of the reaction products of the hydroformylation. Hence, there is no need for an additional solvent. The process is used for the hydroformylation of short chain olefins (C2 to C4). The essential principle of the first version of the LPO process (**gas recycle process**, refer to Fig. 2.3) is that the reactor outlet is a vapor phase which leads to a quantitative retainment of the nonvolatile catalyst complex inside the reactor. By adjusting the syngas feed flow rate and reactor temperature the vapor flow in the reactor outlet is balanced with the aldehyde production rate. In order to slow down the catalyst deactivation a part of the reaction mixture is continuously processed in a catalyst regeneration step. Every 24 month, however, the reactor has to be refilled with fresh catalyst and the reaction mixture containing the old catalyst is removed to recover the catalyst externally [17]. The deactivation of the catalyst has two main reasons, firstly, the formation of rhodium clusters over time, and secondly, poisoning by impurities in the feed, such as sulfur components [17]. While the first reason cannot be avoided, the second one can be reduced by additional cleaning steps in the feedgas supply. The used CSTR operates below 20 bar and at 80 to 120 ^oC with a per pass conversion of 30% [16].

The integrated reactor-separator concept of the gas recycle process avoids additional equipment for the evaporator. The constraint of the fixed phase behavior at the reactor outlet, however, reduces the degree of freedom to optimize the reaction conditions. In order to decouple the parameters of the reactor from the catalyst separation task, the **liquid recycle process** (Fig. 2.4) was developed. Here, the reactor outlet consists of the liquid phase containing the catalyst and the catalyst separation is performed outside of the reactor. The decoupling of reaction and separation enabled the hydroformylation of olefins higher than C3. The improved performance of the reaction step and the reduced gas holdup (since stripping became unnecessary) led to smaller reactors. Due to the reduced gas flow also the recycle compressor could be removed.

Further developments of the liquid recycle process were connected with the use of improved catalyst complexes based on bisphosphites under the trademark SELECTORXX, where XX is the guaranteed n/iso ratio achieved by the catalyst. The process is also mentioned in Bohnen and Cornils [6] under the name Mk4 process 2.5. Very mild reaction conditions of 85-95^oC and 1.5-2 MPa at a propene conversion
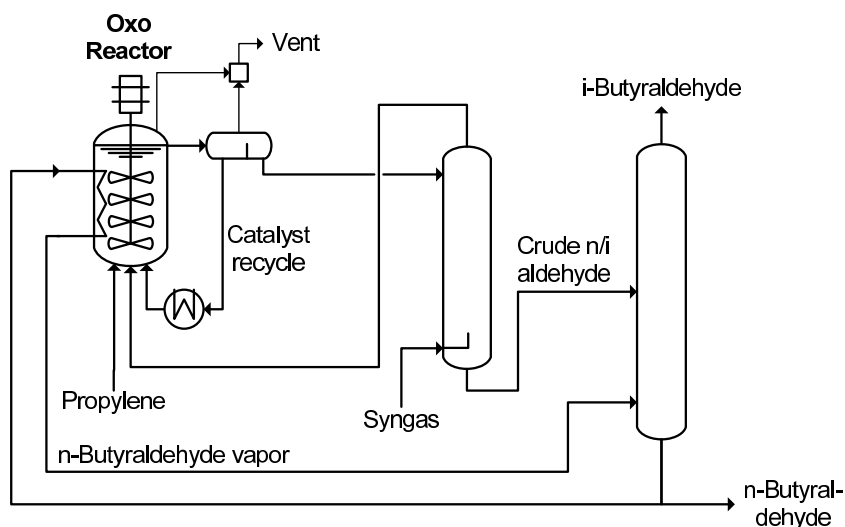
Figure 2.6.: RCRP Process. Adapted from [19].

of 98.7% are reported. The high conversion of olefin and syngas makes a recycling unnecessary, instead the off-gas is burned as fuel. While the bisphosphite process is licenced as SELECTOR30, also a SELECTOR10 process based on TPP has a high market share [18].

Ruhrchemie/Rhone-Poulenc Process

The RCH-RP process is used for the hydroformylation of propene (C3) to butanal. As catalyst a rhodium-TPPTS complex is used. Due to the sulfonate groups of the ligand, the complex is hydrophilic. Hence, the catalyst is contained in an aqueous phase which is sparged with syngas and the gaseous propene. The product aldehyde butanal builds an organic phase and can be easily separated at the top of the reactor. The unconverted olefin, which is solved in the product phase is then stripped with syngas and recycled to the reactor. The catalyst leaching into the organic phase is only about 1 ppb. This simple and efficient process is only applicable for the propene hydroformylation, since the solubility of higher olefins in water is too low to give reasonable reaction rates and the product of lower olefins do not form an organic product phase.

The reactor used in the RCH-RP process is a 120 m^3 CSTR with co-current flow of olefin and syngas from the bottom to the top of the reactor [14].

Due to its simplicity and efficiency the RCH-RP process is the benchmark process of homogeneous catalysis. The process is very energy efficient due to the use of syngas as stripping gas and as reactant, and due to the heat integration of reactor and reboiler of the n/iso aldehyde column via a falling film evaporator [20].

2.2.4. Commercial Process Concepts for Long Chain Olefins

In contrast to short chain olefins, long chain olefins are non-polar liquids at reaction conditions which are only sparingly miscible with water. The aldehyde products do not build a separate phase, since they are miscible with the olefin phase. Due to the high boiling point of long chain olefins ($\geq C_4$) they cannot be separated from the catalyst and product via "gas recycle" and "liquid recycle" processes as applied for short chain olefins, which are gaseous and volatile. The RCH-PR process is only applicable for the propene hydroformylation. Since the water solubility of shorter aldehydes is too high, the catalyst/product separation is difficult. On the other hand, the solubility of olefins higher than C3 in the aqueous phase is not sufficient to yield reasonable reaction rates.

Hence, cobalt based hydroformylation processes are still state-of-the-art for long chain olefins. These processes are mostly based on the Shell process concept using Co/TTP catalyst combined with distillation based catalyst separation.

Adapted Low Pressure UCC Process

With the adapted low pressure UCC process (Fig. 2.7) the only economically viable rhodium based hydroformylation process for long chain olefins was commercialized, so far [21, 6]. The process makes use of a temperature and composition dependent miscibility gap which provides homogeneous reaction conditions at high temperatures and enables a phase separation at lower temperatures without changing the solvent. Applying this concept higher olefins in the range of C6 to C14 can be efficiently converted. The solvent mixture consists of the alkene as reactant and product phase, water as catalyst phase, and NMP as mid-polar solvent. The rhodium catalyst is attached to water soluble TPPTS ligands. In case of heptene, a feasible working point which enables homogeneous reaction and biphasic separation conditions is a mixture with the molar composition of 37% NMP, 54% hepten, and 9% water.
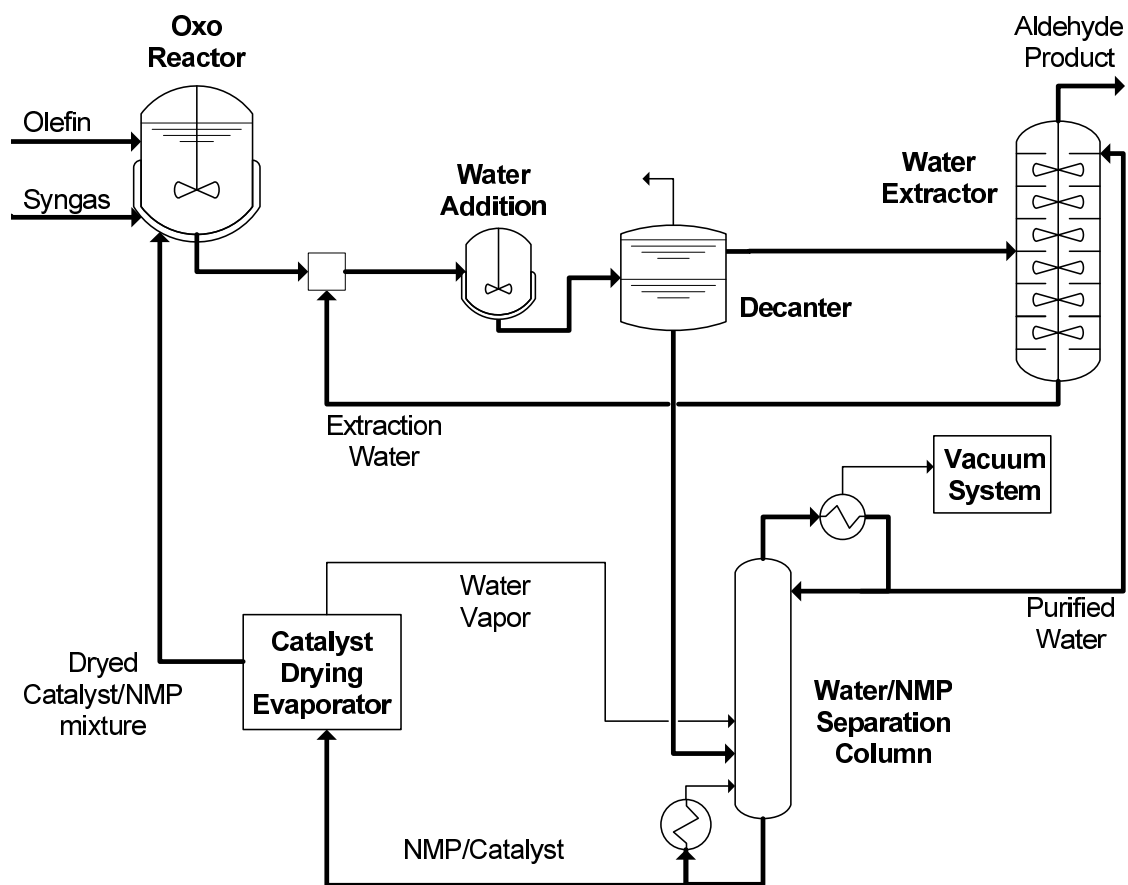
Figure 2.7.: Adapted Low Pressure UCC Process. Adapted from [21].

After the homogeneous reaction in the reactor at high temperature the outlet mixture is cooled down and water is added, yielding a NMP/water phase which contains most of the catalyst, and an organic product phase. Traces of catalyst in the organic phase are then extracted by further water addition. In order to recycle NMP and catalyst the added water has to be separated from the mixture. This is done in two steps, consisting of a distillation were water is separated as light component, and a further drying step to remove traces of water. The purified NMP/catalyst mixture is recycled back to the reactor. The recovered water from the distillation and drying step can be reused for the liquid/liquid separation downstream of the reactor and for the second water extraction step. Hence, the extraction water is always internally recycled. In addition to the water extraction the rhodium concentration in the product can be further reduced by adsorptive filtration over silica gel.

Although the rhodium losses can be reduced to below 20 ppb, the catalyst recovery, which requires vacuum service, drying steps, and a huge water recycle still yields significant equipment costs.

2.2.5. Process Concepts for Long Chain Olefins - Current Research

While, with the adapted low pressure UCC process there is only one commercially applied rhodium-based process available, recent and current research in academia seems to be endless. The hydroformylation of long chain olefins became a prominent example for integrated solvent and process design problems. The high design complexity on the one hand still hinders a commercial implementation of a new hydroformylation process. However, on the other hand it defines a challenging model case to test and develop innovative concepts and methods in academia, such as computer aided process design on multiple scales, development of advanced physical property models, innovative solvent systems and miniplant approaches. The most discussed concepts for rhodium-based hydroformylation of long chain olefins published in scientific literature are shortly summarized in this section. Fig. 2.8 gives a schematic overview of the different concepts according to their underlying principles.
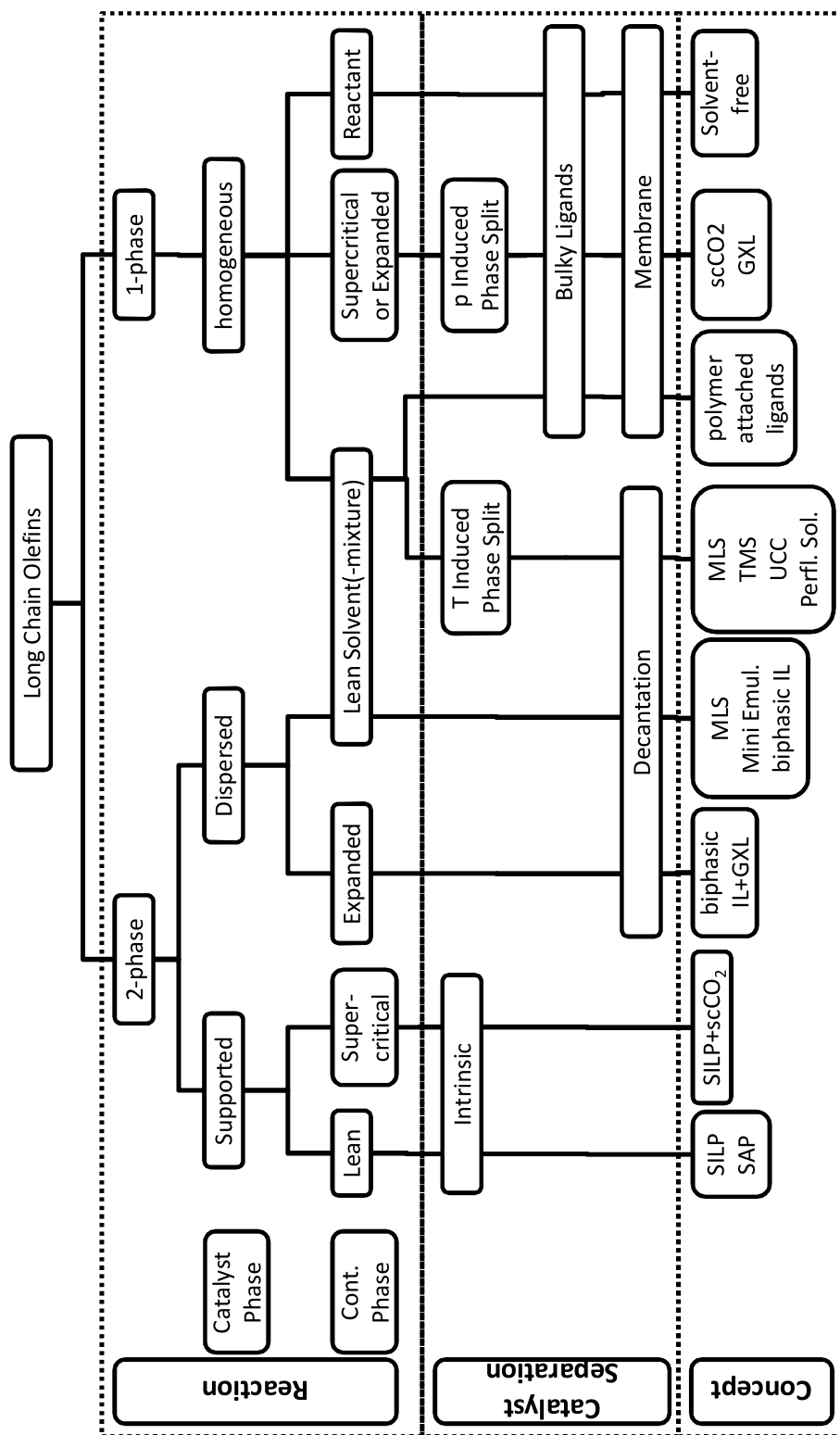
Figure 2.8.: Overview of prominent concepts for rhodium catalyzed hydroformylation of long chain olefins currently investigated in academia.
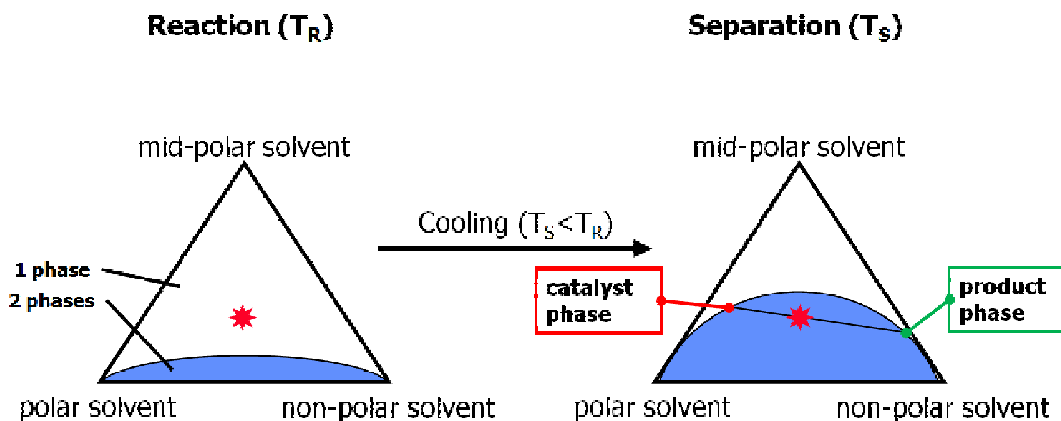
Figure 2.9.: TMS concept.

Thermomorphic Solvent Systems

The concept of thermomorphic solvent systems (TMS), which is also the example system in this thesis, makes use of a temperature depending miscibility gap of a mixed solvent consisting of solvents of different polarity (refer to Fig. 2.9). The miscibility gap that occurs when a polar and a non-polar liquid are mixed can be decreased by adding a mid-polar liquid. Moreover, the size of the two phase region depends on temperature. A suitable TMS for a given reaction provides a homogeneous liquid phase at reaction temperature while a phase split is induced at a lower separation temperature. The catalyst which is attached to polar ligands is then contained in the polar phase.

The concept sounds quite simple, however, the choice of the suitable solvent system is not trivial. If the reactant is considered as one of the TMS solvents, then, besides polar and non-polar solvent, there is at least the product as fourth component that could affect the phase stability. Usually more components than just one reactant and one product are present, which increases the complexity of the phase behavior. The influence of (side) products or reactants could cause heterogeneous phase behavior under reaction conditions or insufficient phase split at separation temperature.

The second aspect is the shape of the two phase region. The distribution of components at separation conditions should be beneficial, e.g. the product should only be contained in the product phase, while the catalyst should only be contained in the catalyst phase. In the before mentioned adapted LPO process for higher olefins

(Chap. 2.2.4) this is obviously not the case since the catalytic phase is still partially solved in the product phase to a non-negligible extent. Hence, additional extraction steps are used to recover the remaining catalyst from the product phase. This extraction procedure requires huge amounts of water which has to be contacted with the product phase in an extraction device that offers high mass transfer area. After the extraction the surplus water has to be removed from the catalyst to enable a catalyst recycle to the reactor. The additional operating and equipment costs due to extraction and solvent regeneration may be significant.

In order to select a suitable TMS Behr developed a theoretical Method based on different pure solvent parameters which represent the polarity of the solvent [10], such as Hansen parameters [22]. However, for the final selection experiments regarding the mixture of solvent system and reaction components have to be performed. Especially the catalyst distribution at separation conditions is difficult to predict due to a lack of reliable thermodynamic models for the catalyst. The model-based identification of the process optimal solvent mixture for TMS in hydroformylation of long chain olefins is subject to current research [23, 24].

Micellar Solvent Systems

Instead of adding a midpolar solvent as in the TMS concept, surfactant is added to a mixture of polar and nonpolar solvent in order to generate a large surface area between the two phases by means of micells [25, 26]. While the three components of a TMS system usually show a convex two phase region, the phase behavior of the micellar solvent system (MSS) is much more complex [27]. The bipolarity of the surfactant molecule, having a polar head and a nonpolar tail, introduces an additional degree of freedom. Thus, the phase diagram of the MLS has to be extended by another dimension yielding a phase rhombus instead of a phase triangle. Depending on the surfactant concentration and temperature a water in oil emulsion can switch into an oil in water emulsion. The MLS is much more sensitive on composition and temperature than a TMS, but the catalyst separation is more effective. In contrast to the TMS where the midpolar solvent actually is selected from a pool of candidates, the surfactant molecule can be specifically designed. The objectives working with a MSS are to provide a wide operating window for the reaction, reduced foaming and reduced surfactant leaching [28].

Perfluorinated Solvents

The concept of perfluorinated solvents is very similar to TMS. It makes use of the phenomenon that highly fluorinated molecules associate to a separate phase, immiscible with organic and aqueous phases. Moreover, the phase behavior can be controlled by temperature, e.g. the fluorous phase mixes with other phases at higher temperatures and separates at lower temperature. For the application in hydroformylation the ligand can be tagged with fluorinated sections, adopting the temperature dependent phase behavior of the fluorinated solvent [29]. It was shown that there is not necessarily a need for a fluorinated solvent, because the fluorinated catalyst may build a separate phase by its own. In case of the hydroformylation of 1-decene a catalyst leaching of 1.18 ppm was measured. Due to the high costs of the fluorinated solvent and ligand industrial application of fluorous biphasic systems will require further advances [30].

Biphasic Ionic Liquid Systems

Ionic liquids (IL) are salts which are liquid at ambient temperatures. Due to their ionic intermolecular forces these liquids have a very low vapor pressure. Depending on the type of anion and cation the properties of the IL, with respect to reactant and product solubility and also the activity and selectivity of catalysts solved in the IL [31, 32] can be tuned. Due to the high number of possible combinations ILs can be designed to meet many kinds of requirements. The homogeneous catalyst can be solved in the IL as long as it contains ionic ligands. The products and reactants of the hydroformylation can be decanted or extracted with organic solvent from the IL while the catalyst remains in the IL.

In case of the hydroformylation using IL very high selectivities and activities have been reported [33, 34] and catalyst leaching below 5 ppb has been achieved [35].

The drawbacks in using IL may be the unknown impact of the IL on the material of pipes and vessels with respect to corrosion. Also long term stability, environmental and health issues may be a quite uncertain aspect. ILs are liquids with rather high viscosity, which may cause problems with transport in pipes and high energy demand for mixing and pumping. Further the industrial application is hindered by the fact that huge amounts of IL are necessary which are about 10-50 times more expensive than the commonly used organic solvents [36]

Peschel et al. calculated the optimal reaction route for the rhodium catalyzed hydro-

formylation in a biphasic IL system [37] and proposed a suitable reactor design [38, 39].

While in most publications about hydroformylation in IL biphasic systems the enhanced olefin solubility compared to aqueous systems is emphasized [19, 40], ILs often suffer from poor syngas solubility.

Supported Ionic Liquid Phase Catalysis

Due to their low vapor pressure and high viscosity ILs can be employed as liquid layer on a solid surface such as silica or monoliths, known as supported ionic liquid phase (SILP). The ionic catalyst is kept inside the IL film, hence the reaction rate depends on the surface area of the solid support. With this approach the drawbacks of IL used as bulk solvent can be avoided [36]. SILP catalysts are highly suitable for continuous gas-phase processes in fixed-bed reactors due to the very low volatility of typical ionic catalyst solutions. The SILP concept was successfully demonstrated for the hydroformylation of short chain olefins [41, 42]. However, the concept appears to be not efficient for long chain olefins due to the bad liquid/IL mass transfer in the pores of the SILP support [36]. A promising concept that could solve this problem is the combination of SILP and supercritical CO_2 [43].

Supported Aqueous Phase Catalysts

The concept of supported aqueous phase catalysis [44] is the forerunner of the just discussed SILP concept using water instead of IL. Due to several problems, such as evaporation of water from the porous support and low solubility of organic molecules, this concept has been more or less substituted by SILP. However, improvements are still ongoing, such as with respect to catalyst molecular design [45].

Membrane Assisted Polymer Attached Ligands

The heterogenization of rhodium based catalysts using inorganic and organic carrier materials to overcome the catalyst separation problem has been investigated [46] but leaching and reduced activity of any kind of immobilization still prevents an industrial applications so far [8].

Solvent Free Hydroformylation

In the context of process intensification (PI) the solvent free hydroformylation was highlighted as it can be efficiently performed in a heat exchanger reactor (HEX reactor). Due to the high heat transfer area a solvent for better heat management is not necessary and smaller reactors can be used. Additionally, the HEX reactor provides increased gas-liquid mass transfer which leads to a higher selectivity. However, the demand for high heat and mass transfer is directly depending on the used catalyst concentration. In case of the HEX reactor a catalyst concentration in the range of $0.03 - 0.3 \text{mol}\%$ with respect to the olefin is used. Due to the mass and heat transfer limitation in the stirred tank, the HEX reactor is the better choice for this range of catalyst concentration. In the work of Enache et al. [47] the catalyst separation is not discussed, but using such high catalyst loading certainly requires a nearly perfect catalyst recovery.

Supercritical Fluids

Supercritical fluids are compressed gases above their critical temperature and pressure. In this state these fluids exhibit extraordinary solvent properties which makes them able to dissolve many organic molecules with low to medium polarity as well as permanent gases. Using this kind of solvent practically no mass transfer resistance occurs. By attaching suitable ligands to the hydroformylation catalyst it can be made soluble in supercritical fluids, such as $scCO_2$ [48]. However, the concept enhances the efficiency of the reaction, but does not solve the catalyst/product separation problem. Some approaches exist where the ligand is designed as such that it dissolves the catalyst in the supercritical fluid while initiating precipitation after decompressing the gas [48]. A very promising concept is the combination of $scCO_2$ and IL [43] to reduce the mass transfer limitations and leaching problems in the application of SILP on hydroformylation of long chain olefins.

Gas Expanded Liquids

In the vicinity of its critical point ($0.9 - 1.2T_c$ and near critical pressure) gases can exhibit liquid like densities. In such a physical state the gas can be solved in common solvents expanding the liquid volume. Depending on the mutual solubility the extent of expansion becomes more or less significant. The expanded liquid appears to have improved phase properties compared to the non-expanded neat solvent, such as lower viscosity (especially for IL/CO_2), or higher diffusion coefficients, making this effect an
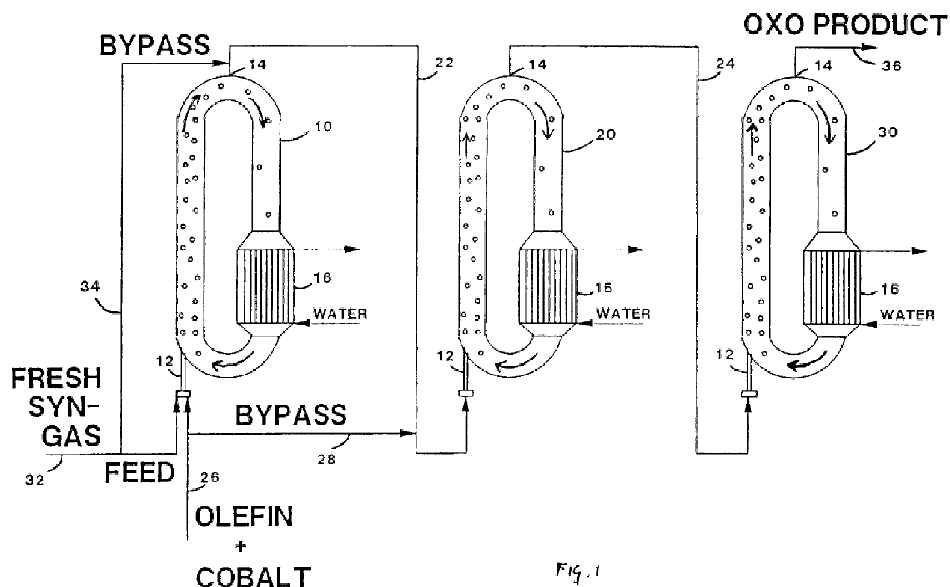
Figure 2.10.: Loop reactors in series as proposed for the Exxon/Kuhlmann process. Adapted from [51].

opportunity for process intensification. The expansion effect can be observed for many gases at very mild conditions enabling a practical implementation at low costs. For multiphase reactions involving gaseous reactants, such as hydroformylation of long chain olefins, the solubilities of the reactant gases can be tuned by the pressure of the expanding gas. In the hydroformylation of 1-octene a much higher regio selectivity was achieved by using CO_2 as expanding gas [49]. It was found that the ratio of H_2 and CO was enhanced by the expanding gas since the solubility of the two gases is affected differently. In the literature also combinations of the GXL concept with other hydroformylation concepts are described, such as GXL + IL [43], or GXL + TMS [50].

2.2.6. State-of-the-Art Hydroformylation Reactors

In most of the above discussed hydroformylation processes a continuously stirred tank reactor with internal or external cooling is used as illustrated in the presented process flow sheets in Fig. 2.3,2.4,2.6, and 2.7. The liquid phase is mostly moving from the bottom to the top of the reactor, which indicates that the reactor is more like a stirred column than like a typical CSTR, especially since often multiple blades are used. Gas is injected at the bottom with a distributor in order to create gas bubbles which move
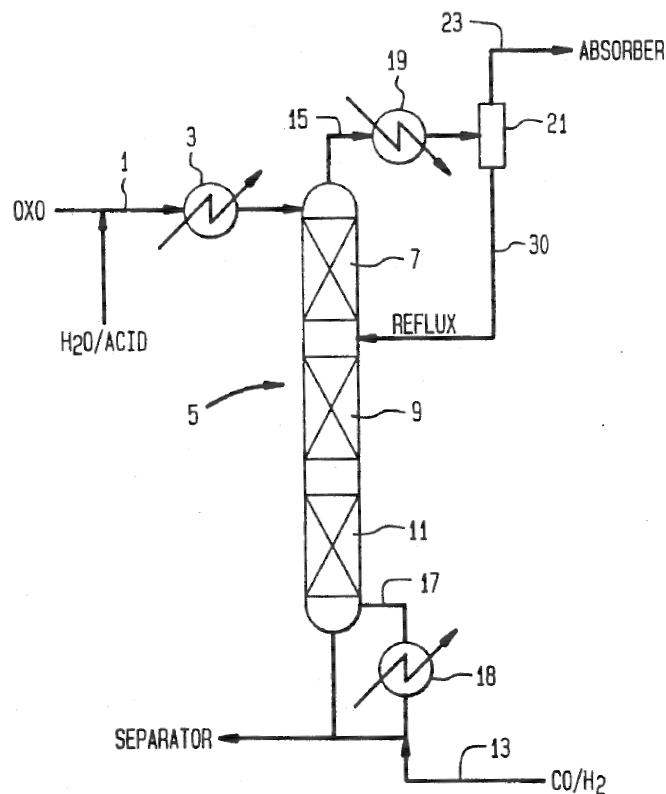
Figure 2.11.: Stripper reactor proposed for the hydroformylation of short chain olefins. Adapted from [53].

more or less co-currently with the liquid phase towards the top of the reactor [6].

In case of the Exxon/Kuhlmann process, which uses unmodified cobalt, a loop reactor is used [6] and patents which describe the use of a series of loop reactors (Fig. 2.10) are published [51]. The loop is arranged vertically in such a manner that the part containing the uprising liquid contains a higher gas holdup. The reactor outlet is located at the top of the loop in order to take out gas and liquid phase. The downcoming part of the reactor is equipped with a heat exchanger to remove the heat of reaction with cooling water. The loop reactor series offers dosing of the feed not only into the first, but also in the following reactors. Besides external loop reactors also internal loop reactors are possible, also with integrated heat exchangers [52].

In case of short chain olefins where the gas recycle method is used special effort was put into the design of the stripper-reactor, where the syngas simultaneously supplies the reactant and removes the product from the catalyst phase [53, 54]. Such a stripper-reactor is designed as packed column with counter-current flow of liquid

and gas phase where liquid flowing downwards. The reactor is divided into an upper stripping section and a lower reaction section (refer to Fig. 2.11). The lower inlet position of the reflux creates a backwash section to reduce catalyst loss into the gas phase.

Bohnen and Cornils report that in the LPO process for short chain olefins with liquid recycle there is a need for high conversion due to missing gas recycle (which is not clear from Fig. 2.4). Hence, several CSTRs in series are used [6]. Further, a single reactor is reported to be a stirred tank with internal or external coolers.

The reactor used in the RCRP process is a CSTR with multiblade stirrer (Fig. 2.6). Due to its low density the aldehyde phase is floating on top of the aqueous catalyst phase and can directly be withdrawn, such as the light phase from a decanter. The innovative aspect is the heat integration of the reactor with the aldehyde separation via a falling film evaporator inside the reactor where aldehyde is evaporated using the heat of reaction thereby cooling the reactor and simultaneously creating stripping vapor for the column.

In case of the solvent free hydroformylation the use of heat exchanger reactors has been reported [47]. However, the feasibility of this concept requires extremely high rhodium loading in order to move the reaction zone towards the gas-liquid interface. Under these conditions high mass and heat transfer achievable with heat exchanger reactors is required. The concepts are exemplified on the hydroformylation of short chain olefins, which have a much higher reaction rate than long chain olefins. However, no information on the catalyst separation is provided.

Wiese et al. [55] reported about the successful application of a tubular reactor (3 m long, 17.8 mm diameter) packed with static mixers for the aqueous biphasic hydroformylation of propene. The reactor is operated at high catalyst loading with residence times about 5 seconds. Downstream of the reactor the catalyst phase is separated via liquid-liquid phase separation and recycled to the reactor. The authors claim the applicability of the concept to hydroformylations with olefin chain length up to C8.

2.3. The Elementary Process Function Concept

The typical process design method in chemical engineering is based on the well established concept of unit operations, which uses available and proven apparatuses to realize certain tasks, such as mixing, separation, and reaction. Within the process
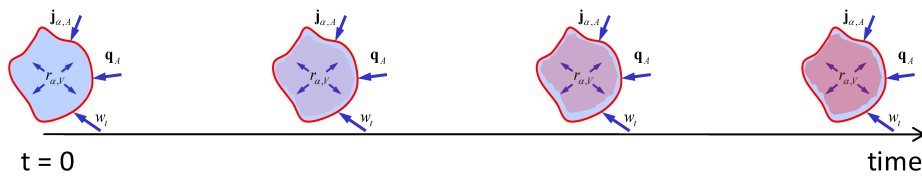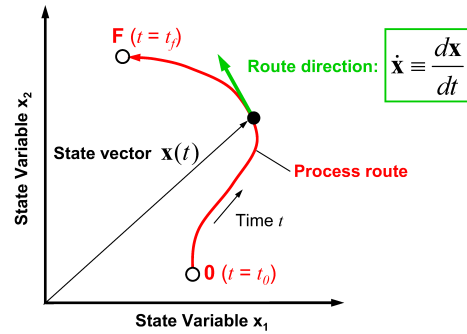
Figure 2.12.: Fluid Element and Travel Route in State Space. Adapted from [56].

design these unit operations are then interconnected by means of material streams in a step-by-step way from reactant conditioning over reaction to product separation and recycling. After the flow sheet of unit operations and material streams is set up, the heat sources and sinks are integrated in order to minimize utility consumption. The approach is very efficient and can be standardized, however, each unit is an own environment which can only be accessed by a limited number of design parameters. Besides the standardized, modular and transferable concept this approach also has some intrinsic disadvantages, such as:

- The optimal process can only be found within the set of available unit operations, which is not necessarily the best possible solution.

- Innovative concepts for a single unit in terms of process intensification are mostly an outcome of increased demand for improvement due to competition, safety, or environmental aspects but they are not included in the normal work flow of the design procedure.

In the concept of elementary process functions from Freund and Sundmacher [3] the chemical process is seen as an optimal travel route of a matter element in the thermodynamic state space, which is controlled by material and energy fluxes on its transformation from a raw material into the final product (Fig. 2.12). Instead of connecting unit operations, the travel path is divided into functional modules, such as reaction, separation or mixing. Within each functional module the optimal travel

Route Direction

$$\dot{\mathbf{x}} = \mathbf{E}(\mathbf{x}) \cdot \mathbf{j}(\mathbf{x}, \mathbf{x}_{eq})$$

Elementary Process Functions

Fluxes

$$\mathbf{E}(\mathbf{x}) = \mathbf{C}^{-1}(\mathbf{x}) \cdot \mathbf{F}$$

$$\mathbf{K}(\mathbf{x}) \cdot \mathbf{f}(\mathbf{d}(\mathbf{x}, \mathbf{x}_{eq})) = \mathbf{j}(\mathbf{x}, \mathbf{x}_{eq})$$

Capacity Matrix:

Sensitivities of Density $\rho(T, p, \mathbf{y})$:
- $\partial\rho(T, p, \mathbf{y})/\partial T$
- $\partial\rho(T, p, \mathbf{y})/\partial p$
- $\partial\rho(T, p, \mathbf{y})/\partial \mathbf{y}$

Sensitivities of Enthalpy $h(T, p, \mathbf{y})$:
- $\partial h(T, p, \mathbf{y})/\partial T$
- $\partial h(T, p, \mathbf{y})/\partial p$
- $\partial h(T, p, \mathbf{y})/\partial \mathbf{y}$

Flux-weighting Matrix:

Geometrical Factors:
- surface areas a_m, a_v, a_q
- volume V or cross sectional area A_c

Reaction Network:
- species mass matrix $\mathbf{M}$
- stoichiometry matrix $\mathbf{N}$

Surface States:
- composition $\mathbf{y}_A$
- enthalpies $\mathbf{h}_A{}^T$

Kinetic Matrix:

Main Coefficients:
- diffusivities
- thermal conductivity
- viscosity
- reactivities
- field coupling coeff.

Cross Coefficients:
- thermo-diffusivity
- thermo-electrical

Driving Force Vector:

Differences between states $\mathbf{x}$ and equilibrium states $\mathbf{x}_{eq}$:
- temperature ΔT
- pressure Δp
- chemical potentials $\Delta\boldsymbol{\mu}$
- velocity $\Delta\mathbf{v}$
- Gibbs enthalpies $\Delta_R\mathbf{G}$
- force potentials $\Delta\psi$

Figure 2.13.: Elementary Process Function Model. Adapted from [56].

route can be found according to the desired objective, such as minimum residence time or maximum selectivity. In order to identify the optimal route a thermodynamic model based on the fundamental balance equations for mass and energy has to be set up for a matter element within each functional module. The travel path from the initial state of the matter element to the final state in thermodynamic state space can be optimized by solving a dynamic optimization problem which is constrained by the balance equations, constitutive equations, and equilibrium relations of the matter element (Fig. 2.12). Freund and Sundmacher also proposed a model formulation which allows a rational assessment of the involved variables by separating the balance equation into a linear combination of a flux vector $\mathbf{j}(\mathbf{x}, \mathbf{x_{eq}})$ and the corresponding elementary process functions $\mathbf{E}(\mathbf{x})$, which represent the unit vectors in thermodynamic state space. Fig. 2.13 shows the structure of the proposed model. Based on the EPF concept Peschel et al. [4] developed a method for the design of chemical reactors which are tailor made for any specific reaction system. As illustrated in Fig. 2.14 the approach consists of three levels with respect to the treatment of the fluxes which control a fluid element (FE) traveling through the reactor. The idea is, according to Fig. 2.12, to calculate the energy and material fluxes on the fluid element as profiles in time by means of solving a dynamic optimization problem (OP). The OP is constrained by balance equations, constitutive equations, equilibrium relations
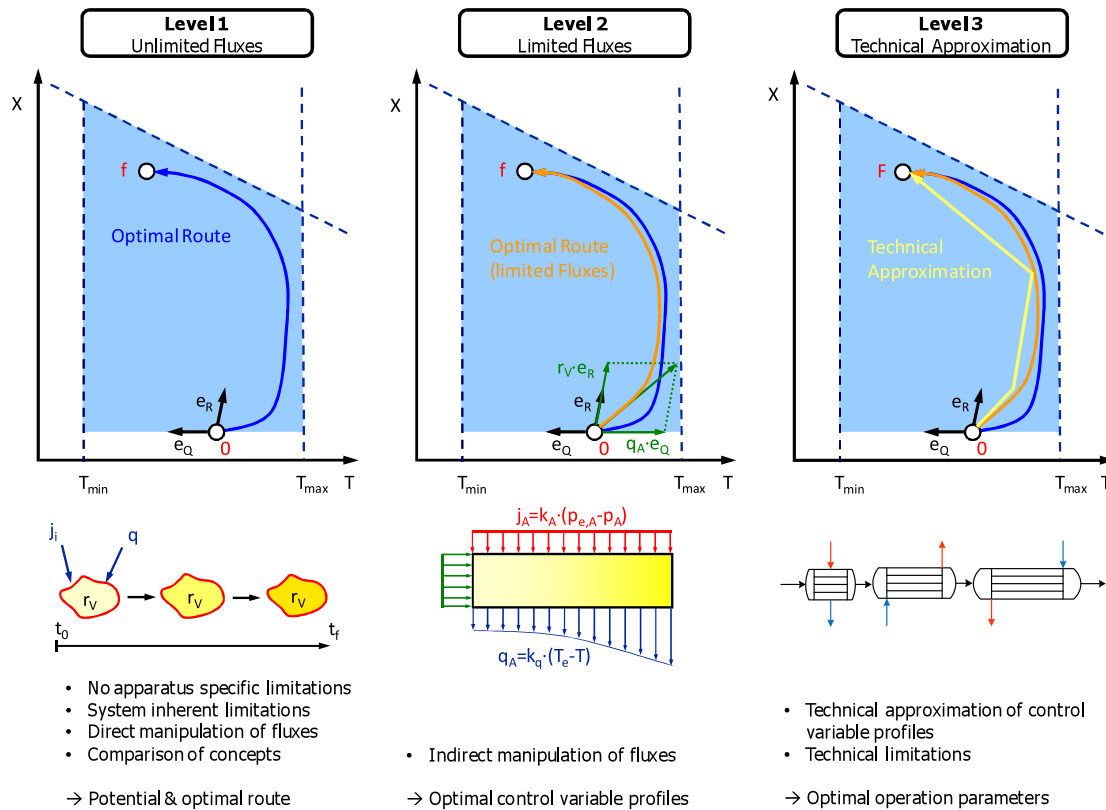
Figure 2.14.: Reactor Design Method of Peschel et al. Adapted from [57].

and physical bounds.

In the first level unlimited fluxes are directly considered as control functions yielding the best possible solution for the OP. This solution defines the reference case to quantify the performance losses due to the technical approximation of the reaction route. On level one all possible fluxes and flux combinations can be screened yielding a most suitable set of fluxes to control the state of the FE.

In level two the best combination of fluxes is further investigated. Instead of manipulating the fluxes directly they are now substituted by their constitutive equations, such as kinetic laws. Hence, additional constraints for the constitutive equations are added to the OP. Thereby the fluxes cannot be directly manipulated anymore, but instead only the driving force and the transport coefficient. Due to the indirect control of the fluxes the optimal reaction route from level one usually cannot be matched anymore. The result of level two are optimal profiles of external control variables in time as well as values for exchange areas.

On the third level the control profiles are translated into a technical approximation by interpreting their dynamic behavior. While on the previous levels a FE which moves through a not yet defined apparatus is considered, now the apparatus has to be re-engineered to yield the dynamic profiles of the control variables. This can be realized as semi-batch process, where no translation into a spatial coordinate is necessary. However, mostly a transformation of the time coordinate into a distributed device in space is beneficial for continuous processes. As an example, a rising cooling temperature profile in time can be translated into a co-current indirect cooling segment in space, if a tubular reactor is considered. On the third level usually many approximations are possible which can be evaluated by comparison with the ideal solution from level 1.

Due to the FE model approach the design method is apparatus independent which does not exclude innovative solutions as in case of predefined reactor concepts. The applicability of the design method was demonstrated on various examples [4, 38, 58, 39, 59].

2.4. Reactor Design for Multiphase Systems

2.4.1. Literature Review

Krishna and Sie [60, 61] developed a selection strategy to chose from several types of reactors depending on the participating phases. They proposed a three level approach consisting of the following steps:

Volume/Surface Area Selection. Determination of the optimal volume to surface area for each phase. In case of gas-liquid systems it corresponds to the ratio of liquid bulk volume to diffusion layer volume, namely the Hinterland ratio. In case of gas-solid systems it corresponds to the particle size.

Contacting Flow Pattern. Determination of the optimal residence time distribution, the optimal dosing/removal strategy for reactants and products, and the relative flow direction of the phases, such as co-current, counter-current, or cross flow.

Flow Regime. The choice of the flow regime addresses interface mass transfer, heat transfer, back-mixing characteristics, and scale up considerations. However, the

decision in level three is more or less predetermined by the decisions on level one and two.

The design procedure is based on qualitative phenomena rather than a rigorous quantitative approach and the result seems to depend very much on the experience of the designer. The method can be summarized as a compilation of good engineering practice rules for multiphase reactor design yielding a suitable reactor from a given set of choices.

Mehta and Kokossis [62] proposed reactor configurations for non-isothermal multiphase systems, incorporating choice of flow pattern, and assuming equilibrium between phases. The method yields optimal networks of standard reactors, also comprising distributed dosing (distributed side-stream reactors) and recycles. However, the optimal solutions presented are mostly very complex and can barely be approximated by a single reactor.

Kelkar and Ng [63] proposed a combined model and knowledge based screening method for non-isothermal multiphase reactors. A generic multiphase reactor model is used considering well mixed bulk phases (gas, liquid, solid), modeled as continuously stirred tank reactor (CSTR), connected via a stagnant film model, modeled as plug flow reactor (PFR), for the interface mass transfer. The model is solved for a specific reaction system and the sensitivities of the objective function, such as selectivity, with respect to the degree of freedom (DoF) is evaluated solving the sensitivity equations in parallel. After each iteration the DoF with the highest sensitivity is adjusted, but also related DoF are adjusted in order to assure feasibility of the parameter set. Such as, if the phase ratio exceeds a certain value also the exchange area is adjusted to be consistent with operation regimes of existing devices. The degree of back-mixing is adjusted by changing the number of CSTRs. If the feasibility check is not strictly performed on each iteration, also new reactor configurations could be identified. Due to the incorporation of the rigorous film model reactions corresponding to the entire range of Hatta numbers can be treated.

2.4.2. EPF-Based Approach

Based on the EPF concept, Peschel et al. [39] extended their reactor design method for multiphase systems by using a sensitivity analysis for the interfacial mass transfer coefficient $k_L a$. The method was exemplified on the hydroformylation of 1-octene in a biphasic liquid system consisting of an organic reactant and product phase and an

ionic liquid catalytic phase which is dispersed in the organic phase. The two liquid phases were assumed to be in equilibrium and the additional gas phase was considered as ideal service phase where the partial pressures in the gas can be ideally optimized. By optimizing the product selectivity for distinct fixed $k_L a$ values the sensitivity of the maximum selectivity with respect to the mass transfer resistance can be analyzed and special criteria on the minimum required mass transfer coefficient can be derived. In the example system a maximum selectivity loss of 1% was assumed and hence a minimum $k_L a$ value of $1 s^{-1}$ was identified. Besides the optimal dosing and temperature profiles over the length of the reactor, also a suitable mixing concept, which provides the minimum $k_L a$ value has to be applied.

For the choice of the mixing concept multiple realizations are possible, which have to be compared with respect to their specific energy requirements, and the most efficient concept can be chosen.

In the specific case a segmented tubular reactor with discrete dosing points for gas and liquid dosing in combination with static mixer elements to provide the necessary $k_L a$ value was suitable to achieve the desired concentration profiles over the reaction coordinate. The heat management was realized with indirect cooling via an external medium with different flow directions on each reactor segment.

The selection of the mixing strategy is easily applicable, but the detailed selection from a set of possible realizations requires besides the specific energy demand several additional aspects to be considered, such as flow regimes. Furthermore, the mixing concept has usually a significant influence on the variable and capital costs of the process, which might have to be considered.

3. Methodological Approach

In this chapter the methodological approach for the identification of the optimal reaction route of the hydroformylation of long chain olefins in TMS is proposed. While this chapter explains the fundamental principles of the method, the application on the specific reaction system is presented in the next chapter.

In order to solve the design problem "optimal reaction route" the most important question is: "What is the objective function?" If the objective is not known then an optimal reaction route does not exist. Although the question of the objective is the most important one, it is not easy to find an answer. There exist many objectives for the design of chemical reactors, each suitable for certain kinds of reaction sys-

Stage 1: Stand-Alone Reactor

Objective
Chemical engineering measure
Result
• **Reaction mechanism**
• **Interpretation of optimal route**

Stage 2: Ideal Recycle

ideal
selective
separation

Objective
Chemical engineering measure
Result
• **Optimal recycle composition**
• **Maximum usage of resources**
• **Criteria on separation section**

Stage 3: Integrated Process

real
separation
S_1

real
separation
S_N

Objective
Economic measure
Result
• **Cost optimal reaction route**
• **and operation parameters of**
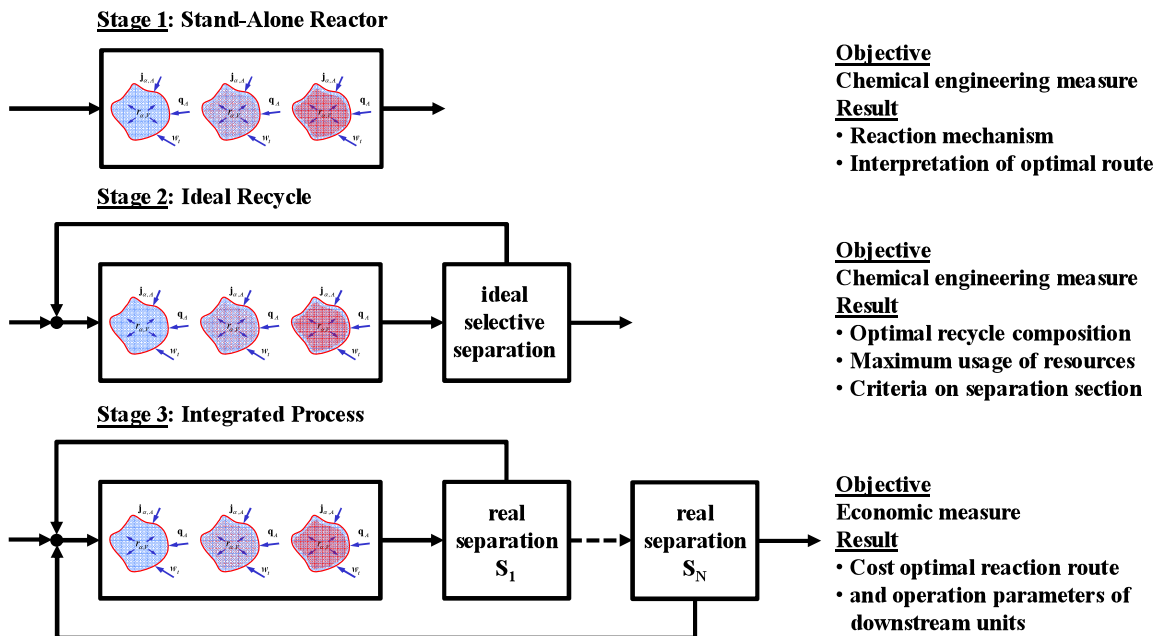 **downstream units**

Figure 3.1.: Design approach for the identification of the process wide optimal reaction concept for liquid multiphase systems. Adapted from [64]

tems. Such objectives are usually chemical engineering measures, such as selectivity, conversion, space-time yield, reaction time, or productivity. The main argument to use these kind of objectives is their independence from external factors, such as location, prices, or authority regulations. Thus, these kind of objectives really measures the physico-chemical performance of the reactor. However, when comparing different chemical engineering objectives one can see that maximizing one objective will always cause a reduction of another objective. Hence, usually only Pareto-optimal solutions can be achieved. The objective that represents process wide optimality is a combination of competing chemical engineering measures where the weighting factors depend on the effort of the downstream process.

If an integrated reaction system is considered where the chemical reactor is a part of, then a local objective such as the mentioned chemical engineering measures might not be optimal regarding the overall process performance. This is also true for each of the other unit operations of the process. An energy optimized distillation column might be locally optimal for a given product spec, but the optimal product spec depends on the overall process performance. If the effort for a certain product separation step is much lower than a high reactor performance, the reactor may even be designed sub-optimal from a local perspective, but the overall process is optimal.

Finally, the overall process performance needs to be maximized. Hence, the aim of this work is to identify the process wide optimal reaction route for the hydroformylation of long chain olefins in TMS. Due to the catalyst separation concept of the TMS which leads to inherent recycle streams there is much feedback which barely can be considered by optimizing a single local chemical engineering objective.

Despite the question if local objectives are suitable for process-wide optimality, chemical engineering measures are perfectly suited for the analysis of the reaction mechanism, model development, and identification of reaction kinetics. Hence, the first two stages of the proposed methodological approach (refer to Fig. 3.1) apply optimization of the isolated reaction section without considering the entire process with respect to local chemical engineering measures. The optimal reaction routes of stage one and two facilitate the understanding of the reaction mechanism and and the interpretation of the process-wide optimal reaction route obtained in stage three. Further, stage one and two support the identification of reasonable reaction conditions for the determination of the reaction kinetics. The different stages of the methodological approach are explained in detail in the next sections.

The calculation of the optimal reaction route on each stage is performed by solving

a dynamic optimization problem according to the EPF concept [3]. The constraints of the optimization problem contain the model equations of the fluid element and specific constraints for each stage. The solutions of the optimization problem, which depend on the choice of the objective function as well as on the constraints, are dynamic profiles of the control variables over the residence time of the fluid element. In order to account for the possibility of feedback via recycling of substances in an early stage of process design, a three stage approach (refer to Fig. 3.1) is proposed and introduced in the following steps.

3.1. Stage 1: Stand-Alone Reactor

In the first stage only the reaction system is considered without recycling (refer to Fig 3.1, first case) and the optimal reaction route with respect to a reaction engineering objective function (e.g. selectivity) is calculated. The optimization problem of stage one can be illustrated as follows.

Objective function:	Maximize selectivity to product S
Control variables:	Mass and energy fluxes into the fluid element $j_i(t)$
	Initial conditions of reactants $n_i(t_0)$ and temperature $T(t_0)$
	Residence time τ
Constraints:	Component mass and energy balance equations
	Reaction kinetics
	Solubilities
	Boundaries (temperature, pressure, STY)
	Initial conditions of non reactants

The detailed model equations depend on the specific example as will be discussed in Chapter 4. In contrast to the following steps the initial conditions of non reactants are always zero, since these compounds are not considered as resource and a recycling is not an option in this stage. The solution of the optimization problem is a set of optimal profiles of control fluxes over the residence time of the fluid element in the reactor in combination with optimal initial conditions of reactants.

The main result of this stage is a deep understanding of the reaction system which facilitates the interpretation of the optimal reaction route of later stages. Further, the optimal reaction route of stage one is used to identify critical periods in the reaction dynamics which facilitate experimental model validation and refinement.

3.2. Stage 2: Reactor with Ideal Recycle

In stage two, initial and end conditions of the dynamic model are coupled in such a way, that components formed by reaction can be recycled selectively to the inlet of the reaction section. This stage represents the reactor with ideal recycle (refer to Fig 3.1, stage 2). The optimization problem of stage two contains the following qualitative compounds:

Objective function:	Maximize selectivity to product S
Control variables:	Mass and energy fluxes into the fluid element $j_i(t)$
	Initial conditions of reactants $n_k(t_0)$ and temperature $T(t_0)$
	Residence time τ
Constraints:	Component mass and energy balance equations
	Reaction kinetics
	Solubilities
	Boundaries (temperature, pressure, STY)
	Initial conditions of non reactants: $n_j(t_0) \leq n_j(t_f)$

The solution of the optimization problem is a set of flux profiles in combination with an optimal composition of the recycle stream, represented by the vector of initial conditions. The composition of the recycle stream yields essential requirements on the separation task downstream of the reactor and supports process design procedure. Although the overall process concept might still not be defined at this stage, but a reasonable working point for the experimental validation and refinement of reaction kinetics can be obtained since recycling is considered.

3.3. Stage 3: Integrated Process

Since the optimal recycle streams usually cannot be realized ideally, in stage three of the methodological approach the process optimal reaction route is calculated based on a specific process, which also fulfills the requirements from stage two regarding the optimal recycle composition (refer to Fig 3.1, stage 3). By closing the recycle streams the initial conditions of non reactant components are determined by the process and only the reactant feed stream and dosing streams can be manipulated as DoF. The result of the optimization problem are optimal flux profiles of the reaction section in combination with optimal parameters of the separation units. Since the objective function of stage three is the minimization of the total production costs, reaction engineering constraints, such as a minimum STY, are not longer necessary. The

qualitative optimization problem of stage three is defined as follows:

Objective function:	Minimize total production costs (depreciation of investment costs, utility costs, raw material costs)
Control variables:	Mass and energy fluxes into the fluid element $j_i(t)$
	Feed stream of reactants N_i
	Residence time τ
	Parameters of separation units
Constraints of fluid element:	Component mass and energy balance equations
	Reaction kinetics
	Solubilities
	Boundaries (temperature, pressure)
Constraints of process model:	Mass and energy balances of the separation units
	Connectivity constraints of process streams
	Cost models for investment
	Boundaries of separation unit parameters (temperature, pressure)

In the next chapter the introduced methodological approach is exemplified on the example of the rhodium catalyzed hydroformylation of 1-dodecene in a TMS. Fig. 3.2 illustrates the practical workflow beginning with validation and refinement of reaction kinetics, validation of the optimal reaction route, and identification of the process-wide optimal reaction route. Further the influence of back-mixing and mass transfer is investigated for the stand-alone reactor as well as for the integrated process.
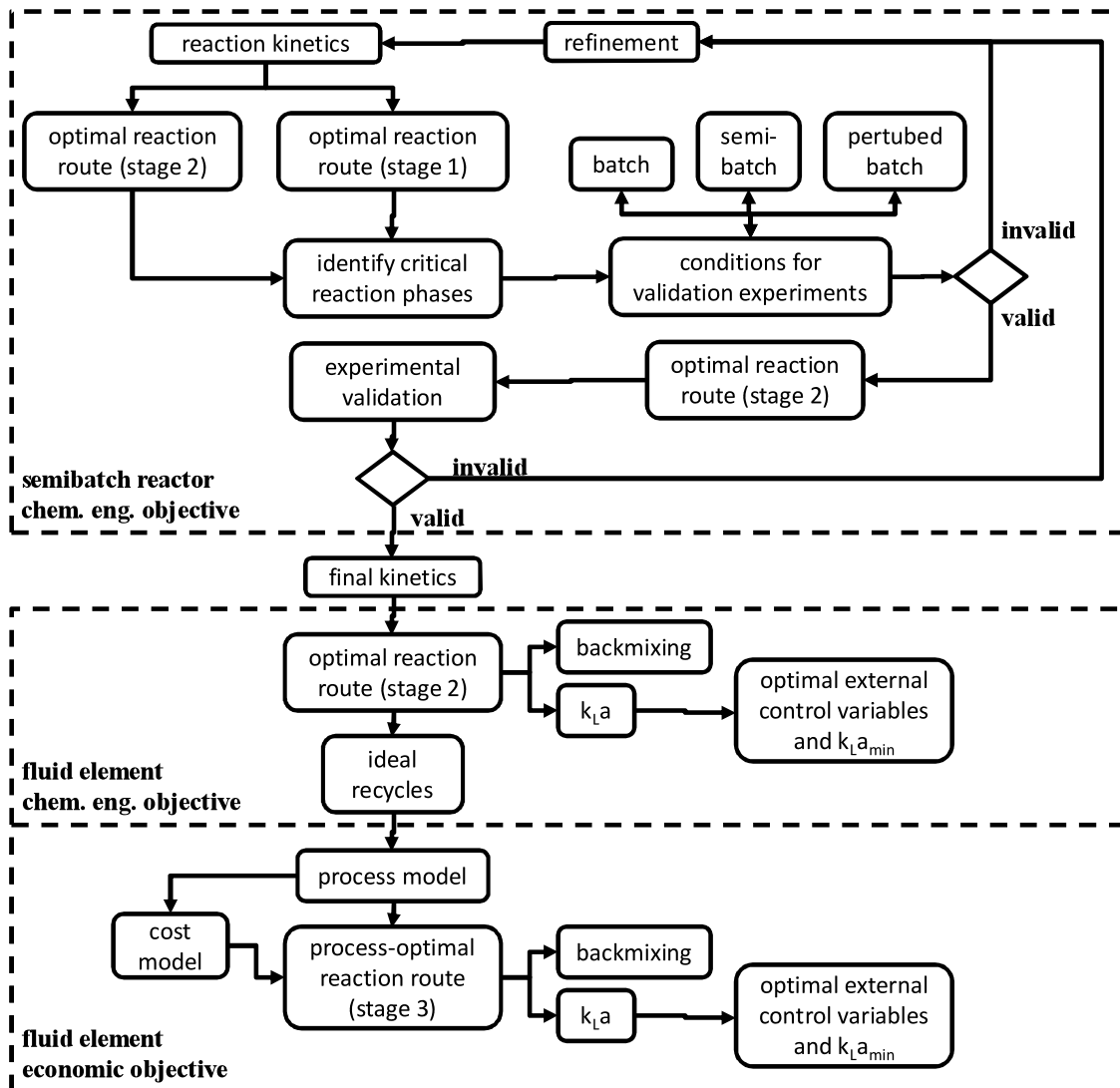
Figure 3.2.: Work flow for the identification of the process wide optimal reaction concept

4. Hydroformylation of 1-Dodecene in Thermomorphic Solvent Systems

4.1. Reaction System and Mathematical Model

4.1.1. Solvent System

The specific example system of this work is the homogeneously catalyzed hydroformylation of 1-dodecene in a TMS consisting of the polar solvent dimethylformamide (DMF), the nonpolar solvent decane (C10an), and the reactants and products of the hydroformylation. Schäfer et al. [65] performed an extensive study on this system using a homogeneous Rhodium(acac)(CO_2)/Biphephos catalyst. In their work, they investigated the LLE behavior experimentally and theoretically using the perturbed chain statistically associating fluid theory (PC-SAFT). Furthermore, reaction performance and catalyst recycling were investigated. The availability of this extensive previous work and the knowledge about this particular TMS makes it an excellent example for our reactor design method.

The purpose of using the TMS system in homogeneously catalyzed hydroformylation of long chain olefins was already described in the introduction. While exhibiting a homogeneous phase under reaction conditions, a reduction of the temperature induces a phase split. After the phase split a dense polar phase which contains the catalyst is in equilibrium with a light organic product phase. The polar catalytic phase is recycled into the reactor. It was shown that the catalyst leaching into the product phase is very low and recycling experiments have been conducted successfully. However, while the catalyst leaching is appreciably low, the solubility of the product in the catalytic phase is less favorable. Schäfer et al. [65] found that a low separation temperature reduces the catalyst leaching. In addition, the biphasic region can only be obtained up to a product mass fraction of 20%. This implies that in case of full conversion around 80% of the product mixture has to be solvent.
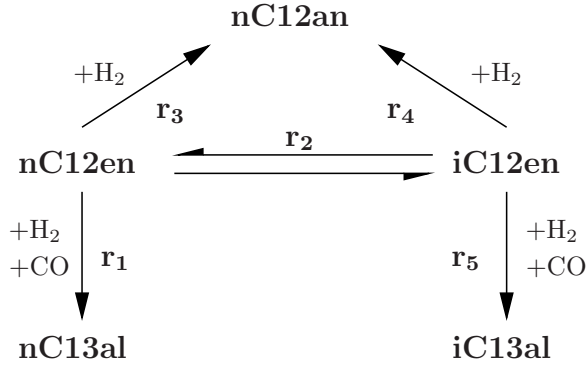
Figure 4.1.: Reaction network of the rhodium catalyzed hydroformylation in TMS as derived by Kiedorf et al. [13]. nC12en = 1-dodecene, iC12en = internal dodecenes, nC12an = n-dodecane, nC13al = n-tridecanal, iC13al = isomeric aldehydes.

4.1.2. Gas Solubilities

Since the hydroformylation reaction system contains the gaseous reactants H_2 and CO the gas solubilities are of high importance in order to calculate the concentrations of gaseous reactants in the liquid phase. Vogelpohl et al. [66] investigated the solubilities of H_2 and CO in the neat solvents decane, DMF, 1-dodecene, and n-dodecanal as well as in binary mixtures of these solvents. Besides experimental measurements the gas solubilities were modeled with PC-SAFT. From the experiments as well as from the PC-SAFT prediction it could be shown that within the experimental conditions the solubilities show rather simple behavior. Hence, for the estimation of the reaction kinetics, a temperature dependent expression for the Henry constant, which is in agreement with the PC-SAFT result has been used by Kiedorf et al. [13]. The equilibrium gas concentration is calculated via Henry's law (Eq. (4.1)) where the gas solubilities are expressed as exponential correlation (Eq. (4.2)). The solubility parameters are given in Tab. A.1.

$$c_i^* = \frac{p_i}{H_i} \tag{4.1}$$

$$H_i = a_{H,0,i} \exp\left(\frac{-E_{A,H,i}}{RT}\right) \qquad , i \in \text{GAS} \tag{4.2}$$

4.1.3. Reaction Network

The identification of the reaction network for the investigated system was performed by Markert et al. [67] and Kiedorf et al. [13] applying perturbation experiments. It

was shown that the complex reaction network can be modeled considering five main reactions (Fig. 4.1). The reactant 1-dodecene (nC12en) can be converted into the desired linear aldehyde n-tridecanal (nC13al) via hydroformylation (r_1). Undesired side reactions are the isomerization of 1-dodecene (r_2) into internal dodecenes (iC12en) and the hydrogenation (r_3) of 1-dodecene into dodecane (nC12an). The internal dodecenes are also subject to hydrogenation (r_4) and hydroformylation (r_5). The hydroformylation of internal dodecenes leads to the formation of undesired branched aldehydes (iC13al). Besides the chemo-selectivity to the linear aldehyde also the n/iso ratio plays an important role, since the n/iso separation is an energy demanding step in the hydroformylation process. The direct formation of branched aldehyde from 1-dodecene was not observed using the Rh/Biphephos catalyst.

4.1.4. Reaction Kinetics

It is well known that the catalytic cycle of the rhodium based hydroformylation is complex and that several catalyst species exist. Kiedorf et al. [13] assumed that in the specific system all reactions are catalyzed by the same active catalyst species which is in equilibrium with its inactive forms and precursors. Based on the full description of the catalytic cycle which combines hydroformylation, isomerization, and hydrogenation they were able to derive the reaction kinetics (Eqs. (4.3)–(4.7)) of the reaction network in Fig. 4.1. Also the catalyst equilibrium (Eq. (4.9)) was derived in order to determine the concentration of active catalyst. The parameters for the reaction kinetics are given in Tab. A.2 of A.1.

$$r_1 = \frac{k_{1,0}C_{\mathrm{nC12en}}C_{\mathrm{H2}}C_{\mathrm{CO}}}{1 + K_{1,1}C_{\mathrm{nC12en}} + K_{1,2}C_{\mathrm{nC13al}} + K_{1,3}C_{\mathrm{H2}}} \tag{4.3}$$

$$r_2 = \frac{k_{2,0}\left(C_{\mathrm{nC12en}} - \frac{C_{\mathrm{iC12en}}}{K_{p,2}}\right)}{1 + K_{2,1}C_{\mathrm{nC12en}} + K_{2,2}C_{\mathrm{iC12en}}} \tag{4.4}$$

$$r_3 = \frac{k_{3,0}\left(C_{\mathrm{nC12en}}C_{\mathrm{H2}} - \frac{C_{\mathrm{nC12an}}}{K_{p,3}}\right)}{1 + K_{3,1}C_{\mathrm{nC12en}} + K_{3,2}C_{\mathrm{nC12an}} + K_{3,3}C_{\mathrm{H2}}} \tag{4.5}$$

$$r_4 = k_{4,0}C_{\mathrm{iC12en}}C_{\mathrm{H2}} \tag{4.6}$$

$$r_5 = k_{5,0}C_{\mathrm{iC12en}}C_{\mathrm{H2}}C_{\mathrm{CO}} \tag{4.7}$$

$$k_{j,0} = k_j^0 \exp\left(\frac{-E_{A,j}}{R}\left(\frac{1}{T} - \frac{1}{378.15}\right)\right) \qquad , j \in \mathrm{RCT} \tag{4.8}$$

$$c_{cat} = \frac{C_{\mathrm{cat,tot}}}{1 + K_{\mathrm{cat,1}}C_{\mathrm{CO}} + K_{\mathrm{cat,2}}\frac{C_{\mathrm{CO}}}{C_{\mathrm{H2}}}} \tag{4.9}$$

From Eqs. (4.4)–(4.5) it can be seen that the isomerization of 1-dodecene (r_2) and the hydrogenation of 1-dodecene (r_3) are both reversible reactions. The respective equilibrium constants were derived from correlations for the Gibbs energy of formation obtained from [68] (parameters are given in the Appendix (Tab. A.3)).

$$K_{p,j} = \exp\left(\frac{-\Delta G_j}{RT}\right) \qquad\qquad , j \in \{2, 3\} \qquad\qquad (4.10)$$

$$\Delta G_j = a_{0,j} + a_{1,j}T + a_{2,j}T^2 \qquad\qquad (4.11)$$

According to the validity of the reaction kinetics the bounds for the reactor optimization are set to:

$$1\text{MPa} \leq P \leq 2\text{MPa} \qquad\qquad (4.12)$$

$$368.15\text{K} \leq T \leq 388.15\text{K} \qquad\qquad (4.13)$$

4.2. Experimental Validation of Kinetic Model

The main requirement for the application of model based optimization techniques are predictive kinetic models. In this section the reaction kinetics of Kiedorf et al. [13], which was introduced in the last chapter, is validated experimentally for various operation modes of a stirred tank reactor, such as batch, semibatch, and perturbed batch operation. It turns out that the original kinetic model has to be refined in order to yield reliable predictions which cover a wide range of physical conditions and operation modes.

Finally, using the refined semibatch reactor model optimal temperature and pressure profiles over time are calculated by means of dynamic optimization. This predicted optimal reaction route is then validated in a real semibatch reactor experiment.

4.2.1. Optimal Control Problem

For the calculation of the optimal reaction route a mathematical model of a stirred tank reactor with gas dosing for semibatch operation is used. The model considers a gas phase (Eq. (4.15)) and a liquid phase (Eq. (4.14)) which are assumed to be ideally mixed. The gas phase can be controlled via dosing fluxes j_i^{gas}, which indirectly affect the concentrations of the gaseous components in the liquid phase via a mass transfer term given by Eq. (4.16). The $(k_L a)_i$ values are obtained experimentally in the non-reactive system without catalyst and are given in Tab. A.1. It is assumed that liquid

and gas volume are constant during the reaction.

$$\dot{C}_{liq,i} = j_i^{\text{GL}} + C_{cat}M_{cat} \sum_{j \in RCT} (v_{j,i}r_j) \qquad , i \in \text{COM} \qquad (4.14)$$

$$\dot{p}_i = j_i^{\text{gas}} - \frac{V_{\text{liq}}}{V_{\text{gas}}} \cdot R \cdot T \cdot j_i^{\text{GL}} \qquad , i \in GAS \qquad (4.15)$$

$$j_i^{\text{GL}} = \begin{cases} (k_L a)_i \left(C_i^* - C_{liq,i} \right) & , i \in \text{GAS} \\ 0 & , i \in \text{COM} \setminus \text{GAS} \end{cases} \qquad (4.16)$$

The general optimization problem OP is written as a nonlinear program. It consists of the objective function Obj, scalar and distributed control variables Ψ and $U(t)$, equality, and inequality constraints. The objective function Obj is the maximization of the selectivity to n-tridecanal S_{nC13al} with respect to 1-dodecene. The set of scalar control variables Ψ contains the initial ratio of 1-dodecene to total dodecene Φ, and the initial partial pressures in the gas phase $p_{\text{H2}}(t_0)$ and $p_{\text{CO}}(t_0)$. Temperature $T(t)$, and gas dosing fluxes $j_{\text{H2}}^{gas}(t)$ and $j_{\text{CO}}^{gas}(t)$ are considered as distributed control variables $U(t)$.

$$\text{Obj} = \max_{U(t),\Psi} S_{\text{nC13al}} \qquad (\text{OP})$$

$$U(t) = T(t), j_{\text{H2}}^{gas}(t), j_{\text{CO}}^{gas}(t)$$

$$\Psi = \Phi, p_{\text{H2}}(t_0), p_{\text{CO}}(t_0)$$

s.t.	Mass balances:	Eqs. (4.14)–(4.15)
	GL mass transfer:	Eqs. (4.16)
	Reaction kinetics:	Eqs. (4.3)–(4.11)
	Gas solubilities:	Eqs. (4.2)–(4.1)
	Bounds:	$p \in [0, 20]$ bar
		$T \in [95, 115]\,^{\circ}\text{C}$
	Conversion:	$X = 1 - \frac{n_{\text{nC12en}}(t_f)}{n_{\text{nC12en}}(t_0)}$
	Selectivity:	$S = \frac{n_{\text{nC13al}}(t_f) - n_{\text{nC13al}}(t_0)}{X \cdot n_{\text{nC12en}}(t_0)}$
	Initial conditions:	$n_{i,\text{liq}} = 0, \ i \in \text{COM} \setminus \{\text{nC12en, iC12en}\}$
		$n_{\text{nC12en}}(t_0) + n_{\text{iC12en}}(t_0) = n_{\text{nC12en,ref}} = 0.85\text{mol}$
		$\Phi = \frac{n_{\text{nC12en}}(t_0)}{n_{\text{nC12en,ref}}}$
	Recycle constraints:	$n_{\text{iC12en,liq}}(t_0) \leq n_{\text{iC12en,liq}}(t_f)$
		$n_{\text{nC12en,liq}}(t_0) \geq n_{\text{nC12en,liq}}(t_f)$
	Scenario constraints:	sgIC:$p_{\text{H2}}(t_0) = p_{\text{CO}}(t_0)$
		sgJ:$j_{\text{H2}}(t) = j_{\text{CO}}(t) = j_{\text{sg}}(t)$
		optT:$T(t) = T = \text{const}$
		noRc:$\Phi = 1$

With increasing degree of freedom the objective function value will of course increase, however, the feasibility of the practical realization of the obtained control profiles usually decreases. In order to investigate the relevance of the different control variables and their interaction different scenarios with varying degree of freedom are investigated and defined as scenario constraints in OP. The following scenarios are considered:

Initial condition of the gas phase (sgIC or optIC) In this scenario the initial partial pressures in the gas phase can either be optimized independently (optIC) or their ratio is fixed to syngas (1:1) condition (sgIC).

Gas dosing flux (sgJ or optJ) In this scenario the dosing fluxes into the gas phase can either be optimized individually (optJ) or their ratio is fixed to syngas (1:1) condition (sgJ).

Temperature profile (optT or dynT) This constraint defines if the temperature can be optimized as profile (dynT) or as optimal constant temperature (optT).

Recycle (Rc or noRc) This constraint defines if the initial dodecene ratio can be optimized, obeying the recycle constraints, or if only 1-dodecene is used as reactant. The recycle constraints make sure that the initially added iso-dodecene is ultimately generated from 1-dodecene and not from an additional feedstock.

4.2.2. Semibatch Reactor Model

While the control variables in the optimization problem are the molar fluxes j_{H2}^{gas} and j_{CO}^{gas}, leading to optimal partial pressure profiles in time, predefined profiles of molar fluxes cannot be confidently realized in the semibatch reactor. Instead, profiles of total pressure can be realized accurately via the pressure control unit (RC-press). However, since the initial conditions of the gas phase can be realized individually, this control turns out to be sufficient to realize the predicted optimal partial pressure profiles (refer to Section 4.2.5), hence only dosing of syngas (1:1) j_{sg}^{gas} is considered in the model. In order to account for the constraint on the gas dosing flux the model equations Eqs. (4.14)-(4.16) are extended about the syngas condition Eq. (4.17) and the ODE of the total pressure (Eq. (4.18)) involving the pressure control term Eq. (4.19).

Regarding temperature, the temperature control unit of the reactor is able to realize profiles of the reactor temperature directly without need for predefined cooling or heating temperature profiles. Furthermore, within the considered temperature range, all temperature profiles are technically attainable without limitation, hence no energy balance and no temperature controller dynamics need to be considered in the model.

$$\dot{j}_i^{gas} = 0.5 \cdot j_{sg}^{\text{gas}} \qquad\qquad , i \in \text{GAS} \qquad (4.17)$$

$$\dot{p}_{\text{total}} = j_{sg}^{\text{gas}} - \frac{V_{\text{liq}}}{V_{\text{gas}}} \cdot R \cdot T \cdot \sum_{i \in \text{GAS}} j_i^{\text{GL}} \qquad\qquad (4.18)$$

$$j_{sg}^{\text{gas}} = K_{\text{control}} \cdot (p_{\text{control}}(t) - p_{\text{total}}) \qquad\qquad (4.19)$$

4.2.3. Validation in Different Operation Modes

In order to validate the kinetic parameters in the RC1 autoclave in various operation modes, several experiments have been performed. Fig. 4.2 shows a selection of dynamic concentration and corresponding temperature and pressure profiles over time for batch, semibatch, and perturbed batch operation.

Batch operation In batch operation (Fig. 4.2(a) and Fig. 4.2(b)) no dosing of syngas is performed as the reaction goes on. Initially, no gas is solved in the liquid phase and the initial total pressure in the gas phase is set to 20 bar with H_2 to CO ratio of 1. The mass transfer into the liquid phase is rapid and the solved gas is quickly consumed via hydroformylation reaction. Due to the missing gas dosing the pressure drops quite fast, yielding a depletion of H_2, thus reducing the rate of the hydroformylation reaction. Since the CO concentration in the liquid is low, there is no significant inhibition of the isomerization reaction, which lowers the selectivity to n-tridecanal. Since the kinetic parameters in Kiedorf et al. [13] have been entirely obtained from batch experiments the batch case can be predicted quite accurately.

Semibatch operation In semibatch operation (Fig. 4.2(c) and Fig. 4.2(d)) the same initial conditions as in the batch case are used, but the depletion of gas is avioded by dosing of syngas ($j_{H2}^{gas} = j_{CO}^{gas} = j_{sg}^{gas}$), keeping a constant total pressure of 20 bar. In this way high concentrations of gas in the liquid phase are maintained over the entire reaction time. The experimental data shows, that the isomerization is significantly reduced compared to the batch operation, which can be explained by the high CO concentration in the liquid phase. The model prediction using the original parameters

(a) Batch, 105^oC

(b) Batch, 105^oC

(c) Semibatch, 105^oC

(d) Semibatch, 105^oC

(e) Perturbed batch
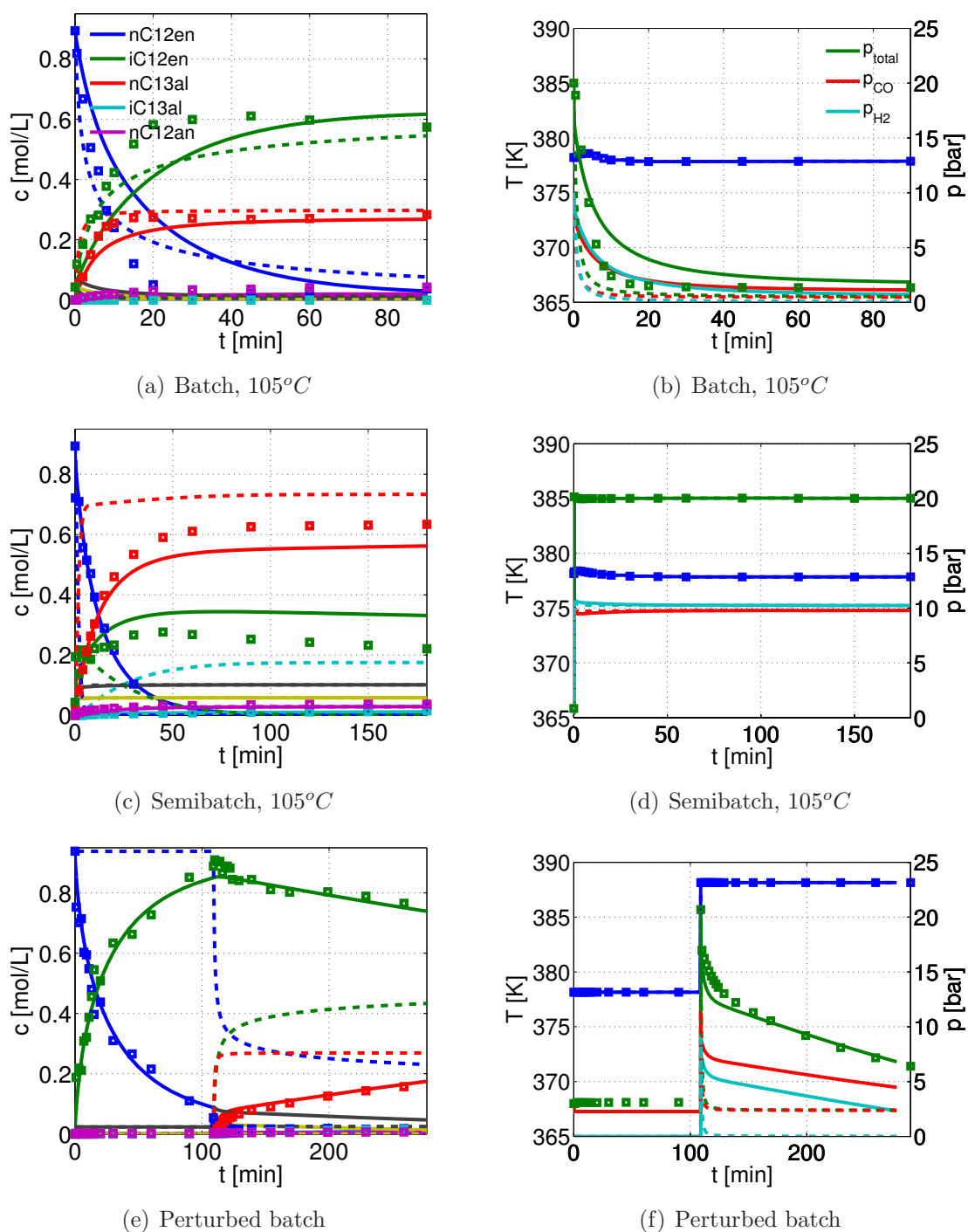
(f) Perturbed batch

Figure 4.2.: Reference experiments for model validation. a)–b): Batch operation, $p_{H2}^0 = p_{CO}^0$, $p_{total}^0 = 20 bar$, $T = 105^oC$. c)–d): Semibatch operation, $p_{H2}^0 = p_{CO}^0$, $j_{H2} = j_{CO}$, $p_{total} = 20 bar$, $T = 105^oC$. e)–f): Perturbed batch operation with initial isomerization at $p_{CO}^0 = 3 bar$ and $T = 105^oC$, and subsequent hydroformylation via perturbation with syngas (1:1) up to $p_{tot,pert} = 20 bar$, $T = 115^oC$. Symbols: experimental data. Dashed lines: model prediction with original parameters of Kiedorf et al. [13]. Solid lines: model prediction with refined parameters.

overestimates the dynamics of the reaction system significantly. Also the production of iso-aldehydes is overestimated. The reason for the fast dynamics can be found in the nature of the batch experiments used for the estimation of the original parameters. Since in the batch experiments a state of high CO concentration in the liquid phase is only reached for a very short time at the beginning of the experiment, there is a lag of information about the influence of high CO concentrations on the reaction kinetics. Particularly, since all reactions are inhibited, the inhibition constants in Eq. 4.9 should be refined. The high confidence interval of $K_{cat,1}$ in Kiedorf et al. [13] (refer to Tab. A.5) also results from the missing information about the influence of CO within batch operation. The overestimation of the iso-aldehyde formation can be explained with the same arguments. Since during the investigation of the iso-aldehyde formation the situation with high iso-dodecene concentration and high CO concentration never occurred, the rate of iso aldehyde formation was overestimated.

Perturbed batch operation The perturbed batch (Fig. 4.2(e) and Fig. 4.2(f)) represents two subsequent batch experiments in series to validate the model regarding its CO sensitivity. During a first isomerization phase where only CO atmosphere at 3 bar is applied, the 1-dodecene is almost totally converted into iso-dodecene. The subsequent hydroformylation phase is initiated via a perturbation with syngas (1:1) up to 20 bar. At the same time the temperature is increased from 95^oC to 115^oC to enhance the rate of reisomerization. Using the original parameters the model predicts a constant 1-dodecene concentration until the hydroformylation starts. According to Eq. 4.9 the missing hydrogen leads to a total deactivation of the active catalyst, hence, the initial isomerization phase cannot be reproduced.

4.2.4. Refinement of Kinetic Parameters

In this work the kinetic model will be used to calculate the optimal reaction route considering a large range of experimental conditions. Hence, the kinetic parameters are fitted to semibatch experiments in a first step, to cover high gas concentrations in the liquid phase as well. The model prediction using the refined parameters is also shown in Fig. 4.2 represented by solid lines. As illustrated, using the refined parameters leads to a satisfying reproduction of all scenarios. Within the parameter estimation only the frequency factors $k_{0,j}$, and the inhibition constants of Eq. 4.9 have been modified. In order to cover the perturbed batch conditions it was necessary to introduce an exponent for the CO concentration in Eq. 4.9 indicating a more complex influence of CO on the formation of catalytic resting state. During the fitting the original parameter $K_{cat,2}$ was estimated to zero, yielding no effect of hydrogen on the
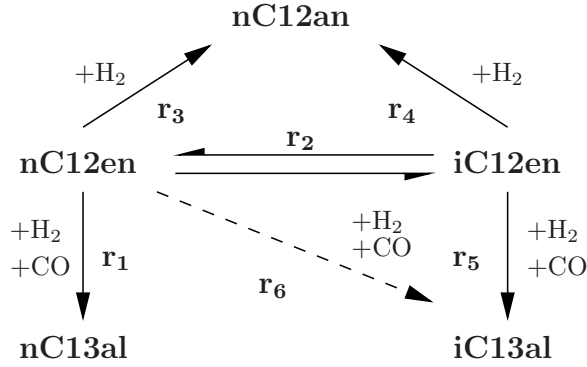
Figure 4.3.: Refined reaction network of the rhodium/biphephos catalyzed hydroformylation. nC12en = 1-dodecene, iC12en = iso-dodecenes, nC12an = n-dodecane, nC13al = n-tridecanal, iC13al = iso-aldehydes. Reaction r_6 was added within model extension in this work.

amount of active catalyst under the investigated conditions, which is in agreement with the observations of van Leeuwen [7].

$$C_{\text{cat}} = \frac{C_{\text{cat,tot}}}{1 + K_{\text{cat,1}} C_{\text{CO}}^{K_{\text{cat,3}}}} \tag{4.20}$$

Additionally, a new reaction (r_6, see Fig. 4.1) had to be added to accurately reproduce the formation of iso-aldehyde during semibatch operation.

$$r_6 = k_{6,0}(T) C_{\text{nC12en}} C_{\text{H2}} C_{\text{CO}} \tag{4.21}$$

The refined parameters are listed in Tab. A.4, whereas the original parameters can be found in Kiedorf et al. [13]. It should be emphasized that the confidence intervals of the refined parameters are much smaller than those of the original parameters (refer to Tab. A.5), supporting the made assumptions, such as the reaction order of CO and the additional direct formation of iso-aldehyde from 1-dodecene.

4.2.5. Selectivity Optimization: Scenario Screening

In order to identify a reasonable set of control variables various optimization scenarios with different degree of freedom have been screened. Main control variables are the initial partial pressures of H_2 and CO, dosing fluxes of H_2 and CO over time, and the temperature profile. These control variables are subject to the scenario constraints defined in the optimal control problem (OP)

Furthermore, the initial ratio of 1-dodecene to iso-dodecene was set as degree of

(a) Without recycle   (b) With recycle
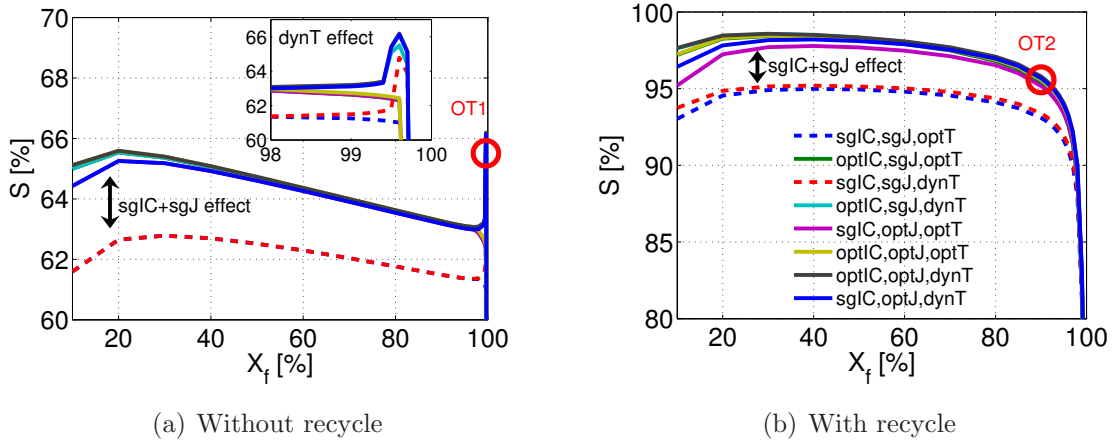
Figure 4.4.: Maximum attainable selectivity over conversion for various control scenarios with different degree of freedom. Red circle: Chosen optimal control for experimental validation OT1 (a), OT2 (b).

freedom, representing the possibility of recycling of iso-dodecene after the reaction. In order to allow only ratios which correspond to feasible recycle compositions, such that the initial amount of iso-dodecene has to be lower or equal to the final amount, additional constraints (recycle constraints) were included into the optimization problem (OP).

In Fig. 4.4 all investigated scenarios are illustrated and in particular a comparison between recycle (Fig. 4.4(b)) and non-recycle conditions (Fig. 4.4(a)) was made. It can be seen that the recycling of iso-dodecene, represented by optimal initial 1-dodecene to iso-dodecene ratios Φ yields a significant increase in selectivity of approximately 30% over the entire range of conversion. As the conversion approaches 1 there is no iso-dodecene left to recycle, hence the solutions of both cases converge. However, since in some cases recycling is not possible, and due to validation purposes, both cases are further investigated.

The lines of the different scenarios in Fig. 4.4 can be grouped into two groups of similar behavior. The classification is possible in both cases, with and without recycle condition. The lower branch represents scenarios with syngas initial conditions (sgIC), except when individual gas dosing (optJ) is allowed. Due to individual gas dosing the non-optimal initial conditions in the gas phase can be sufficiently compensated. It can be concluded that an optimal gas phase composition leads to an increase in selectivity of about 2%, hence should be considered as control strategy.

A second classification can be made with respect to a dynamic or isothermal tem-

perature profile (dynT or optT). Whenever allowing a dynamic temperature profile in the scenarios without recycle, a significant increase in selectivity can be observed at high conversions ($X \geq 0.97$). The reason for that is the reisomerization which becomes feasible at high conversions, hence low 1-dodecene concentrations. While under conditions with high 1-dodecene concentrations low temperatures are optimal, high temperatures are more beneficial in order to accelerate the slow reisomerization and subsequent hydroformylation step.

For the further validation of the optimal reaction route two scenarios are selected, one for the case with recycle, and one for the case without recycle. In case without recycle the highest selectivity is obtained at full conversion, thus this point is taken for experimental validation. In contrast, in the scenario with recycle the selectivity decreases with increasing conversion. In order to chose an advantageous point with respect to the entire process, a point at high conversion and high selectivity is chosen. Another advantage of choosing points at high conversion is that the experimental errors are much higher for low conversions due to the short reaction time.

Optimal route without recycle (OT1) In case of no recycling a scenario at high conversion ($X = 0.996$, refer to red circle in Fig. 4.4(a)) with optimal initial condition in the gas phase (optIC), syngas dosing (sgJ) and dynamic temperature profile (dynT) is chosen. Since the individual dosing of H_2 and CO is more difficult to realize than the setup of an optimal initial condition, dosing of syngas is preferred.

Optimal route with recycle (OT2) In case of recycling, a scenario at lower conversion ($X = 0.90$, refer to red circle in Fig. 4.4(b)) with optimal initial conditions in the gas phase (optIC), with syngas dosing (sgJ), isothermal temperature profile, and optimal initial ratio of 1-dodecene to iso-dodecene Φ is chosen.

4.2.6. Optimal Reaction Route

Predicted Optimal Control

Optimal route without recycle (OT1) The optimal control profiles of OT1 are illustrated in Fig. 4.5(a). Starting with optimal initial gas phase conditions, syngas dosing (1:1) is applied to maintain a constant total pressure of 20 bar. The temperature is kept at 95^oC up to 12 min, followed by a constant temperature increase up to 115^oC over 30 min. The now reached reaction conditions are maintained up to 180

(a) OT1: Without recycle   (b) OT2: With recycle
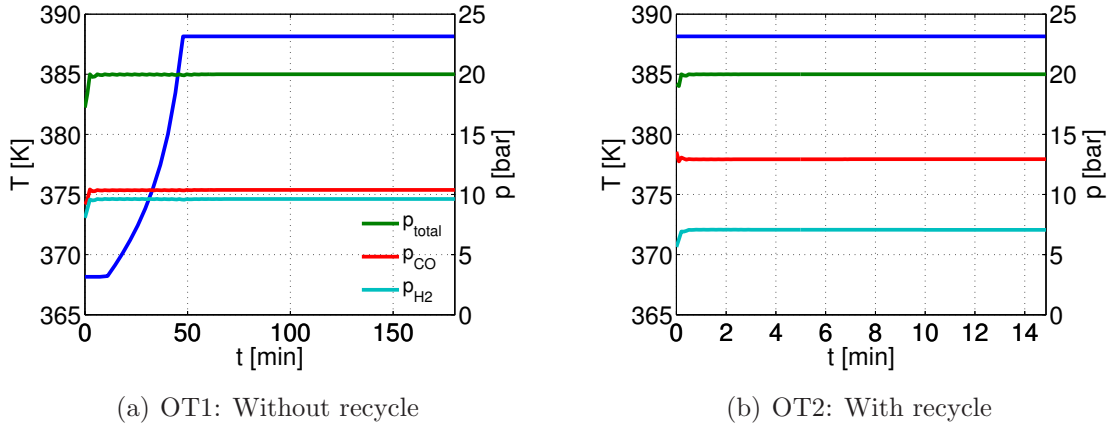
Figure 4.5.: Predicted optimal control profiles.

min to reach a conversion of $X = 0.996$.

Optimal route with recycle (OT2)   The optimal control profiles of OT2 are illustrated in Fig. 4.5(b). According to the chosen final conversion of $X_f = 0.9$ the optimal initial ratio of 1-dodecene to iso-dodecene is 1:4.7, corresponding to $\Phi = 0.1765$. Under these conditions constant control profiles are sufficient to approximate the optimal control. The optimal temperature and total pressure is at the upper bound of $T = 115^oC$ and $p_{total} = 20bar$, respectively. The optimal initial condition in the gas phase is $p_{H2}^0 = 5.6bar$ and $p_{CO}^0 = 14.4bar$, which leads to nearly constant partial pressure profiles over the entire reaction time applying syngas (1:1) dosing. Since the chosen final conversion is $X_f = 0.9$ the predicted reaction time is only 15 min.

Validation of Optimal Control

Optimal route without recycle (OT1)   In order to set the desired optimal initial condition in the gas phase, an excess of CO is needed. Since the optimal syngas composition is not directly available it has to be composed stage-wise. Firstly, CO is introduced into the reactor until the excess pressure of CO of $p_{CO} = 2.34bar$ is reached. Afterwards, syngas (1:1) is dosed until the total pressure of $p_{total} = 20bar$ is reached. 11 min after the initial condition of the gas phase is set, the temperature is increased as ramp profile ($0.54\ K/min$) until it reaches the maximum temperature of $T = 115^oC$ after 50 min. Fig. 4.6(b) compares the predicted control profiles with the actually realized profiles. The experimental realization of both, temperature and pressure profile can be achieved very accurate. Regarding the concentrations in the liquid phase (Fig. 4.6(a)), the prediction and the simulation using the actual control

(a) Without recycle

(b) Without recycle

(c) With recycle

(d) With recycle
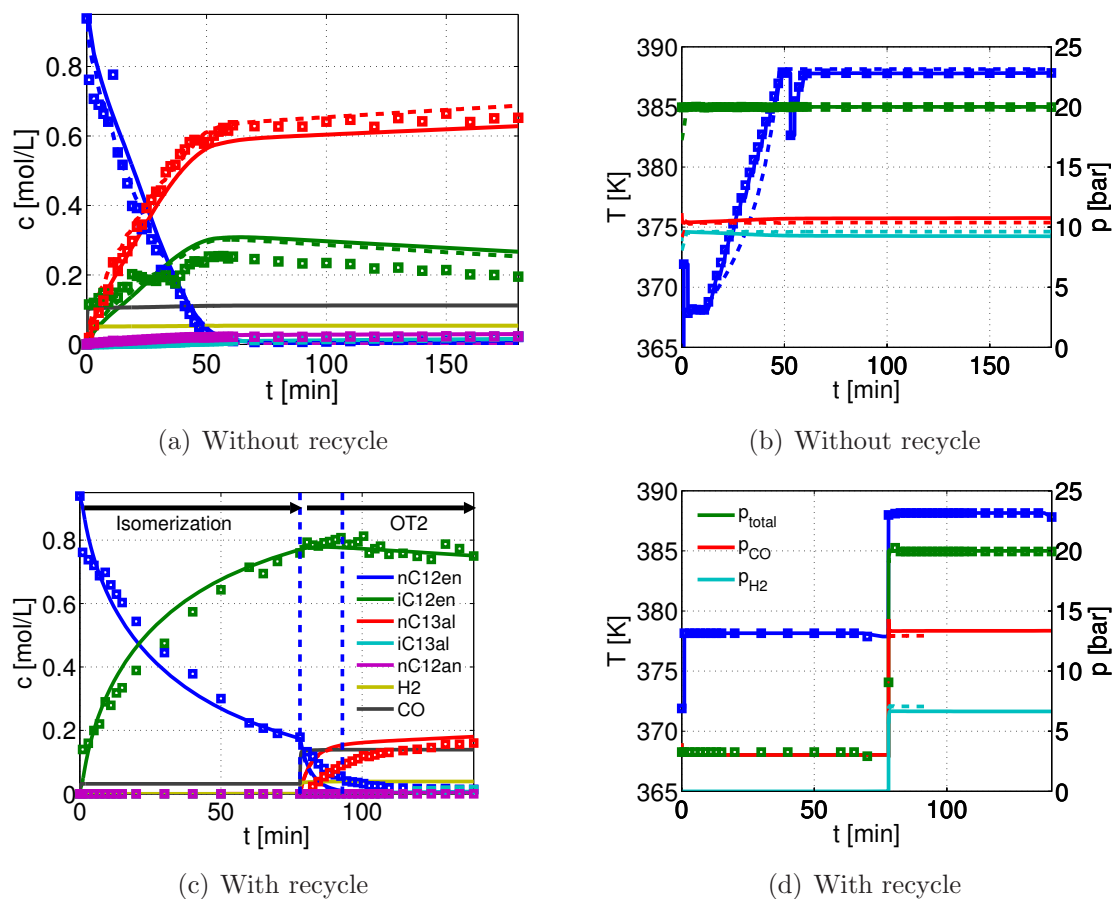
Figure 4.6.: Experimental validation of selectivity optimal reaction routes with corresponding control profiles. Solid lines: Simulation result applying the actual experimental temperature profile and pressure control model. Dashed lines: Simulation applying the predicted control profiles.

agree well with the experimental data, although the prediction yields a higher amount of linear aldehyde, which may be caused by the small deviation of the temperature profile or deviation in the initial conditions. The concentration of iso-dodecene is overestimated.

Optimal route with recycle (OT2)   For the realization of the second control trajectory optimal initial conditions of both, gas and liquid phase have to be adjusted. In order to generate the optimal initial dodecene ratio, an isomerization step is performed prior to the actual control experiment. Since the isomerization can be performed under CO atmosphere, the excess pressure of CO ($\Delta p_{\mathrm{CO}} = 8.8 bar$) and the initial dodecene ratio ($\Phi = 0.1765$) can be realized conveniently in one step. However, since it was already validated that the isomerization can be predicted accurately at $p_{\mathrm{CO}} = 3 bar$, this pressure was chosen for the isomerization step. In this way the optimal initial dodecene ratio can be achieved more reliably. Hence, the isomerization is performed at a lower pressure of $3 bar$, followed by a perturbation with CO up to $p_{\mathrm{CO}} = 8.8 bar$ and a subsequent dosing of syngas (1:1) up to $p_{\mathrm{total}} = 20 bar$. Regarding the temperature, again, the isomerization step is performed at $T = 105^o C$, since this temperature was used for validation already. At the end of the isomerization the temperature was increased to the desired optimal temperature of $T = 115^o C$. As illustrated in Fig. 4.6(d), predicted and actually realized control profiles match with the experimental data. Fig. 4.6(c) shows that the initial dodecene ratio could be achieved very precisely by using the isomerization as pretreatment.

The predicted optimal trajectory actually requires only 15 min, but the experiment was performed for 60 min to gain more data points. Apparently, the dynamics in the actual time interval is over-predicted and the real system behaves much slower. The model was not validated under such high CO pressures so far, and the inhibition by CO appears to be under-predicted. However, despite the speed of reaction, the trend in selectivity behavior is reliable and indeed, much higher selectivities are gained applying the proposed OT2 control (refer to Fig. 4.7).

Although the initial dodecene ratio matches the optimal value, the experimental data indicate that the isomerization reaction is actually not totally in equilibrium, since reisomerization takes place. However, the observed reisomerization is likely to be within the experimental error range.
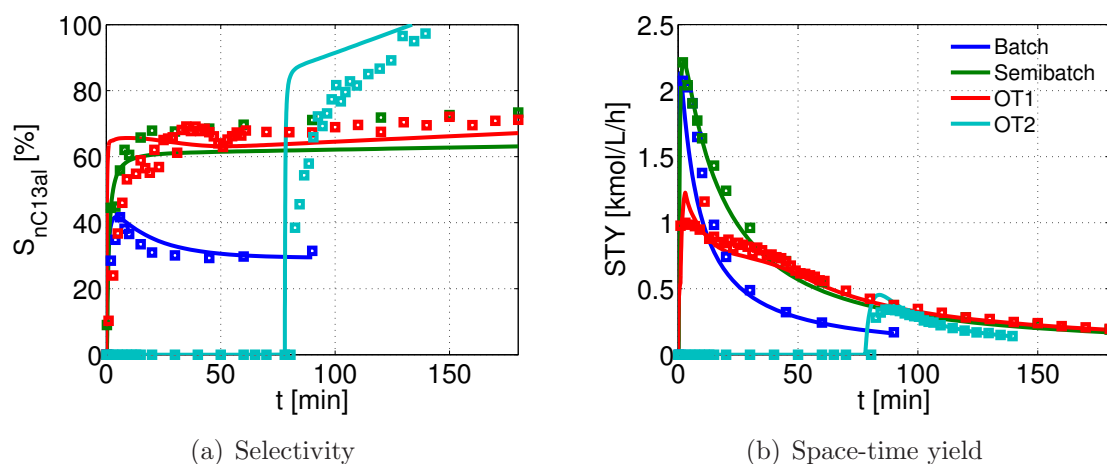
Figure 4.7.: Dynamic behavior of selectivity S and space-time yield STY. Comparison of different operation modes. Solid lines: Model prediction. Symbols: Experimental data.

4.2.7. Comparison of Operation Modes

In Fig. 4.7 all discussed scenarios are compared with respect to their dynamic selectivity and resulting space-time yield behavior. Due to the fast depletion of CO in the liquid phase during batch operation, the isomerization is the dominating reaction in this mode. The selectivity behavior appears to be proportional to the behavior of the CO concentration in the liquid phase, which increases initially due to mass transfer from the gas into the liquid phase, followed by consumption due to reaction. Hence, the inhibition of the isomerization and the selectivity shows a maximum as well. The respective STY shows a high maximum value at short reaction times which decreases as the reaction goes on.

Applying semibatch operation the gas depletion can be avoided, hence high CO concentrations can be maintained, resulting in selectivities approximately twice as much as obtained in the batch case. While the STY in semibatch operation starts at similar values as the batch case, it decreases slower with higher reaction times, indicating a more efficient reaction.

In contrast to the model prediction in case of OT1, which shows an increased selectivity applying an optimal CO to H_2 ratio, compared to the semibatch case, the experimental data show no difference between semibatch and OT1 with respect to selectivity. However, there is a difference regarding the STY. The STY of OT1 starts with only half of the value of the semibatch case, but towards higher reaction times

both scenarios converge to the same STY.

Since the isomerization is the dominating side reaction, the selectivity can be further increased by choosing an optimal initial dodecene ratio. In this way the isomerization reaction is near to equilibrium and the hydroformylation of 1-dodecene is dominating. The expected behavior in case of OT2 can be successfully validated, although the selectivity is over-predicted, while the STY shows only a small deviation. In case of OT2 the x-axis has to be shifted to the left about the time of the isomerization phase in order to directly compare the four cases. When doing so, the space time yield of OT2 appears to be the lowest, caused by the much lower 1-dodecene concentrations in the reactor.

When evaluating the selectivity care has to be taken in order not to mix up the phase where no net production of iso-dodecene occurs (up to 110 min) and the following reisomerization. During the reisomerization phase ($t \geq 110$ min) the linear aldehyde is partially produced indirectly from iso-dodecene via reisomerization, hence the selectivity cannot be based on 1-dodecene anymore. However, for the short time interval without net production of iso-dodecene (78 min $\leq t \leq 110$ min) n-aldehyde is only produced from 1-dodecene.

4.3. Stand-Alone Reactor

The validated and refined reaction kinetics are now used within a general dynamic model which allows the prediction of an optimal reaction route over time without technology related limitations on the material and heat fluxes. Hence, the gas phase is now considered as ideal service phase, thus component fluxes into the liquid phase can be optimized directly without the limit of a gas phase capacity. The gas solubility and the feasible pressure range of the kinetic parameters are the only limitations on the material flux. Since the heat flux is unlimited any temperature can be realized, hence no energy balance is considered, but the temperature is a degree of freedom. As in case of pressure, temperature is also limited to be within the feasible range of kinetic parameters.

Since the influence of back-mixing is not included in the just mentioned EPF concept, it is investigated by evaluating a cascade model of CSTRs in series, which are subject to optimal dosing and temperature. As known from theory, the ideal CSTR represents the extreme case of total back-mixing, while plug flow, as assumed in the EPF model, represents totally segregated flow. In a cascade of CSTRs the amount of back-mixing

increases with the number of tanks until plug flow behavior is approached when the tank number approaches infinity. Practically, however, the tank number necessary to approach plug flow is in the range of 10 to 40 tanks.

Both models are further introduced in the next sections.

4.3.1. Kinetic Model

Fluid Element

The optimal reaction route can be visualized by following a fluid element entering the reactor at time t_0 and leaving it at time t_f. During the journey the state variables of the fluid element are optimally adjusted in time by external material and energy fluxes. Besides external fluxes there are also internal fluxes influencing the state variables, such as reaction and diffusion flux. Besides scaling by the catalyst concentration, the reaction flux can only be manipulated on a lower level, namely catalyst design or solvent design. This is not an option in this example. The diffusion flux can be neglected when the fluid element is small enough that it can be considered as ideally mixed. The governing equations of such a fluid element are the following.

$$\frac{\mathrm{d}n_{i,\mathrm{liq}}}{\mathrm{d}t} = j_i + c_{\mathrm{cat}} V_{\mathrm{liq}} M_{\mathrm{cat}} \sum_{j \in \mathrm{RCT}} v_{i,j} r_j \tag{4.22}$$

$$c_{\mathrm{liq},i} = \frac{n_{\mathrm{liq},i}}{V_{\mathrm{liq}}} \tag{4.23}$$

$$V_{\mathrm{liq}} = \sum_{i \in \mathrm{COM}} \frac{n_{i,\mathrm{liq}} M_i}{\rho_i} \tag{4.24}$$

CSTR Cascade

As known from application for certain reactions back-mixing may yield a better reactor performance than segregated flow. Otherwise no stirred tank reactors would be in use. This is especially the case when low reactant concentrations are beneficial in order to reduce unwanted side reactions. Since low reactant concentrations lead to high reaction times it would require extremely long tubular reactor with constant reactant dosing over its length. However, in principle the fluid element model will yield the optimal reaction route, but during the interpretation of the flux profiles back-mixing has to be considered as possible approximation. Watching the fluid element inside the ideal CSTR we will realize the same dosing profile over time as predicted

Table 4.1.: Solvent composition of kinetic experiments in the open-loop optimization and in reactor outlet of the closed-loop optimization.

Variable	Value	Unit
ω_{nC12en}	0.2	g_{nC12en}/g
ω_{C10an}	0.48	g_{C10an}/g
ω_{DMF}	0.32	g_{DMF}/g
x_{cat}	10^{-4}	$mol_{\text{cat}}/mol_{\text{nC12en}}$

by the optimal flux profiles. However, a drawback of any real CSTR is the unfavorable residence time distribution. The time course of different fluid elements is not synchronized because their tracks cross randomly in time, which is not possible for plug flow. For this reason the CSTR is actually never the optimal reactor, but since real processes never work ideally the overall process performance - in terms of costs, space or handling - of a CSTR could be superior to the PFR.

In order to validate the optimal reaction route obtained from the fluid element model and to investigate the effect of back-mixing a cascade model of ideal CSTRs is implemented. Each CSTR represents an ideally back-mixed compartment with optimal temperature and dosing fluxes. Each tank operates at outlet conditions. Increasing the number of tanks in the cascade, means reducing the amount of back-mixing and approaching segregated flow. Hence, the higher the number of tanks, the closer the solution of the fluid element should be approached. The design equations of the cascade model are the following.

$$\dot{n}_{i,\text{out,liq},s} = \dot{n}_{i,\text{in,liq},s} + j_{i,s} + c_{\text{cat},s} V_{\text{liq},s} M_{\text{cat}} \sum_{j \in \text{RCT}} v_{i,j} r_{j,s} \tag{4.25}$$

$$c_{\text{liq},i,s} = \frac{\dot{n}_{\text{out,liq},i,s}}{\dot{V}_{\text{out,liq},s}} \tag{4.26}$$

$$\dot{V}_{\text{out,liq},s} = \sum_{i \in \text{COM}} \frac{\dot{n}_{i,\text{out,liq},s} M_i}{\rho_{i,s}} \tag{4.27}$$

$$\dot{n}_{i,\text{in,liq},s} = \dot{n}_{i,\text{out,liq},s-1} \tag{4.28}$$

$$V_s = V_{s-1} \tag{4.29}$$

As constraint the volume of each tank is the same but not fixed.
The solvent and catalyst ratios given in Tab. 4.1 are fixed in order to guarantee the validity of the reaction kinetics and the feasibility of the liquid-liquid phase split.

4.3.2. Optimization Problem

The optimization problem of the stand-alone reaction route differs from the previous chapter, as the equations for the gas phase and mass transfer are missing. Further, since the fluxes are unlimited the initial conditions of gas components are degrees of freedom. The total amount of 1-dodecene is fixed to 1 mole as arbitrarily chosen reference value. 1-Dodecene can be allocated as initial amount and distributed flux but the sum has to be the same.

Several candidates are possible as objective function, such as product selectivity (S), space-time yield (STY), n/iso-product ratio, conversion, or productivity. However, product selectivity and space-time yield are further investigated. As in the previous chapter different constraints on the fluxes, such as a fixed H_2 to CO ratio of the gas dosing flux (syngas condition) or a constant temperature profile are investigated in order to evaluate the potential of additional degree of freedom. Additionally, the influence of recycling is considered with the recycle condition. The full optimization problem is defined in the following.

$$\text{Obj}_\text{S} = \max_{U(t), \Psi} S_\text{nC13al} \qquad \text{(OP)}$$

$$U(t) = T(t), j_\text{nC12en}(t), j_\text{H2}(t), j_\text{CO}(t)$$

$$\Psi = \Phi, n_i(t_0)$$

s.t. Mass balances: EPF: Eqs. (4.22)–(4.24)
   CSTR: Eqs. (4.25)–(4.29)

Reaction kinetics: Eqs. (4.3)–(4.11)

Gas solubilities: Eqs. (4.2)–(4.1)

Bounds: $p \in [10, 20]\,\text{bar}$
   $T \in [95, 115]\,^\circ\text{C}$

Conversion: $X = 1 - \frac{n_\text{nC12en}(t_f)}{n_\text{nC12en,ref}}$

Selectivity: $S = \frac{n_\text{nC13al}(t_f) - n_\text{nC13al}(t_0)}{X \cdot n_\text{nC12en,ref}}$

STY: $STY = \frac{n_\text{nC13al}(t_f) - n_\text{nC13al}(t_0)}{\int_{t_0}^{t_f} V_\text{liq}(\tau)\text{d}\tau} \geq STY_\text{ref}$

Initial conditions: $n_\text{i,liq} = 0, \; i \in \text{COM} \setminus \{\text{nC12en}, \text{iC12en}, \text{H}_2, \text{CO}\}$
   $n_\text{nC12en}(t_0) + \int_{t_0}^{t_f} j_\text{nC12en}(\tau)\text{d}\tau = n_\text{nC12en,ref} = 1\text{mol}$

Recycle constraints: $n_\text{iC12en,liq}(t_0) \leq \Phi \cdot n_\text{iC12en,liq}(t_f)$
   $n_\text{nC12en,liq}(t_0) \geq \Phi \cdot n_\text{nC12en,liq}(t_f)$

Scenario constraints: sgJ:$j_\text{H2}(t) = j_\text{CO}(t) = j_\text{sg}(t)$
   optT:$T(t) = T = \text{const}$
   noRc:$\Phi = 0$

(a) Selectivity (b) STY

(c) n/iso Ratio (d) Residence Time

Figure 4.8.: Comparison of different objective functions with recycle condition.

4.3.3. Choice of Objective

The first task in optimizing anything is the definition of the objective function in order to evaluate optimality. From a chemical engineering point of view, many objectives are possible which can be used to measure the performance of a reaction system. However, from an economic point of view there is only one objective, production costs. So we could immediately start to optimize production costs, after we set up all relevant cost models concerning the whole process. But before the process can be set up, the reaction behavior and the resulting performance should be understood. Reaction engineering objectives are perfectly suited to develop a deep understanding of the behavior of the reaction system, which is needed for the interpretation of the cost optimization. This is very important because an optimization of the complex process involving different cost models and prices represents a combination of various reaction engineering objectives. For the example system of hydroformylation the

objectives selectivity (max S), space-time yield (max STY), n/iso aldehyde ratio (max n/iso), and residence time (min t) are compared in the following. The solutions shown in Fig. 4.8 are corresponding to the optimization without flux constraints and with possible recycling, hence, allowing the highest degree of freedom. Each line in the figure corresponds to a certain objective function and the relation between different objectives can be concluded from the four figures.

Maximum Selectivity Fig. 4.8(a) shows the selectivity to n-aldehyde from 1-dodecene over conversion of 1-dodecene. The maximum selectivity is of course obtained from the selectivity maximization (blue). Obviously choosing another objective will lead to much lower selectivities of at least 35%. The STY maximization yields the highest selectivities below 60% conversion. Beyond 60% conversion a switch of reaction regime occurs, which leads to higher STY on the expense of selectivity. The n/iso maximization (red) yields the 3rd highest selectivity for low conversion and the 2nd best for high conversion. But the attained selectivity is still not desirable. The lowest selectivity is obtained by the minimization of reaction time. This objective will provide reaction conditions which facilitate the fastest overall reaction rate. Obviously, the main reaction is slower compared to at least one side reaction. So from the figure one can conclude that the three objectives STY, n/iso, and residence time are actually not suitable to yield sufficiently high selectivity.

Maximum Space-Time-Yield Fig. 4.8(b) shows the STY over conversion of 1-dodecene. Only two lines can be distinguished. The green line corresponds to the objective max STY, while the optimization of all other objectives obviously yields a reduction of STY until the conversion dependent lower bound on STY is reached. That means, that choosing an objective other than max STY will yield either higher reaction times or lower selectivities, or both. Looking at the line of max STY (green) the STY monotonously decreases with increasing conversion, but at a conversion of 60% a similar behavior occurs as already seen in Fig. 4.8(a). The additional STY is gained on costs of selectivity. The same behavior occurs in Fig. 4.8(d) (green line), where the reaction time decreases beyond 60% conversion. Since STY represents essentially the ratio of selectivity and reaction time, the reaction time seems to be the greater level in order to increase STY than selectivity. Hence, in the second reaction regime the selectivity gain is less than the gain in time reduction.

Maximum n/iso aldehyde ratio Fig. 4.8(c) shows the n/iso aldehyde ratio depending on conversion of 1-dodecene. Maximizing this ratio (red line) yields very high

64

values over a wide range of conversion. Beyond 95% conversion the ratio drops, but just down to 99%. The other objectives yield very similar n/iso ratios which are in the range of 99%. Remarkably, the max S curve shows the highest loss in n/iso ratio beyond 95% conversion; down to 95%. Concluding, any objective seems suitable for ensuring sufficiently high n/iso ratios, but maximizing n/iso ratio yields low selectivity and STY, hence, it is not recommended as objective which represents the process optimality.

Minimum reaction time   Fig. 4.8(d) shows the reaction time over conversion of 1-dodecene. The minimum reaction time is obtained by the corresponding objective, which, as discussed earlier, is a result of enhancement of at least one side reaction, but no product formation (Fig. 4.8(a)). The other objectives yield reaction times which are about one magnitude higher than the minimum reaction time. The highest reaction times are obtained from the objectives max S and max STY which are in the range of 1 min to 100 min. The kink in the max STY curve was explained earlier.

After the evaluation of the different objectives choosing selectivity seems to be the best approximation of the process demands. Although maximum selectivity inversely correlates with STY, but the other performance measures are in a feasible range. Hence, for the further optimization problems in this chapter selectivity is chosen as objective.

4.3.4. Screening of Intensification Options

(a) zero initial gas

(b) optimal initial gas
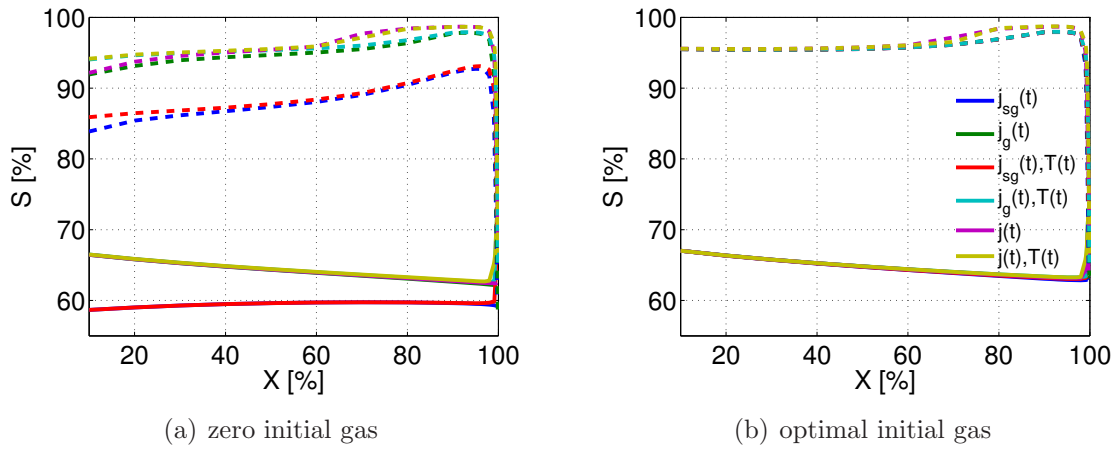
Figure 4.9.: Influence of initial concentration of gas components in liquid phase. Comparison of different intensification concepts as constraints on the control fluxes of the fluid element. Recycle condition (dashed), no recycle (solid).
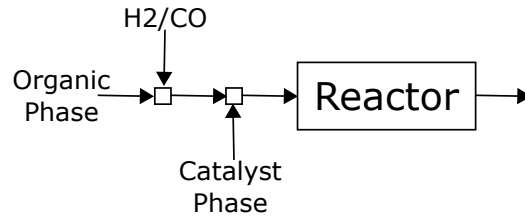
Figure 4.10.: Realization of optimal initial condition for H_2 and CO.

In order to identify the optimal reaction route it is important to screen different intensification options to evaluate the benefit of more or less degree of freedom. The objective function value improves with higher degree of freedom on the optimization parameters. However, so does the complexity of the control profiles and thus the technical realization. Hence, it is important to know the deviation from the optimal solution when less degree of freedom, hence, more easily realizable control fluxes are used.

In the concept of elementary process functions the initial conditions of reactants inside the fluid element is proposed to be a degree of freedom as the fluxes are. When dealing with multiphase systems, however, this should be carefully investigated, because it depends on which point in the history of the fluid element we start to control

it. According to the idea of dividing the production process into functional modules, the setup of the initial condition is actually the result of the functional module "mixing" upstream of the module "reaction". The end condition of the module "mixing" is defined by the optimal reaction route.

Fig. 4.9 illustrates that even if ideal fluxes without considering mass transfer are used, the choice of the initial concentration of gas in the liquid phase makes a big difference in the attainable objective function value. If the initial concentration of gas in the liquid is set to zero, as it is normally the case in gas-liquid reactions, then the attainable selectivity using syngas with a H2/CO ratio of 1 is about 10% lower than with an optimal H2/CO ratio. This, as explained in the previous chapter, is due to the fact that syngas is consumed equimolar by reaction, but the optimal gas concentrations in the liquid are not equal. That means, the equimolar dosing of gas is optimal, but the concentrations of H_2 and CO affect the reaction rates differently. When assuming that the initial condition is a degree of freedom one must consider that the setup of this initial condition is the result of fluxes and it is better to include this gas mixing process into the optimal reaction route. Otherwise one will observe the result of Fig. 4.9(b) and one will believe that there is no difference between the unconstrained flux $j_g(t)$ and the constrained flux $j_{sg}(t)$.

As the optimal adjustment of the initial condition of gas in the liquid phase is crucial for the reactor performance, the scheme illustrated in Fig. 4.10 is proposed for the feed pretreatment upstream of the reactor. Alternatively, the catalyst phase can be injected in a premixing segment of the reactor.

In the following it is assumed that the initial gas condition is realized according to the scheme shown in Fig. 4.10, thus, zero initial gas conditions are not considered further.

4.3.5. Optimal Reaction Route

Table 4.2.: Performance measures of different intensification options.

Trajectory	S [%]	X [%]	$\frac{n}{n+i}$ [-]	STY [$\frac{mol}{m^3h}$]	τ [min]	Potential [%]
noRc,j(t),T(t)	72.95	99.70	94.69	92	400	±0
Rc,jsg(t),T	97.92	93.00	98.45	272	15	+24.97
Rc,j(t),T	98.68	93.00	98.98	272	15	+25.73

(a) Flux profiles

(b) Temperature and pressure profiles

(c) Concentration profiles

(d) Reaction rate profiles
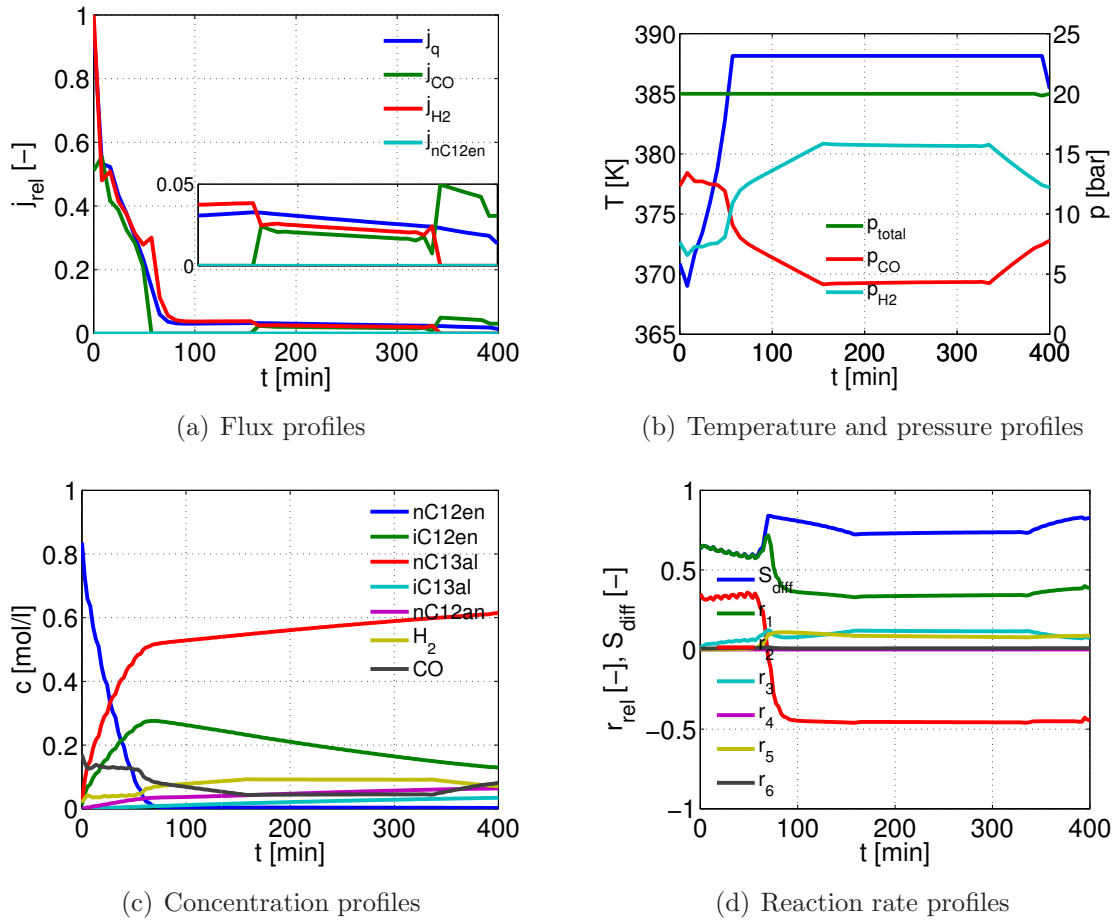
Figure 4.11.: Optimal reaction route without recycle and unconstrained fluxes (first line in Tab. 4.2). $X_f = 99.7\%$

Tab. 4.2 summarizes the performance measures of the most promising reaction routes corresponding to the maximum of the curves shown in Fig. 4.9(b). In case of similar performance the concept with the lowest degree of freedom is chosen.

Optimal route without recycle (OT1)   Comparing the selectivity of the solutions without recycle, no remarkable difference between the different intensification options can be seen. The only difference occurs at almost full conversion; it is that allowing a dynamic temperature profile will lead to higher selectivity because this enhances the re-isomerization reaction (Fig. 4.11(d)). Because this reaction is very slow, options with a constant temperature profile will violate the minimum STY constraint earlier. The effect of the temperature profile can be seen in Fig. 4.11(b). This reaction route consists of two phases each having different optimal conditions. The first phase promotes the main reaction by providing optimal gas concentrations in the liquid phase

(a) Flux profiles

(b) Temperature and pressure profiles

(c) Concentration profiles

(d) Reaction rate profiles
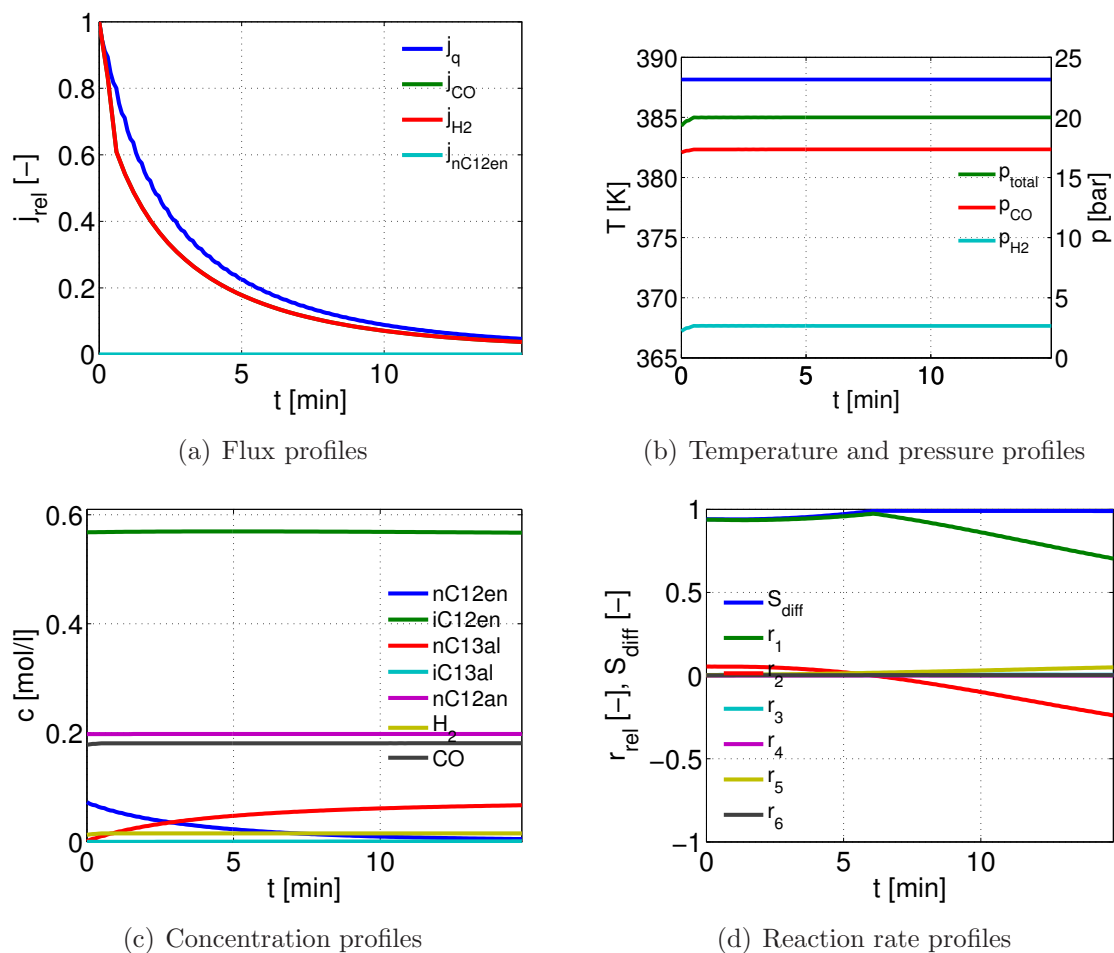
Figure 4.12.: Optimal reaction route with recycle, syngas dosing, and constant temperature profile. (second line in Tab. 4.2). $X_f = 93\%$

and an increasing temperature profile. Since the parallel isomerization reaction cannot be avoided, the second reaction phase enhances the re-isomerization by providing a maximum temperature and an inversion of the H_2/CO ratio in the liquid phase and corresponding gas phase (Fig.4.11(b)). From the lower differential selectivity in the first reaction phase (Fig. 4.11(d)) it can be concluded that the contribution of the second reaction phase to the reaction performance is much higher than the first reaction phase. Fig. 4.11(d) and Fig. 4.11(c) show that the re-isomerization phase promotes the formation of iso-aldehyde.

Optimal route with recycle and syngas constraint (OT2) Fig. 4.12 shows the consequences of the combination of dodecene recycling conditions and dosing of syngas with fixed H_2/CO ratio of 1. The gas flux is illustrated in Fig. 4.12(a). Both, H_2

(a) Flux profiles

(b) Temperature and pressure profiles

(c) Concentration profiles

(d) Reaction rate profiles
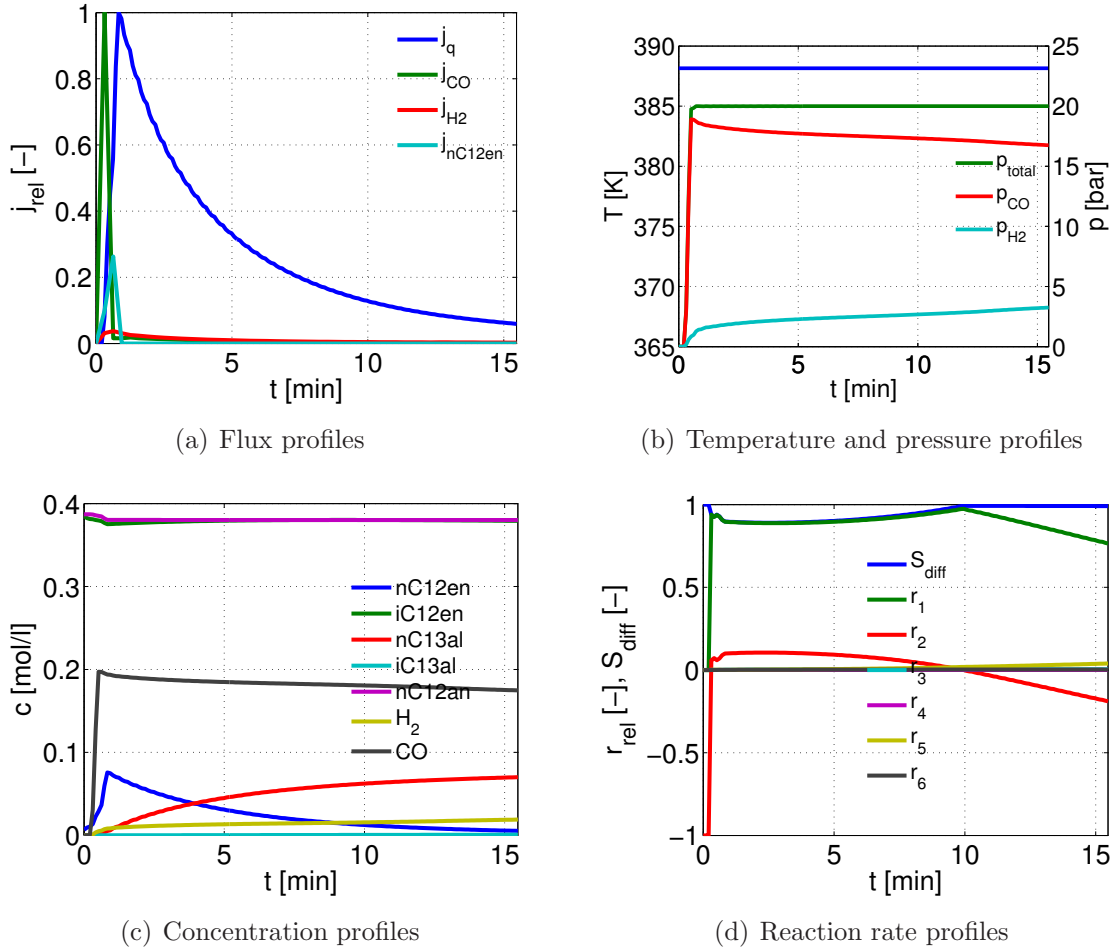
Figure 4.13.: Optimal reaction route with recycle, unconstrained gas and liquid dosing fluxes, and constant temperature profile (third line in Tab. 4.2). $X_f = 93\%$

and CO flux are similar due to the syngas constraint. An optimal CO and H_2 concentration is chosen by the optimizer which can be maintained over the entire reaction time via an optimal syngas dosing profile. The high initial concentration of internal dodecene and alkane 4.12(c) provided by the recycle condition, suppresses the hydrogenation and isomerization side reactions (Fig. 4.12(d)) compared to the previous reaction route. In contrast to the reaction route without recycle the reaction time is much shorter and essentially only one reaction phase can be observed. Although the isomerization reaction switches direction there is no distinct switch of reaction phase as without recycle. This is because the concentration of isomer and alkane are kept rather constant, hence also the corresponding side reactions are always near to its equilibrium and thus no obvious switch of reaction regime occurs.

Best optimal route (OT3) The profiles of the best optimal reaction route calculated with unconstrained fluxes and recycle condition is shown in Fig. 4.13. Initially a very high excess of internal dodecene is set followed by a pure re-isomerization, which is facilitated by having no gas dissolved in the liquid phase, initially. This condition is chosen by the optimizer, thus it is not a zero gas constraint. After the short reisomerization phase 1-dodecene is injected as pulse and an optimal gas ratio in the liquid phase is set up by sequentiol dosing of CO and then H_2 in a pulse manner followed by very low dosing of H_2 in order to maintain a low H_2 concentration in the liquid phase. The temperature is kept at maximum over the whole reaction time (Fig. 4.13(b)) by an optimal heat flux profile.

4.3.6. Influence of Back-Mixing

(a) Selectivity   (b) Space-Time Yield
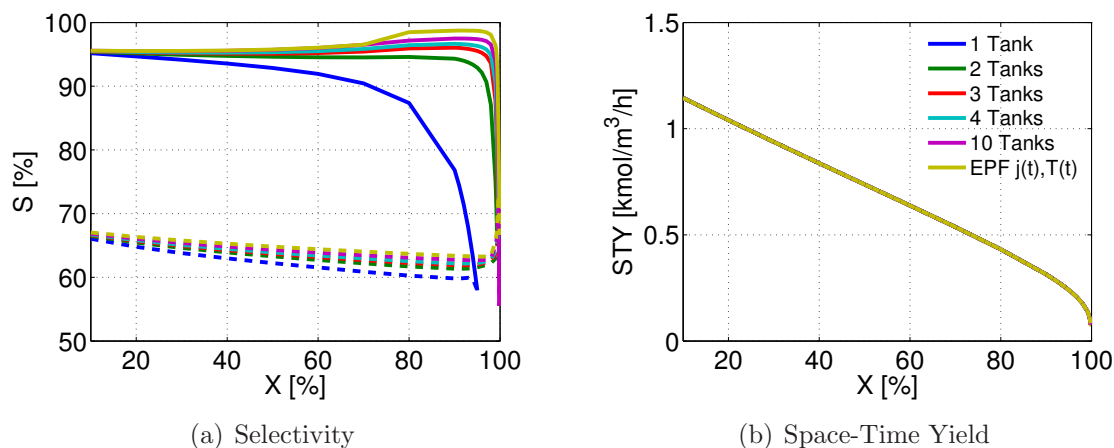
Figure 4.14.: Influence of back-mixing on the maximum attainable selectivity. Comparison of optimal reaction route and optimized cascades of CSTRs. Comparison of recycle and no recycle.

In order to investigate the effect of back-mixing CSTR cascades with varying tank number are compared to the optimal solution from the EPF approach allowing the highest degree of freedom on the optimization problem.

While the selectivity of the optimal reaction route and the cascades does not decrease with increasing conversion up to 90%, the selectivity of the single CSTR decreases monotonously (Fig. 4.14(a)). This behavior can be explained from the observation of the optimal reaction route that the two reaction regimes with different optimal conditions exist which require a certain degree of freedom on the control fluxes. Due

to its limited degree of freedom the single CSTR can only provide suitable conditions for one reaction phase. However, since the formation of the desired product always involves a hydroformylation and an isomerization phase, there are always at least two optimal reaction conditions required. In addition, the dilution effect of the CSTR leads to lower achievable STY for the same selectivity. Since, as shown in Fig. 4.14(b), selectivity is gained from lower STY, the CSTR reaches the minimum STY constraint at lower selectivity than reaction routes with higher degree of freedom.

For cascades of higher order, up to a conversion of 70% no remarkable difference can be observed. For conversion beyond 70% the optimal route as well as the cascades with more than two tanks show a selectivity increase. At its optimum the optimal route shows a selectivity of 98% which is more than 2% more than the cascade with 10 tanks.

One can conclude that total back-mixing (a single CSTR) is definitely not suitable for the process due to two reasons. The reaction system requires a higher degree for the control fluxes to provide optimal conditions for two reaction regimes and the dilution due to back-mixing leads to unfavorable STY, leading to very large reaction volumes and residence times. However, some degree of back-mixing seems feasible since a cascade of 4 CSTRs leads to a good approximation of the optimal reaction route. However, the suitability of a cascade of CSTRs depends on conversion, since beyond 80% conversion even a cascade with 10 CSTRs yields a 2% selectivity loss compared to the optimal reaction route.

Since the desired conversion depends on the downstream process it is not possible to decide which number of CSTRs is optimal for the process. This is only one example why the reactor design should always be done by considering the integrated system of reactor, process, and recycles. In the next section such an integrated reactor design will be demonstrated.

4.3.7. Influence of Mass Transfer - Limited Fluxes

So far, the presented reaction routes were based on unlimited control fluxes, hence without considering transport resistances and driving forces. Thus, those reaction routes represent the theoretical optimum which sets a benchmark for the evaluation of further technical approximations. Due to the limitation of the fluxes by transport resistance and driving forces the theoretical optimum usually cannot be reached ideally. Instead of manipulating a specific flux directly, it is now manipulated indirectly

via external control variables, such as cooling temperature instead of heat flux. The transfer coefficients are used as scaling factors. In this section the technical feasibility of the limited fluxes is investigated and transfer coefficients and external control variable profiles are calculated. The model equations are now extended by the energy balance and constitutive equations for the control fluxes.

$$\left(\sum_{i\in\text{CH}} n_i \cdot c_{p,i}\right) \frac{\mathrm{d}T}{\mathrm{d}t} = j_q + m_{\text{cat}} \sum_{j\in\text{RCT}} \Delta_R h_j r_j \tag{4.30}$$

$$j_q = k_q \cdot a_q \cdot V_{\text{liq}} \cdot (T_c - T) \tag{4.31}$$

$$j_i = (k_L a)_{liq} \cdot V_{\text{liq}} \cdot (c_i^* - c_i), \, i \in \text{GAS} \tag{4.32}$$

Also, the optimal control problem has to be changed (refer to OP). Instead of the fluxes, appropriate external control variables have to be optimized. Hence, the set of control functions $U(t)$ now contains the cooling temperature T_c, since an indirect cooling strategy is proposed. The 1-dodecene dosing flux is again directly optimized, representing direct injection. The gas phase is now manipulated via the partial pressure profiles p_{H2} and p_{CO} in order to manipulate the driving force of the gas dosing flux. The set of optimization parameters Ψ still contains the initial conditions. As elucidated earlier, zero initial conditions for the gas do not have to be investigated anymore.

Further, the consecutive equations for the heat and gas dosing fluxes are added to the OP. The mass transfer coefficient $k_L a$ and the heat exchange area a_q are fixed and adjusted to yield a reasonable scaling of the driving forces. The transfer coefficient k_q is fixed to a typical value for gas-liquid systems [69] of 500 $\frac{W}{m^2 K}$. Instead of optimizing the driving force profile and keeping the transfer coefficient fixed, one could also optimize a transfer coefficient or exchange area profile by keeping the external control variable (such as cooling temperature) or the driving force fixed (such as $T - T_c$). However, the simultaneous optimization of transfer coefficient and driving force will yield non-unique solutions due to the missing penalty on the objective function.

The physical bounds have to be extended by the bounds for the external control variables (T_c). The lower bound of T_c is the cooling water temperature and the upper bound is steam temperature at 30 bar. At last, the scenario of no recycle is removed, since no recycle leads to undesired performance. Since it is still of interest to investigate the influence of a fixed syngas ratio the syngas constraint can still be applied on the gas dosing flux enabled via scenario constraint sgJ.

$$\text{Obj} = \max_{U(t),\Psi} S_{\text{nC13al}} \qquad\qquad\qquad (\text{OP})$$

$$U(t) = T_c(t), j_{\text{nC12en}}(t), p_{\text{H2}}(t), p_{\text{CO}}(t)$$

$$\Psi = n_i(t_0)$$

s.t.

Mass balances:	EPF: Eqs. (4.22)–(4.24)	
Energy balances:	EPF: Eq. (4.30)	
Reaction kinetics:	Eqs. (4.3)–(4.11)	
Gas solubilities:	Eqs. (4.2)–(4.1)	
Flux equations:	Eqs. (4.31)–(4.32)	

Bounds: $\quad p \in [0,20]\,\text{bar}$

$\qquad\qquad T \in [95,115]\,^{\circ}\text{C}$

$\qquad\qquad T_c \in [25,234]\,^{\circ}\text{C}$

Conversion: $\quad X = 1 - \dfrac{n_{\text{nC12en}}(t_f)}{n_{\text{nC12en,ref}}}$

Selectivity: $\quad S = \dfrac{n_{\text{nC13al}}(t_f) - n_{\text{nC13al}}(t_0)}{X \cdot n_{\text{nC12en,ref}}}$

STY: $\quad STY = \dfrac{n_{\text{nC13al}}(t_f) - n_{\text{nC13al}}(t_0)}{\int_{t_0}^{t_f} V_{\text{liq}}(\tau)\,\mathrm{d}\tau} \geq STY_{\text{ref}}$

Initial conditions: $\quad n_{i,\text{liq}} = 0,\ i \in \text{COM} \setminus \{\text{nC12en}, \text{iC12en}, \text{H}_2, \text{CO}\}$

$\qquad\qquad n_{\text{nC12en}}(t_0) + \int_{t_0}^{t_f} j_{\text{nC12en}}(\tau)\,\mathrm{d}\tau = n_{\text{nC12en,ref}} = 1\text{mol}$

Recycle constraints: $\quad n_{\text{iC12en,liq}}(t_0) \leq n_{\text{iC12en,liq}}(t_f)$

$\qquad\qquad n_{\text{nC12en,liq}}(t_0) \geq n_{\text{nC12en,liq}}(t_f)$

Scenario constraints: $\quad \text{sgJ:} j_{\text{H2}}(t) = j_{\text{CO}}(t) = j_{\text{sg}}(t)$

Figure 4.15.: Influence of mass transfer on the maximum attainable selectivity. Comparison of OT2.1 and OT2.2. Comparison of different catalyst concentrations on the mass transfer behavior: solid lines: $x_{cat} = 10^{-4}$, dashed lines: $x_{cat} = 2 \cdot 10^{-4}$, dotted lines: $x_{cat} = 4 \cdot 10^{-4}$

For evaluation of limited fluxes, the two best cases of the previous section, $Rc, j(t), T$ and $Rc, j_{sg}(t), T$ are analyzed. While the cooling temperature is optimized as profile in time, $k_L a$ and a_q are fixed. It turned out that by setting a heat exchange area in the range of 1-5 $\frac{m^2}{m^3}$, all temperatures are attainable within the bounds of the cooling temperature profile. This corresponds to a transfer area of an empty tube of diameter $0.8 - 4m$ and can be considered as easily achievable.

More attention has to be paid to the mass transfer coefficient $k_L a$. As proposed by Peschel et al. [39], a sensitivity study with respect to the $k_L a$ is performed by changing the $k_L a$ value and solving OP for each fixed $k_L a$. This was done for the best two cases of the previous section and the results are illustrated in Fig. 4.15. For better understanding the reader should focus on the solid lines first. Starting at the right side of the figure, the selectivity corresponds to the optimal value obtained with unlimited fluxes (refer to Fig.4.9(b)). Reducing the $k_L a$ value, hence increasing the mass transfer resistance, has no effect on selectivity until around $k_L a = 0.01s^{-1}$, while beyond this value a sharp decrease of selectivity occurs. Interestingly, shortly before the collapse of selectivity the two solutions of OP merge into a single solution. Obviously, the control policy of the favored solution cannot be maintained beyond a certain mass transfer resistance. The reason for this behavior is the lower bound on the STY, since the favored solution OT2.2 yields slightly longer residence times than

(a) Relative Control Profiles

(b) Flux profiles

(c) Concentration profiles

(d) Reaction rate profiles
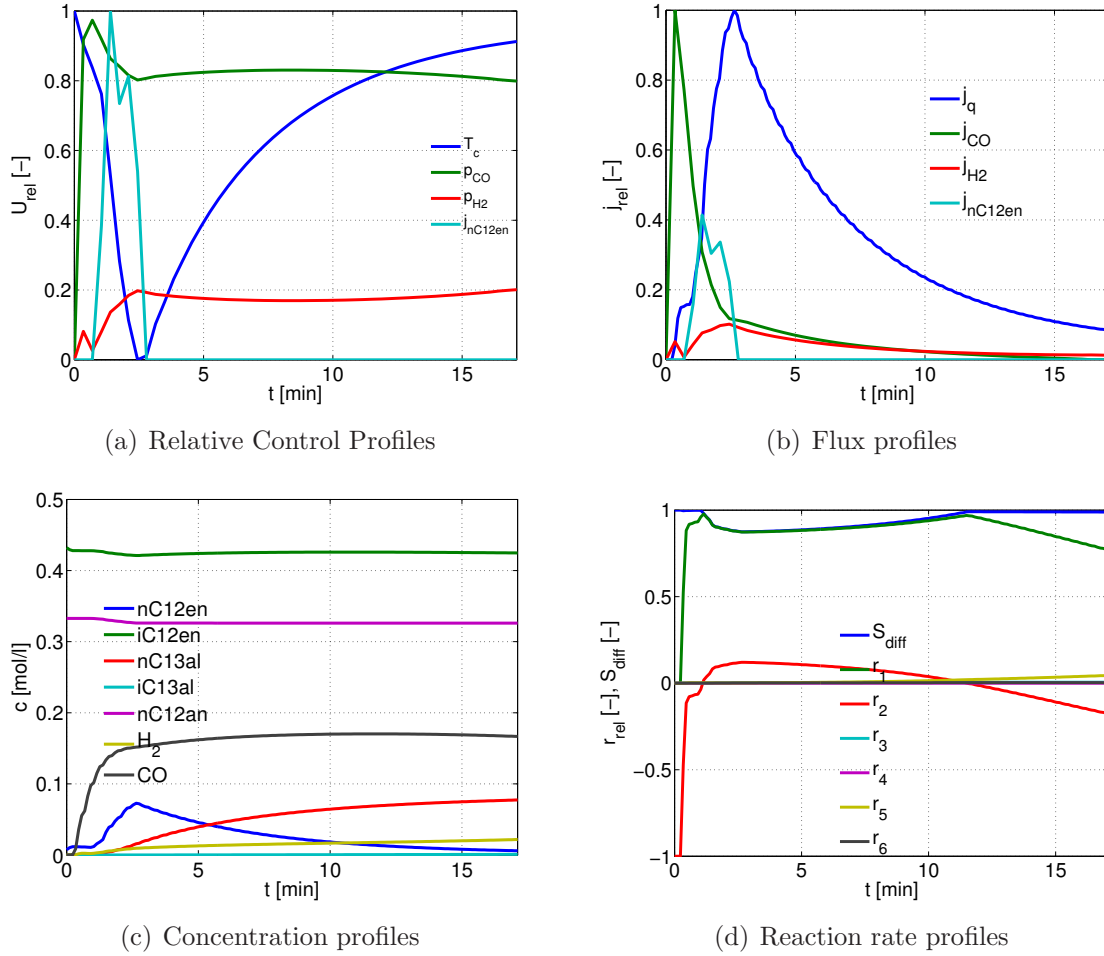
Figure 4.16.: Optimal reaction route OT2.2 at limited mass transfer ($k_L a = 0.02 s^{-1}$). $X_f = 93\%$

OT2.1, which cannot be afforded beyond a critical $k_L a$ value. In order to determine a set of external control profiles, a decision on the desired $k_L a$ value has to be made. Peschel et al.[39] proposed to choose a value corresponding to an acceptable selectivity loss of 1 %. However, due to a much higher catalyst concentration and different reaction kinetics their required $k_L a$ value was two orders of magnitude higher than in this case, which also yields much higher effort to realize this value. For the low catalyst concentration considered in this work, much lower $k_L a$ values are required, hence the acceptable selectivity loss is decreased to 0.2%. Thus, a minimum $k_L a$ of $0.02 s^{-1}$ is chosen (refer to black dotted line in Fig. 4.15). The corresponding control profiles, concentrations, fluxes, and reaction rates are illustrated in Fig. 4.16.

Fig. 4.16(a) shows the profiles of the external control variables. After a short pe-

riod of 1 min 1-dodecene is dosed for about three minutes. The initial condition of the gases is chosen to be zero by the optimizer, followed by immediate increase of the CO partial pressure to nearly 20 bar accompanied by a marginal increase of H_2 partial pressure. This control policy enhances the re-isomerization of the recycled internal dodecene (refer to Fig. 4.16(d)). The re-isomerization is stopped as 1-dodecene is dosed. At this time the H_2 partial pressure rises until the end of the dosing period while the CO partial pressure decreases to stay at the maximum total pressure bound of 20 bar. After the end of the 1-dodecene dosing period the partial pressures are kept at a more or less constant level, at a partial pressure ratio of about $CO/H_2 = 4$. The cooling temperature profile follows the heat flux (Fig. 4.16(b)) due to heat of reaction in order to keep a constant upper reaction temperature of 105^oC (not shown). It consists of two sections, beginning with a linearly decreasing profile from the beginning of the trajectory until the end of the 1-dodecene dosing period. Followed by an increasing profile with decreasing slope until the end of the trajectory.

Influence of catalyst concentration on mass transfer. Since the required mass transfer rate depends on the rate of reaction, a change of the catalyst concentration yields different mass transfer requirements. Fig. 4.15 illustrates the effect of different catalyst concentrations on the attainable selectivity. In case of the chosen trajectory OT2.2, an increase of the catalyst concentration while keeping $k_La = 0.02s^{-1}$ would yield a change of control policy to OT2.1, thus a different reactor design and lower selectivity. Thus, in order to keep the old control policy and high selectivity at higher catalyst concentration the k_La value has to be increased accordingly.

4.3.8. Summary

In this chapter the validated reaction kinetics obtained after experimental validation of the optimal reaction route is applied within a reactor independent fluid element model. This enables a further exploitation of the state space than within the constraints of the experimentally used semibatch reactor.

In a first step different chemical engineering objectives are analyzed in order to identify the most suitable objective and to get a clue of the intercorrelation of different objectives. From the comparison selectivity is chosen as most representative objective since this objective does not yield very extreme values of the other performance measures.

After the identification of selectivity as suitable objective optimal reaction routes

are calculated for different DoF and varying conversion in order to get Pareto fronts of selectivity and conversion. As in the experimental validation section, it turned out that the setup of optimal initial conditions of gaseous reactants is a crucial aspect for obtaining maximum selectivity. Further, recycling of internal dodecene and dodecane yields about 20% higher selectivities than without recycling due to the inhibition of side reactions.

The influence of backmixing is investigated by comparing the optimal reaction route with the highest DoF with cascades of CSTRs with varying tank number. It turned out that backmixing yields performance losses compared to the optimal route, however, a cascade of four CSTRs yields a good approach to the optimum. The higher tank number offers more DoF, which enables more suitable reaction conditions the different dynamic phases of the reaction.

At last the influence of mass transfer is investigated by substituting the unlimited fluxes in the fluid element model with constitutive mass transfer equations and performing sensitivity analysis on the $k_L a$ value. It could be shown that the minimum required $k_L a$ value depends on the catalyst concentration and that the improper choice of the $k_L a$ may yield a switch of the optimal control policy. Finally, for the minimum required $k_L a$ value of $0.02 s^{-1}$, according to the experimentally considered catalyst concentration, optimal profiles of cooling temperature, 1-dodecene dosing flux and gas dosing fluxes.

4.4. Process-Wide Optimal Route

In the previous chapter it was shown, that there exists an optimal recycle composition which enhances the reactor performance by means of higher product selectivity. Further, it is beneficial to recycle all of the produced internal dodecene to the reactor in order to reduce the rate of isomerization, which leads to a reduction of side product formation, such as alkanes and branched aldehyde. It is now the task to practically realize such a recycle composition by means of real process equipment. In this chapter an integrated process is proposed, which aims to realize the desired recycle composition suggested in the previous chapter.

Although it is unlikely to exactly realize the desired recycle composition, due to the nonidealities in the separation units, but at least the deviation from the optimal performance can be quantified. If the deviation is too high, an alternative process realization has to be found.

A second very important aspect of this chapter is that the problem of multiple objective functions can be reduced to a single objective, namely total production costs. In previous chapters different performance measures, such as selectivity, space time yield, residence time, conversion, and n/iso-ratio where introduced, but their relative weights towards an overall performance was unknown. By using an economic model for the operating and investment costs of the process the relative weights of the different performance measures will be intrinsically supplied. The performance measures not only affect the operating costs by means of utility consumption, and raw material demand, but also the size of the equipment. The equipment size and costs essentially determine the practical feasibility of a new reaction concept.

In order to investigate the influence of realistic recycles and to evaluate production costs, a flowsheet (Fig. 4.17) is developed based on general process design principles [69]. Although alternative separation processes such as crystallization [70] or hybrid separation processes [71, 72] are currently under investigation for the specific solvent system, this work is exemplified based on distillation separation since it is still the most important and most applied separation technology in industry. While methods for the identification of the optimal process structure for this specific system are currently developed [73], the process structure in this work is fixed. However, the operation parameters of the considered separation units are degrees of freedom. Simultaneous optimization of process and reaction route in this context refers to an optimization problem containing distributed control functions related to the fluid element model and parameters related to the downstream units which are optimized according to the same objective function.

4.4.1. Overall Process
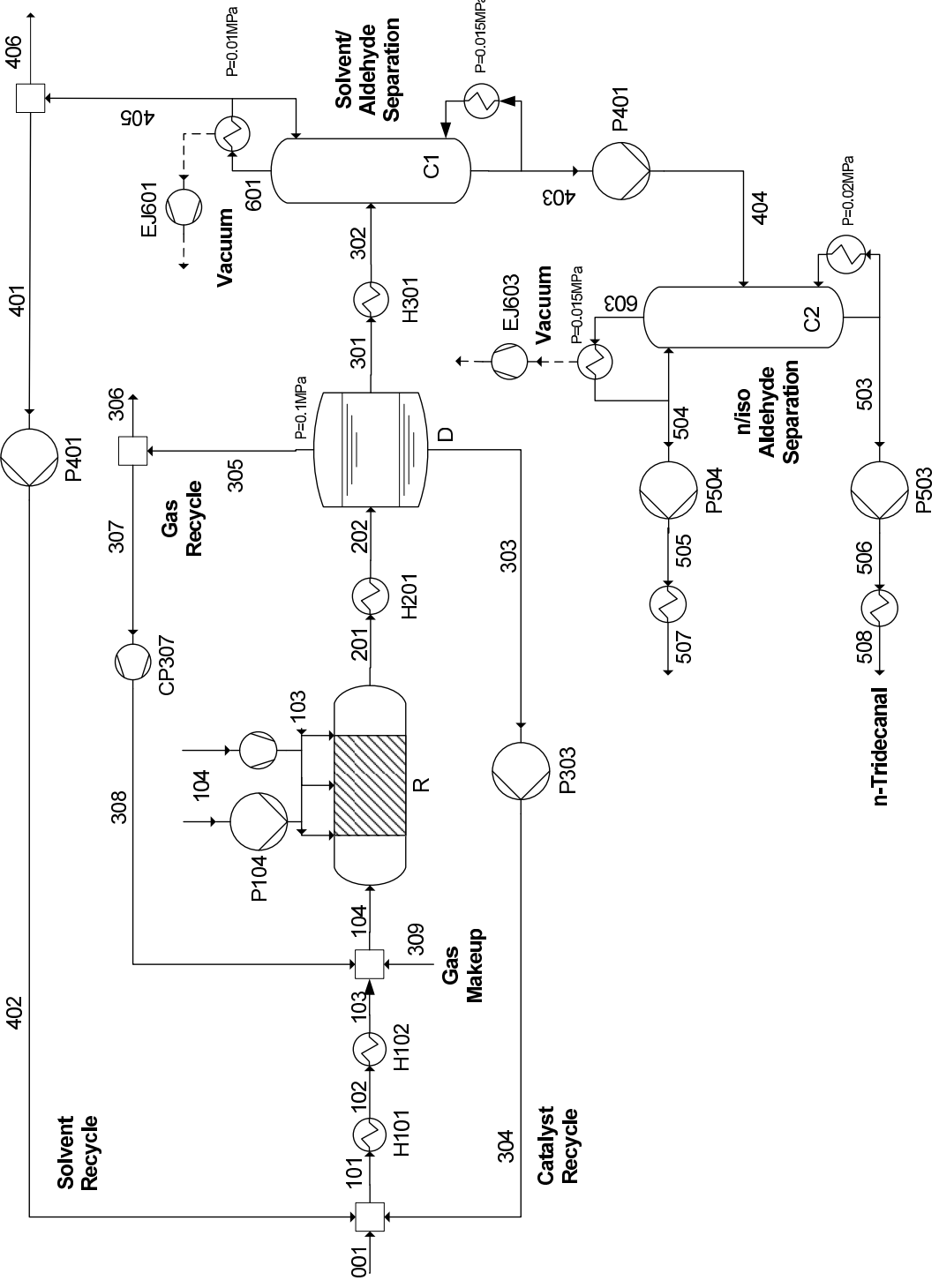
Figure 4.17.: Flowsheet of the proposed hydroformylation process.

The overall process can be divided into four main sections. Beginning with the reaction section, where reactant feed streams and recycle streams are converted into product. Followed by a syngas and catalyst recovery section, where aqueous solvent, which contains the catalyst, and unconverted syngas are separated from the organic solvent, which contains the product. In the solvent recovery section the aldehydes are separated from the remaining organic solvent and intermediate reactants. At last the linear aldehyde product is obtained from the bottom stream of the n/iso aldehyde separation section.

In contrast to the previous chapter, the ideal recycle composition is constrained by three phenomena. At first, the recycle gas composition is constrained by the gas-liquid-liquid equilibrium in the syngas and catalyst recovery section. Further, the catalyst recycle not only contains the polar solvent and the catalyst, but also parts of product and intermediates according to the phase equilibrium. Finally, the organic solvent recycle contains not only decane, but also intermediates and product. Hence, the real recycle streams only inherit limited degree of freedom compared to the previous chapter.

Applying the TMS concept, a liquid-liquid phase separation is induced by lowering the temperature to ambient conditions. However, in this special case two separation problems can be integrated into one device by reducing temperature and pressure at the same time. Due to the pressure reduction remaining syngas, which is still solved inside the liquid phase can be flashed and separated from the liquid phases. Recovered catalyst and syngas is recycled to the reaction section.

After the reactants are mixed with the recycle streams coming from the solvent and catalyst recovery section, stream 101 is either cooled down in cooler H101, or heated up in heater H102 to reactor inlet temperature. Recycle gas is directly dosed into the reactor R in order to start the reaction.

As applied in the previous chapters the reaction section is considered as an optimized path of a fluid element of the mixture, which is subject to optimally adjusted fluxes of energy and material providing optimal reaction conditions at each time point.

Downstream of the reaction section the outlet stream 201 is cooled to ambient temperature in cooler H201 and subsequently depressurized to ambient pressure via valve V201 in order to initiate a gas-liquid-liquid phase split in decanter D. The aqueous phase 303, mostly containing DMF and the catalyst, is recycled to the reactor via pump P303, while the product rich organic phase 301 is fed into the solvent recov-

ery section. All of the remaining gas which was dissolved in the reactor outlet is assumed to be totally separated from the liquid phases in the decanter (stream 305) and recycled to the reactor via compressor CP307. The non-polar phase leaving the decanter (stream 301) is preheated to bubble point temperature in heater H301 before entering the solvent/aldehyde separation column C1. In this column n-decane, remaining DMF, unconverted dodecene, and dodecane is removed from the mixture as distillate (stream 405) and recycled to the reactor via pump P401. The bottom stream of column C1 (stream 403), containing mainly the aldehyde mixture is fed to the n/iso separation column C2 via pump P403. The desired linear aldehyde product is obtained as bottom stream of C2 (stream 503) while the distillate (stream 504) contains the branched aldehyde. Since the aldehydes tend to form aldolcondensates at temperatures above 180°C both distillation columns operate at vacuum conditions in order to lower the boiling point of the mixtures. Since the outlet streams of column C2 are below ambient pressure at elevated temperature they have to be pressurized via pump P503 and P504 and cooled via heat exchanger H506 and H507 to meet boundary limit conditions (B.L.).

In the following, the balance equations and connectivity constraints of each unit are described in detail. From the material and energy balances utilities (refer to A.4) as well as equipment sizes (refer to A.5) are calculated which enables the determination of operating and investment costs (refer to A.6).

4.4.2. Reaction Section

In order not to limit the design space a priori, an apparatus independent formulation of the reaction section according to the concept of elementary process functions (EPF) [3] was applied. Instead of assuming a predefined type of reactor the Lagrangian formalism is used to model the evolution of states of a fluid element over the reaction coordinate.

The fluid element model consists of the mass and energy balances of the liquid phase (Eqs. (4.33)–(4.34)), equations to describe liquid volume (Eq. (4.36)), heat capacities (Eq. (4.38)), solubilities (Eq. (4.2)), and reaction kinetics (Eqs. (4.3)–(4.9)). The

parameters for the substance properties are given in Tab. A.7 and Tab. A.6 of A.2.

$$\frac{\mathrm{d}n_{i,\text{liq}}}{\mathrm{d}t} = j_i + c_{\text{cat}}V_{\text{liq}}M_{\text{cat}} \sum_{j \in \text{RCT}} v_{i,j}r_j \tag{4.33}$$

$$\sum_{i \in \text{COM}} (n_{i,\text{liq}}c_{p,i}) \frac{\mathrm{d}T}{\mathrm{d}t} = j_q + c_{\text{cat}}V_{\text{liq}}M_{\text{cat}} \sum_{i \in \text{COM}} \left(h_i \sum_{j \in \text{RCT}} v_{i,j}r_j \right) \tag{4.34}$$

$$c_{\text{liq},i} = \frac{n_{\text{liq},i}}{V_{\text{liq}}} \tag{4.35}$$

$$V_{\text{liq}} = \sum_{i \in \text{COM}} \frac{n_{i,\text{liq}}M_i}{\rho_i} \tag{4.36}$$

$$\rho_i = a_{\rho,0,i} + a_{\rho,1,i}T \tag{4.37}$$

$$h_i = h_{f,0,i}(T_0) + \sum_{j=1}^{4} p_{Cp,j,i}(T - T_0)^j \tag{4.38}$$

Since the fluid element model is formulated according to the Lagrangian observer, which describes the space-independent time course of the steady state trajectory, the streams of the flowsheet and the initial and end conditions of the fluid element have to be connected (Eqs. (4.40)–(4.43)). The initial size of the fluid element is determined by its initial amount of substance, which can be chosen to scale the optimization problem. Here it was set to $n_{\text{liq,ref}} = 1kmol$.

$$n_{\text{liq}}(t_0) = n_{\text{liq,ref}} \tag{4.39}$$

$$\frac{\dot{n}_{i,103}}{\dot{n}_{102}} = \frac{\int_{t_0}^{t_f} j_i(\hat{t})\mathrm{d}\hat{t}}{n_{\text{liq}}(t_0)} \qquad , i \in \text{COM} \tag{4.40}$$

$$x_{i,102} = x_{\text{liq},i}(t_0) \tag{4.41}$$

$$x_{i,201} = x_{\text{liq},i}(t_f) \tag{4.42}$$

$$\frac{\dot{n}_{102}}{\dot{n}_{201}} = \frac{n_{\text{liq}}(t_0)}{n_{\text{liq}}(t_f)} \tag{4.43}$$

4.4.3. Catalyst Separation Section

From experimental investigations of Schäfer et al. [65] it was found that the temperature dependency of the distribution coefficients of non-catalytic components during the liquid-liquid separation is not very significant. However, the catalyst leaching into the organic phase is strongly temperature dependent and it was shown that lower temperatures lead to a lower catalyst leaching. Since the catalyst losses are not considered in this work the decanter temperature was set at a constant value of

$T_D = 298.15K$. Instead, more effort was put on the accurate description of the composition dependency of the distribution coefficients. In order to avoid the solution of an LLE calculation within the optimization, the distribution coefficients were expressed as second order polynomials with conversion as independent variable (Eq. (4.45)). The parameters for the correlation (Tab. A.8) were obtained from fitting to UNIFAC Dortmund, which is in good agreement with the experimental data [65]. To correlate conversion to the distribution coefficient, typical mixtures at the reactor outlet were generated from the selectivity optimal open-loop trajectory. The deviation between UNIFAC and the correlation is below 5%. The decanter model then consists of the following equations.

$$\dot{n}_{\text{nC13al},202} \cdot M_{\text{nC13al}} \leq \omega_{\text{nC13al,max}} \cdot \sum_i (\dot{n}_{i,202} \cdot M_i) \qquad , i \in \text{COM} \setminus \text{GAS} \qquad (4.44)$$

$$k_{LLE,i}(X) = a_{0,i} + a_{1,i} \cdot X + a_{2,i} \cdot X^2 \qquad , i \in \text{COM} \setminus \text{GAS} \qquad (4.45)$$

$$x_{i,303} = k_{LLE,i}(X) \cdot x_{i,301} \qquad , i \in \text{COM} \setminus \text{GAS} \qquad (4.46)$$

$$\dot{n}_{i,202} = \dot{n}_{i,301} + \dot{n}_{i,303} + \dot{n}_{i,305} \qquad , i \in \text{COM} \qquad (4.47)$$

$$\dot{n}_{i,202} = \dot{n}_{i,301} + \dot{n}_{i,303} \qquad , i \in \text{COM} \setminus \text{GAS} \qquad (4.48)$$

$$\dot{n}_{i,s} = 0 \qquad , i \in \text{GAS}, s \in \{301, 303\} \qquad (4.49)$$

$$\dot{n}_{i,305} = \begin{cases} \dot{n}_{i,202} & , i \in \text{GAS} \\ 0 & , else \end{cases} \qquad (4.50)$$

$$\dot{n}_{i,s} = \dot{n}_{i,s-1} \qquad , i \in COM, s \in \{202, 302, 304, 305, 306\} \qquad (4.51)$$

Eq. (4.44) represents the phase split criterion, since it was shown by Schäfer et al. [65] that an aldehyde weight fraction of above 20% in the product stream prevents the phase split. Eqs. (4.45) and (4.46) account for the LLE distribution of the non-gaseous components in the aqueous and non-aqueous phase. For sake of simplicity it is assumed that the dissolved gases from the reactor outlet can be totally separated in the decanter (see Eqs. (4.49) and (4.50)). Eqs. (4.47) and (4.48) represent the total molar balances in the decanter, whereas Eqs. (4.50) and (4.51) describe the coupling of adjacent fluxes.

In addition to the presented decanter model also the solvent and catalyst ratios introduced in the stand-alone reactor section are fixed.

4.4.4. Distillation Columns

As mentioned earlier, the distillation columns C1 and C2 operate at vacuum conditions in order to reduce the boiling point of the mixtures below 180ºC. Due to

the low absolute pressure a low column pressure drop is required. Since packed beds provide lower pressure drop per theoretical stage than trays, unstructured packing of Rasching Rings is used as phase contacting material.

In order to depressurize the columns to sub-ambient pressure non-condensable gases have to be continuously removed. Although, syngas is completely removed from the liquid phase in the decanter (refer to assumption 4.49) non-condensable gases will continuously enter the column as air in-leakage via small orifices distributed over the column surface, especially around fittings, nozzles, manholes, etc. This leak flow of air has to be continuously removed by evacuation. For this purpose motor driven or steam driven devices can be used. Usually, steam ejectors are used to generate the sub-ambient pressures in vacuum distillation since there are no moving parts and very low suction pressures can be generated at low operating costs.

In order to determine operating and investment costs the number of equilibrium stages and the reflux ratio of the columns is calculated using the short-cut method of Fenske–Underwood–Gilliland. In this method the minimum number of stages is determined at infinite reflux by assuming a constant relative volatility of key components over the column. Hence, the minimum number of stages can be explicitly obtained for a given purity of the key components according to the following equations.

$$N_{\min} = \frac{\log(\frac{\dot{n}_{D,LK} \cdot \dot{n}_{B,HK}}{\dot{n}_{B,LK} \cdot \dot{n}_{D,HK}})}{log(\bar{\alpha}_{LK,HK})} \tag{4.52}$$

where $\dot{n}_{D,LK}$ denotes the molar flow rate of the light key LK in the distillate stream D, and $\dot{n}_{B,HK}$ is the molar flow rate of the heavy key HK in the bottom stream B. The molar flow rate of the key components is determined by the recovery ratio ζ which is a degree of freedom in the optimization problem.

$$\dot{n}_{D,LK} = \zeta_{LK} \cdot \dot{n}_{in,LK} \tag{4.53}$$

$$\dot{n}_{B,HK} = \zeta_{HK} \cdot \dot{n}_{in,HK} \tag{4.54}$$

The mean relative volatilities between distillate stream D and bottom stream B are defined as follows.

$$\bar{\alpha}_{i,j} = \sqrt{\alpha_{i,j}(T_D) \cdot \alpha_{i,j}(T_B)} \tag{4.55}$$

The temperature dependent relative volatilities are calculated as the ratio of the vapor pressures of component i and j.

$$\alpha_{i,j}(T) = \frac{p_{vap,i}(T)}{p_{vap,j}(T)} \tag{4.56}$$

Temperature dependent correlations and parameters for the vapor pressure are given in Appendix A.9. With the minimum number of stages and the total molar balance of the column the entire set of component flow rates can be calculated.

$$\dot{n}_{\mathrm{B},i} = \frac{\dot{n}_{\mathrm{in},i}}{1 + \frac{\dot{n}_{\mathrm{D,HK}}}{\dot{n}_{\mathrm{B,HK}}} \cdot \bar{\alpha}_{i,\mathrm{HK}}^{N_{\min}}} \tag{4.57}$$

$$\dot{n}_{\mathrm{in},i} = \dot{n}_{\mathrm{D},i} + \dot{n}_{\mathrm{B},i} \tag{4.58}$$

Vacuum Service

(a) Air leakage constant

(b) Steam requirement
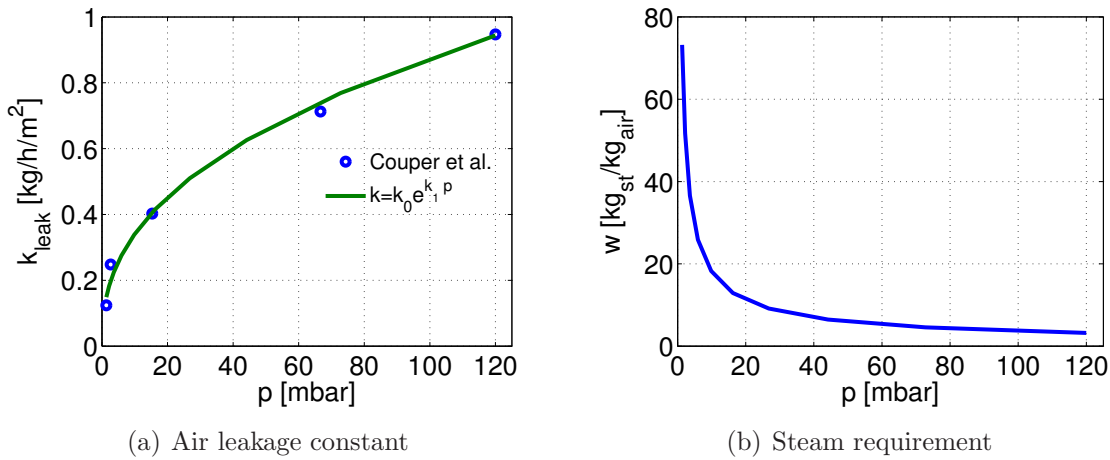
Figure 4.18.: Correlations for vacuum service in distillation columns using 2-stage steam ejector with barometric intercondenser.

In order to determine the operating and investment costs of the steam ejectors the air leakage flow into the column has to be continuously removed after the condenser. A correlation for the leak flow can be found in [74] and is illustrated in Fig. 4.18(a).

$$\dot{m}_{\mathrm{air}} = k_{\mathrm{leak}}(p) \cdot V^{2/3} \tag{4.59}$$

$$k_{\mathrm{leak}}(p) = 0.0967 \cdot p_{\mathrm{cond}}^{0.4105} \tag{4.60}$$

Pressure is in MPa, volume of the column in m^3 and the mass flow in kg/min.

For a given ejector type and suction pressure the necessary amount of steam can be estimated from Fig. 4.18(b). For the pressure range relevant for this process a 2-stage ejector with barometric inter-condenser and 100% air to be removed is assumed. With this constellation suction pressures between 100 and 7 mmHg can be

continuously maintained. The curve from Fig. 4.18(b) corresponding to the chosen ejector type can be represented by the following correlation.

$$\frac{\dot{m}_{\text{steam}}}{\dot{m}_{\text{air}}} = 0.1496 \cdot p_{\text{cond}}^{-0.6941} \tag{4.61}$$

Using the correlation of Pikulik and Diaz [75] the investment costs of the steam ejector can be estimated from the air flow and the suction pressure as follows.

$$X_{\text{ejec}} = \frac{\dot{m}_{\text{air}}}{p_{\text{cond}}} \tag{4.62}$$

$$\text{BC}_{\text{ejec}} = \text{BC}_0 \cdot \left(\frac{X_{\text{ejec}}}{\text{BC}_1}\right)^{\text{BC}_2} \tag{4.63}$$

$$0.1 \leq X_{\text{ejec}} \leq 100 \tag{4.64}$$

4.4.5. Optimization Problem

As concluded from the analysis of various chemical engineering objectives in the previous chapter, it is clear, that a generalized objective needs to be defined which contains the correct weighting factors between the possible performance measures. These weighting factors result from the costs associated with the technology that compensates a possible lag in the respective performance measure. For example, if the n/iso aldehyde ratio in the reactor is too low it could be increased by a higher separation efficiency in the n/iso separation column C2. The combined operation and investment costs of the column, that are needed to reach the desired n/iso ratio define the weighting factor of the n/iso ratio of the reactor compared to the other possible objectives.

For the optimization of total production costs in addition to the reactor model the mass and energy balances of the process equipment, models for the utility demand, unit sizes, and cost models for utilities, raw material, and equipment have been added to the optimization problem. The optimization problem for the integrated system of reactor and process is then defined as follows.

$$\text{Obj} = \min_{U(t)} \left(\frac{\frac{C_{\text{invest}}}{3a} + C_{\text{util}} + C_{\text{rawmat}}}{\dot{n}_{503,\text{nC13al}}}\right) \tag{OP3}$$

$$U_R(t) = j_q(t), j_{\text{CO}}(t), j_{\text{H2}}(t), j_{\text{nC12en}}(t), t_f$$

$$U_P(t) = \dot{n}_{i,001}, \dot{n}_{i,104}, \xi_{\text{LK,c}}, \xi_{\text{HK,c}}, RR_{\text{c}}, P_{\text{reb,c}}, x_{\text{purge,s}}$$

s.t.   **Reaction section:**

Fluid element model:	Eqs. (4.33)–(4.38)
Reaction kinetics:	Eqs. (4.3)–(4.11)
T,p bounds:	Eqs. (4.12)–(4.13)
Catalyst concentration:	Eq. (A.1)
Solvent composition:	Eqs. (A.2)–(A.3)
Process model:	
Coupling conditions:	Eqs. (4.40)–(4.43)
Decanter:	Eqs. (4.44)–(4.51)
Distillation columns:	Eqs. (4.52)–(4.58)
Connectivity constraints:	Eqs. (A.4)–(A.41)
Utilities:	Eqs. (A.43)–(A.65)
Sizing:	Eqs. (A.66)–(A.107)
Cost models:	Eqs. (A.108)–(A.117)
Product specifications:	$\dot{n}_{503} = 0.1\frac{kmol}{min}$

Although the TMS concept is actually an approach to recover the expensive rhodium catalyst from the product, the catalyst loss is not included in the economic model. The catalyst loss is caused by leaching of catalyst into the organic phase. The leaching is mainly influenced by temperature and solvent composition. That means, that the catalyst loss could actually be minimized by an optimal decanter temperature and an optimal reactor outlet composition. However, during the time this thesis was prepared no adequate thermodynamic or empirical mathematical model which quantitatively describes catalyst leaching was available. Further, experimental data at this time were scarce and not comprehensive enough to develop such a model. Hence, in this work is is assumed that the catalyst loss is not influenced by the reactor outlet composition, thus reactor design does not affect catalyst loss. However, the catalyst contained inside the reactor is considered as investment costs, since it depends on the size of the reaction volume. Although the detailed mechanism of catalyst loss is not investigated in therms of an optimal reactor outlet composition, the effect on process economics is assessed via an sensitivity study assuming a constant leaching rate into the organic phase (refer to Section 4.4.11).

4.4.6. Screening of Intensification Options

In order to derive the process-wide optimal reaction concept in terms of production costs, OP3 (Eqs. (OP3)) has to be solved. In contrast to the optimization of the stand-alone reactor, control fluxes of the reaction section and process parameters are optimized simultaneously. In analogy to the stand-alone reactor different

Table 4.3.: Screening of intensification options.

Case	S	X	tau	STY	n/(n+i)	Utility	Invest	Costs	rel. Costs
	%	%	min	$\frac{mol}{m^3 h}$	%	$\frac{\$}{kmol}$	$\frac{\$}{kmol}$	$\frac{\$}{kmol}$	%
$j_{sg}(t)$	97.0	97.2	241.7	41.7	97.8	77.0	22.8	730.4	+0.4
$j_{sg}(t), T(t)$	97.0	97.4	268.8	38.0	97.9	77.0	22.9	730.3	+0.4
$j_g(t)$	97.0	97.2	242.3	42.0	97.9	77.0	22.3	729.7	+0.3
$j(t)$	97.0	97.2	242.2	42.5	97.9	76.9	22.1	728.9	+0.2
$j_g(t), T(t)$	97.0	97.2	232.8	41.9	98.0	76.9	22.2	728.5	+0.1
$j(t), T(t)$	97.1	97.1	236.7	42.4	97.9	76.8	22.0	727.8	±0.0

intensification options, representing different degree of freedom, are investigated in a screening. Since in the multi-objective problem of the stand-alone reactor optimization the weighting factors of different performance measures were uncertain, some of them had to be fixed or bounded, such as conversion or STY, in order to generate a Pareto front and to avoid trivial solutions, such as a maximum selectivity at zero conversion. Having the generalized objective production costs the weighting factors are implicitly available and a unique optimum can be calculated.

In Tab. 4.3 the optimal solutions for the investigated intensification options are shown. The deviation of the objective value is very small (maximum 0.4%) indicating that the optimum can actually be approached already with a small degree of freedom since the benefit of using more degree of freedom by more complex control profiles is marginal. All optimal solutions show a conversion of 1-dodecene around 97%, which corresponds to the right bound of the plateau of the selectivity optimum obtained in the optimization of the stand-alone reactor (refer to Fig. 4.9). At the level of the stand-alone reactor, however, no distinction between the optimal points on the plateau could be made. The left bound of the plateau was associated with a lower conversion, hence a higher recycle, and the right side was associated with a high reaction time and low STY, hence a bigger reaction volume. The result of the cost optimization reveals that high conversion is economically more beneficial than a huge recycle of unreacted olefins.

Tab. 4.3 also shows that the process concept that defines the attainable recycle conditions is suitable, since the very high selectivities, that were only obtained by including the recycle condition, can be realized. Further, the sensitivity of the solution on the syngas constraint has almost vanished, since the gas recycle and the mixing of recycle gas and solvent provides an optimal initial condition of the gas in the liquid phase.

(a) Fluxes

(b) Reaction rates

(c) Temperature and pressure

(d) Concentrations in liquid
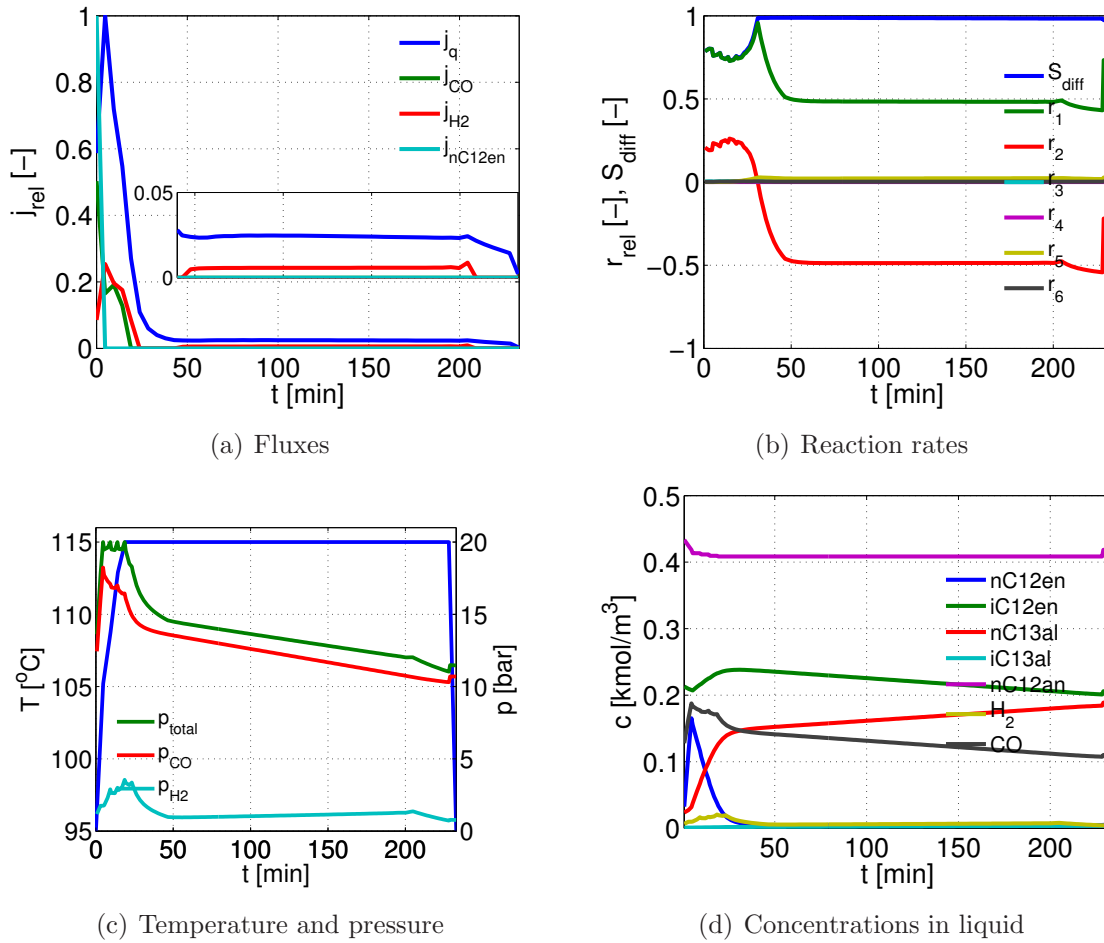
Figure 4.19.: Process wide optimal reaction route considering operation without distributed liquid dosing $(j_g(t), T(t))$.

For the analysis of the reaction route and process performance the optimal solution without liquid dosing is further investigated since taking liquid dosing into account will only lead to small cost reduction of 0.1%.

4.4.7. Optimal Reaction Route

In this section the chosen optimal reaction route without liquid dosing $(jg(t), T(t))$ is further analyzed. The profiles of the control fluxes are illustrated in Fig. 4.19(a) and Fig. 4.19(b). The highest values of the fluxes occur in the first part of the reaction route up to 30 minutes. Initially H_2 and CO are dosed independently with a slightly higher H_2 flux. The gas flux decreases rapidly towards zero at about 25 minutes
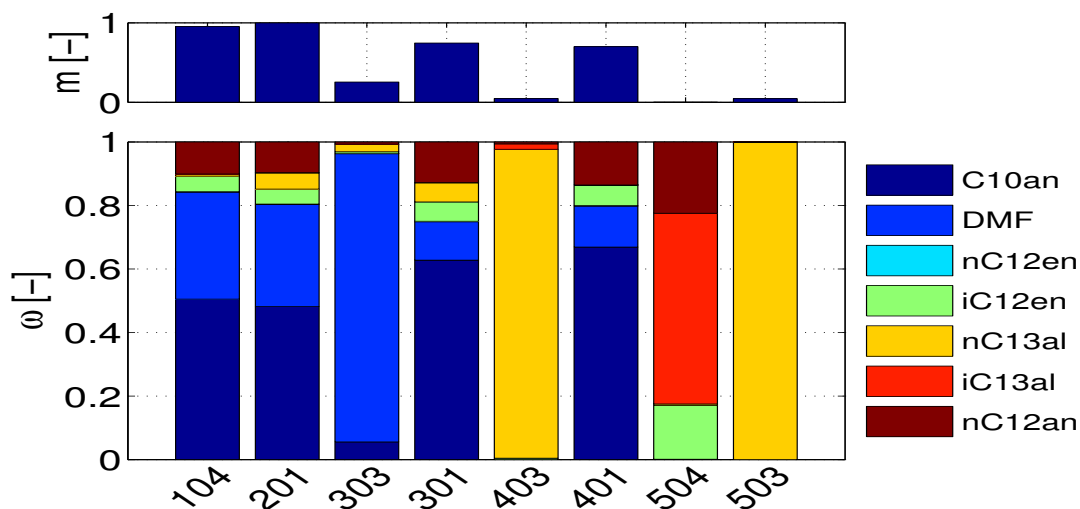
Figure 4.20.: Stream distribution associated with the optimal reaction route considering operation without distributed liquid dosing $(j_g(t), T(t))$.

followed by a batch phase without dosing for 20 min. Shortly before 50 minutes H_2 is dosed as constant profile up to 210 minutes, again followed by a batch phase. Since the heat flux is coupled to the heat of reaction it represents the intensity of the net reaction. Thus, the reaction proceeds in two regimes, a fast reaction regime up to 30 minutes followed by a slow reaction regime with a constant reaction rate until the end of the reaction.

The fluxes in Fig. 4.19(b) correspond to partial pressure and temperature profiles which are shown in Fig. 4.19(c). The optimal temperature profile is a ramp from minimum to maximum temperature over 20 minutes followed by a constant maximum temperature. In the gas phase an excess of CO with a decreasing CO profile is optimal, whereas the partial pressure of hydrogen increases in the first period and maintains at a low level in the second period. In contrast to the selectivity optimal route of the stand alone reactor 4.11(b) the total pressure is not kept constant until the end of the reaction time, which leads to a reduction of the gas recycle stream.

Fig. 4.19(d) shows the concentration profiles of the liquid phase. It can be seen that the initial conditions result directly from the recycles. The concentrations of the side products dodecane and internal dodecene are at a high level, dodecane concentration being about twice the internal dodecene concentration. The high level of these side products leads to a reduction of the reversible side reactions. It should be noted that, in contrast to the result of the stand-alone reactor, the initial concentration of aldehydes is greater than zero, caused by the catalyst recycle. As a result of the two

(a) Total Cost Distribution

(b) Utility Cost Distribution

(c) Investment Cost Distribution
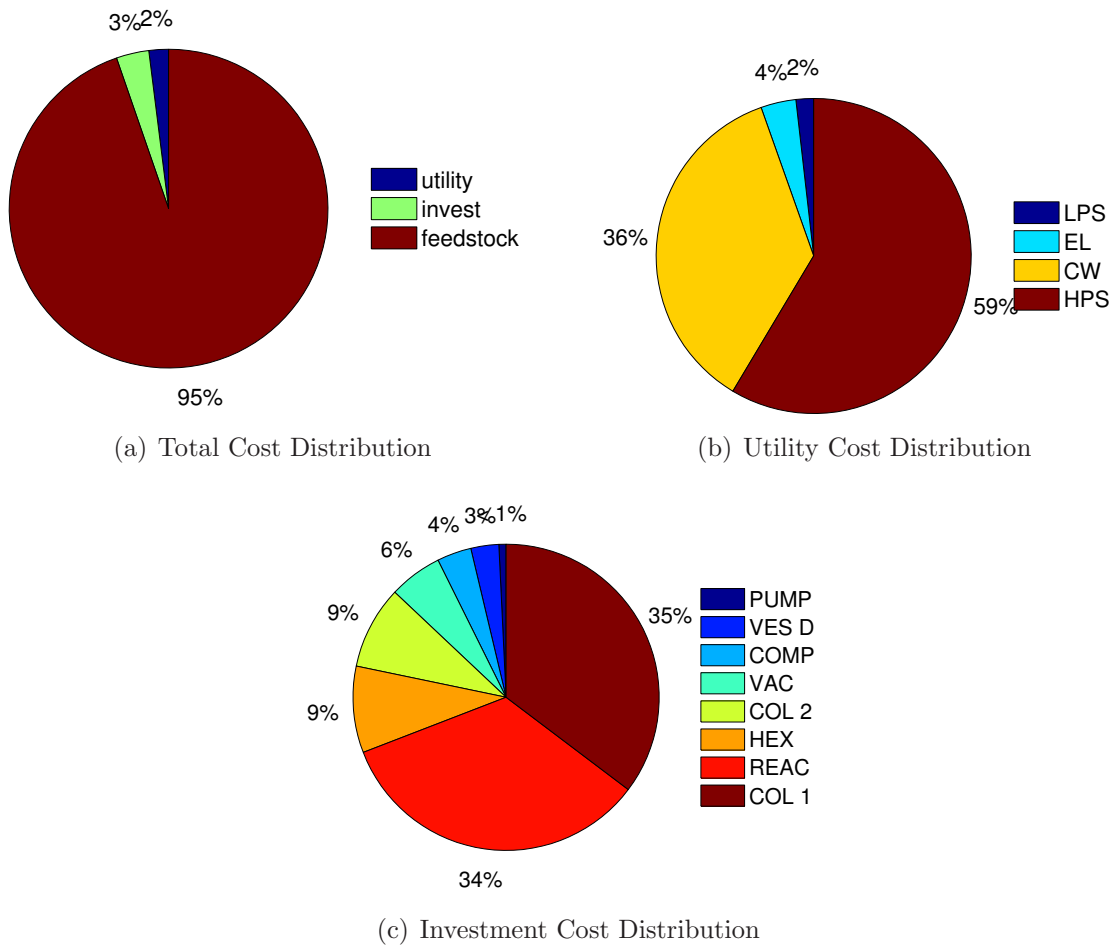
Figure 4.21.: Costs associated with the optimal reaction route considering operation without distributed liquid dosing $(j_g(t), T(t))$.

reaction regimes, also the concentration profiles exhibit two regimes. The first regime is similar to a batch process with respect to 1-dodecene. After the 1-dodecene level reaches a low value the re-isomerization takes place, where the level of 1-dodecene remains constant until the end of the reaction time at about 230 minutes.

The reaction route is embedded into the flux distribution of the process (Fig. 4.20) as it converts the reactor inlet flux (104) into the reactor outlet flux (201). Since the 1-dodecene and syngas is added to the reaction the mass flow of the reactor outlet is higher than the inlet. Main products in the reactor outlet are dodecane, internal dodecene, and the linear aldehyde. The liquid part of the reactor outlet is then divided into the catalyst recycle 303, which contains most of the DMF and some linear aldehyde, and into the organic phase (301) entering column C1. The aldehydes leave the solvent separation column C1 as bottom stream 403 already with a high purity. Solvent and intermediates are recycled back to reactor in stream 401. The iso aldehyde fraction of column C2 (504) contains a rather high content of dodecane and internal dodecene, but the mass flow itself is negligible compared to the product flow rate (503).

The costs associated with the process are shown in Fig. 4.21. The total production costs are mainly determined by the costs of the feedstock, in particular 1-dodecene. The utility costs are dominated by the costs for high pressure steam for columns and heaters. Cooling water contributes as second highest utility cost followed by electricity for pumps and compressors, and low pressure steam for the ejectors. The main equipment contributing to the capital investment are the reactor and the solvent separation column. The investment for the aldehyde separation column is as high as the investment for all heat exchangers. The vacuum equipment is slightly more expensive than the compressors. It can be seen that in case of vacuum service the investment for the equipment is rather high, while the running expenses are relatively low. The benefit of vacuum distillation is clearly higher than the expenses it takes. After the decanter vessel the liquid pumps have the smallest investment costs.

4.4.8. Influence of Back-Mixing

As discussed previously, the EPF concept is essentially based on a plug flow behavior of the fluid element. Back-mixing is actually the interaction of fluid elements of different age which could be modeled in two ways. The first way would be to introduce dosing and removal fluxes, that remove material of the fluid element at time t_1 and distribute it to different points in time to the same fluid element. This requires inte-

Table 4.4.: Performance of cascades of CSTRs with various tank numbers without intermediate liquid dosing.

Case	S	X	tau	V	n/(n+i)	Utility	Invest	Costs	rel. Costs
	%	%	min	m^3	%	$\frac{\$}{kmol}$	$\frac{\$}{kmol}$	$\frac{\$}{kmol}$	%
1 CSTR	96.3	93.0	159.1	155.3	96.9	77.6	27.4	740.6	+1.8
2 CSTR	96.5	96.4	156.4	139.0	97.2	77.2	27.8	737.5	+1.3
3 CSTR	96.7	96.8	171.2	148.6	97.6	77.0	29.1	736.7	+1.2
10 CSTR	96.8	96.7	117.2	100.5	97.8	76.9	31.5	737.1	+1.3
$j(t), T(t)$	97.1	97.1	236.7	151.4	97.9	76.8	22.0	727.8	±0.0

Table 4.5.: Performance of cascades of CSTRs with various tank numbers with intermediate liquid dosing.

Case	S	X	tau	V	n/(n+i)	Utility	Invest	Costs	rel. Costs
	%	%	min	m^3	%	$\frac{\$}{kmol}$	$\frac{\$}{kmol}$	$\frac{\$}{kmol}$	%
1 CSTR	96.3	93.0	159.1	155.3	96.9	77.6	27.4	740.6	+1.8
2 CSTR	96.8	90.0	151.1	132.2	97.5	77.2	27.5	735.2	+1.0
3 CSTR	96.9	88.0	156.1	128.9	97.7	77.0	28.2	734.1	+0.9
10 CSTR	97.1	75.0	134.4	114.0	98.2	76.8	32.9	736.5	+1.2
$j(t), T(t)$	97.1	97.1	236.7	151.4	97.9	76.8	22.0	727.8	±0.0

gral constraints on the fluxes. The second way would be a population balance model of a population of fluid elements of different age which are able to exchange fluxes with each other. In any case the optimization problem would become very complex and model reduction methods have to be used, such as moment approximations of the integral parts which have been widely used in the field of fluid dynamics [76], crystallization [77], or biological virus production models [78].

However, such an extension of the EPF concept is not part of this thesis, hence the possibility of cost reduction due to back-mixing is investigated by comparison of the optimal EPF reaction route with an optimized cascade of CSTRs. As introduced previously, the cascade is subject to optimal fluxes and temperatures in each tank. In order to investigate the pure effect of back-mixing in a first scenario no dosing of liquid is allowed, since this would overlap with the back-mixing effect. In the second scenario dosing of liquid is possible. To change the degree of back-mixing the number of tanks of the cascade is changed. The single CSTR represents ideal back-mixing while increasing the number of tanks decreases back-mixing. Tab. 4.4 and Tab. 4.5 summarize the results of the two scenarios. In both cases a cascade with three tanks represents the cost-optimal configuration. This leads to the conclusion that an ideally segregated flow as represented by the EPF solution is actually not necessary, which might be important to know for the technical approximation of the optimal reaction route.

The cascade with three tanks without liquid dosing (Tab. 4.4) leads to 1.3% higher productions costs, which is due to lower conversion and selectivity compared to the optimal reaction route. Allowing for liquid dosing the production costs can be reduced, but they are still 0.9% higher than the optimal solution (Tab. 4.5). In both scenarios it can be seen that increasing the number of tanks in the cascade leads to higher investment costs, although the total reactor volume of the cascade is smaller than the EPF solution, but according to the economy of scale, increasing the number is more expensive than increasing the volume. Comparing the performance of the cascades with and without liquid dosing, one can conclude that liquid dosing leads to higher selectivities (about 0.3%) but much lower conversion.

4.4.9. Variation of Olefin Price

As shown in the previous section, the olefin price has the highest impact on the total production costs. Now it lies on hand to investigate the effect of the olefin price on the process and reactor performance. Therefore the olefin price is varied as constant pa-
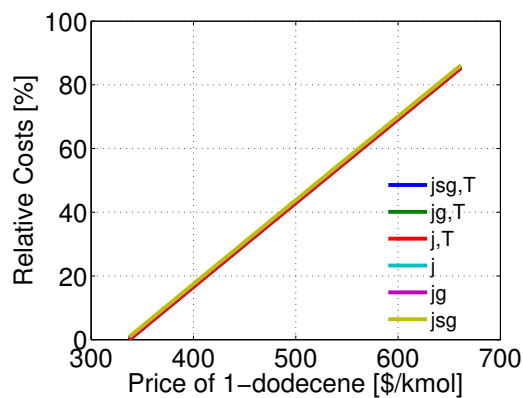
(a) Relative Production Costs
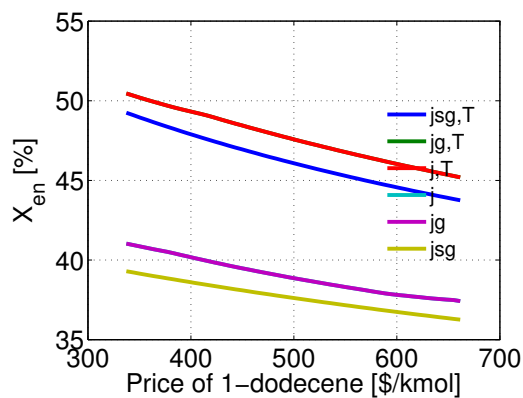
(b) Conversion of Olefin
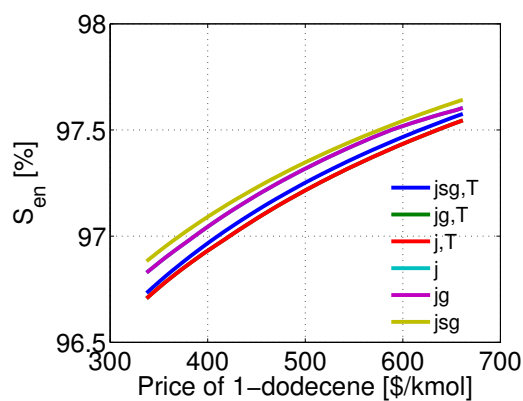
(c) Selectivity
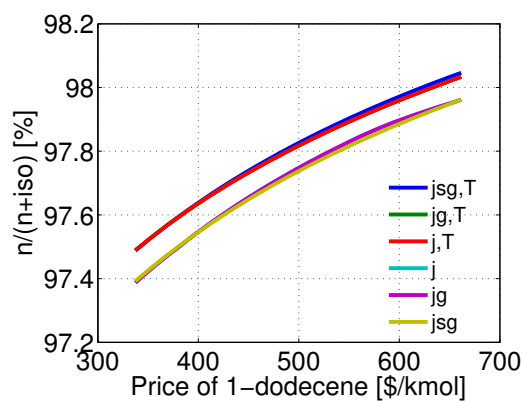
(d) n/iso Aldehyde Ratio

Figure 4.22.: Influence of olefin price on total production costs and reactor performance. Comparison of different intensification options.

(a) Fluxes

(b) Concentrations

(c) Investment Costs

(d) Mass Fractions
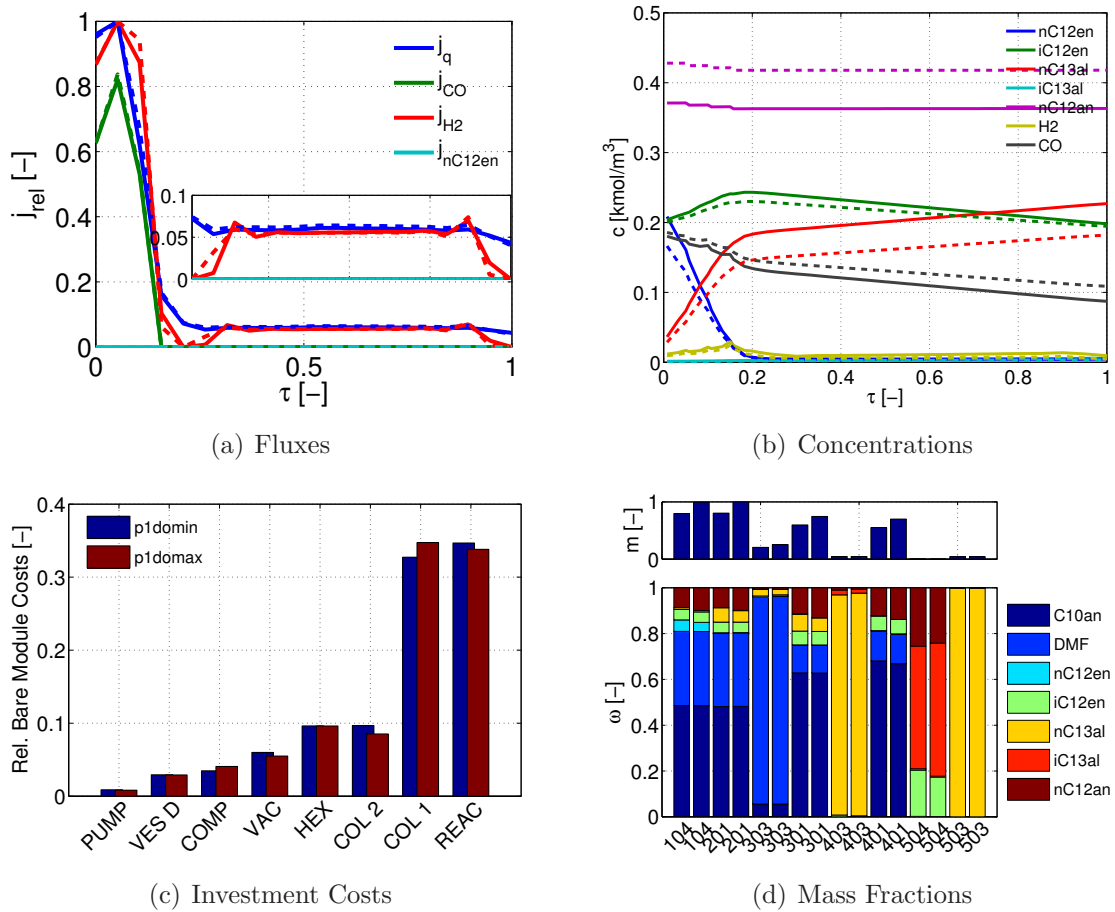
Figure 4.23.: Comparison of cost optimal reaction route at minimum (solid) and maximum (dashed) olefin price.

Table 4.6.: Comparison of main cost factors for minimum and maximum olefin price.

Costs	$P_{\text{olefin,min}}$ [$\$/kmol$]	$P_{\text{olefin,max}}$ [$\$/kmol$]	Rel. Change [%]
1-Dodecene	352.16	682.01	93.67
H_2	4.14	4.10	-0.87
CO	4.09	4.07	-0.50
Feedstock	360.38	690.18	91.51
Decan	$1.52 \cdot 10^{-3}$	$3.57 \cdot 10^{-4}$	-76.47
DMF	$1.23 \cdot 10^{-5}$	$1.90 \cdot 10^{-6}$	-84.57
Solvent	$1.53 \cdot 10^{-3}$	$3.59 \cdot 10^{-3}$	-76.53
Electricity	0.56	0.73	30.99
Cooling water	4.37	5.36	22.60
LP Steam	0.22	0.26	16.65
HP Steam	6.98	8.70	24.66
Utilities	12.13	15.05	24.06
Invest	21.40	24.62	15.07
Total	393.92	729.85	85.28

rameter in the optimization problem and for each price an optimization with respect to total production costs is solved. Fig. 4.22 shows how total production costs and reactor performance change with olefin price. The total production costs increase with increasing olefin price in a linear manner (Fig. 4.22(a)). The difference of different intensification options can be considered as constant over the investigated olefin price range. As the olefin price increases, the conversion of olefin decreases (Fig. 4.22(b)), Product selectivity (Fig. 4.22(c)) and n/iso aldehyde ratio (Fig. 4.22(d)) increase. This result shows that increasing the price of the feedstock leads to an improvement of reactor performance with respect to product selectivity on the expense of a higher reactant recycle due to lower conversion.

How does this improvement of the reactor performance happen? In order to answer this question the scenarios of maximum (which corresponds to the nominal olefin price) and minimum olefin price will be investigated in more detail. Since the difference between the investigated intensification options does not change with the olefin price, the optimal reaction route without liquid dosing and variable temperature $(jg(t), T(t))$ is used for the comparison.

Fig. 4.23(a) shows that only minor changes occur in the profiles of control fluxes

over the dimensionless reaction time. However, looking at the concentration profiles (Fig. 4.23(b)), the concentration level of dodecane is increased (dashed lines) if the maximum olefin price is considered. Since the initial condition of dodecane is mainly determined by the solvent separation column, it means, that the separation efficiency of the column has to be increased in order to recycle more of the alkane. The higher alkane level in the reactor reduces the reversible alkane formation reaction (r_3) which increases the selectivity to tridecanal. The reason why the alkane level is not at this higher level for all reaction routes is, that more alkane leads to higher dilution in the reactor, hence a larger reaction volume and reactor costs (Fig. 4.23(c)). The additional alkane increases also duties of heat exchangers (Fig. 4.23(c)) and pumps due to the higher flow rates. This effect is further amplified by the phase splitting condition in the decanter, which requires a constant mass fraction of decane and DMF. Thus, at higher dilution due to recycling the amount of solvent needs to be increased in order to guarantee the liquid-liquid phase split, hence the catalyst separation step. From Fig. 4.23(c) it can also be seen that the investment costs of the solvent separation column are higher at maximum olefin price, but the costs of the aldehyde separation column are almost the same.

Tab. 4.6 gives a comparison of the operating costs. Assuming the minimum olefin price, which is 50% of the nominal price, the total production costs decrease about 55%. Due to the higher selectivity and lower conversion at maximum olefin price less hydrogen and CO is consumed. The solvent makeup is about one magnitude smaller because the separation efficiency of the solvent column is higher, hence less solvent leaves with the iso-aldehyde stream (505). In no case a purge stream is required.

Since the control profiles of the reactor are qualitatively the same over a wide range of olefin price, the optimal reaction route seems to be robust with respect to this aspect.
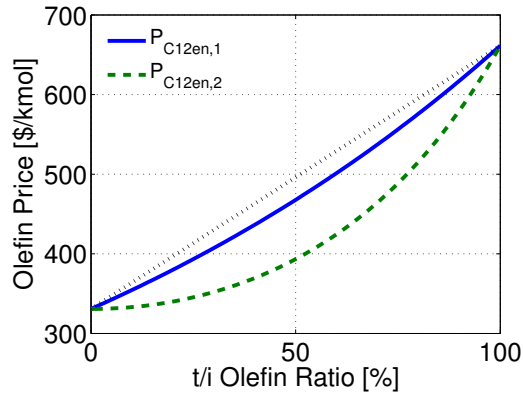
Figure 4.24.: Olefin blend price depending on the ratio of terminal to internal olefin (t/i ratio). Dotted line represents linear relation for comparison.
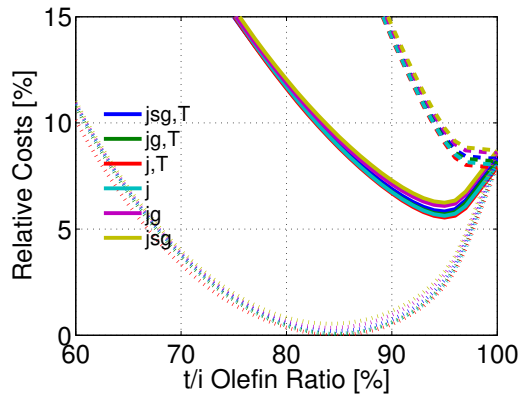
Figure 4.25.: Minimum production costs depending on olefin feed composition. Comparison of different blend price correlations: constant price (dashed lines), price correlation 1 (Eq. 4.65) (solid lines), price correlation 2 (Eq. 4.66) (solid lines).

4.4.10. Composition of the Olefin Feedstock

Since the rhodium catalyst is able to isomerize the olefin in both directions, from 1-dodecene to internal dodecene and reverse, the question arises, if it would be beneficial for the process to use internal dodecene as feedstock directly. As shown from the evaluation of the main cost aspects in the process, the 1-dodecene feedstock is the most expensive part, essentially determining the production costs. Until now only pure 1-dodecene was considered as feedstock. However, assuming that a blend of dodecene with lower ratio of terminal (t) to internal (i) olefin would be much cheaper compared to highly pure 1-dodecene, there might be a chance for process optimization by optimizing the t/i ratio.

Table 4.7.: Comparison of intensification options for optimal olefin feed composition with variable price of the olefin blend. Olefin blend price according to correlation 1 (Eq. 4.65)

Case	n/i C12en	S_{C12en}	X_{C12en}	STY	n/(n+i)	Utility	Invest	Costs	rel. Costs
	%	%	%	$\frac{mol}{m^3h}$	%	$\frac{\$}{kmol}$	$\frac{\$}{kmol}$	$\frac{\$}{kmol}$	%
$jsg(t)$	95.0	96.2	42.3	51.2	96.9	75.8	20.3	716.8	+0.7
$jg(t)$	95.0	96.2	43.2	55.8	96.9	75.8	19.6	715.7	+0.5
$jsg(t), T(t)$	95.0	96.0	54.4	42.8	96.9	75.5	20.1	714.0	+0.3
$jg(t), T(t)$	95.0	96.0	53.9	47.3	97.0	75.5	19.3	713.1	+0.1
$j(t)$	95.0	96.1	52.9	49.3	96.7	75.5	18.9	712.6	+0.1
$j(t), T(t)$	95.0	96.1	51.9	49.6	96.7	75.4	19.0	712.0	±0.0
$j(t), T(t)$	100.0	97.6	44.3	151.4	97.9	76.8	22.0	727.8	+2.2

Table 4.8.: Comparison of intensification options for optimal olefin feed composition with variable price of the olefin blend. Olefin blend price according to correlation 2 (Eq. 4.66)

Case	n/i C12en	S_{C12en}	X_{C12en}	STY	n/(n+i)	Utility	Invest	Costs	rel. Costs
	%	%	%	$\frac{mol}{m^3h}$	%	$\frac{\$}{kmol}$	$\frac{\$}{kmol}$	$\frac{\$}{kmol}$	%
$jsg(t)$	84.0	91.1	49.7	65.6	93.4	72.1	16.0	678.3	+0.5
$jg(t)$	84.0	90.7	53.6	77.1	93.7	72.1	15.1	677.0	+0.3
$jsg(t), T(t)$	85.0	90.5	64.2	59.3	93.7	71.9	15.6	676.0	+0.2
$jg(t), T(t)$	85.0	90.3	64.2	70.3	94.0	71.9	14.7	675.0	+0.1
$j(t)$	85.0	90.8	61.9	73.0	93.7	72.0	14.6	675.2	+0.1
$j(t), T(t)$	85.0	90.7	61.6	73.3	93.8	71.9	14.6	674.7	±0.0
$j(t), T(t)$	100.0	97.6	44.3	151.4	97.9	76.8	22.0	727.8	+7.9

Table 4.9.: Comparison of optimal reaction routes for different olefin blend price correlations.

Case	t/i C12en	S_{C12en}	X_{C12en}	τ	STY	n/(n+i)	Costs	rel. Costs
	%	%	%	min	$\frac{mol}{m^3h}$	%	$\frac{\$}{kmol}$	%
$P_{\text{olefin}} = \text{const}$	100.0	97.5	45.2	232.0	41.5	98.0	729.9	±0
$P_{\text{olefin}} = f(t/i)$	95.0	96.0	54.1	280.7	47.4	97.0	713.1	-2.3
$P_{\text{olefin}} = f(t/i)^2$	85.0	90.3	64.2	282.8	70.3	94.0	675.0	-7.5

Table 4.10.: Comparison of main cost factors of optimal reaction routes of different correlations of the olefin blend price.

Costs Potential	$P_{\text{olefin}} = \text{const}$ [%]	$P_{\text{olefin}} = f(t/i)$ [%]	$P_{\text{olefin}} = f(t/i)^2$ [%]
1-Dodecene	0.00	-1.34	-5.76
H_2	0.00	1.59	7.97
CO	0.00	0.96	3.91
Feedstock	0.00	-1.31	-5.62
Decan	0.00	751.58	107590.43
DMF	0.00	1487.05	754739.86
Solvent	0.00	755.49	111025.66
Electricity	0.00	-33.27	-59.80
Cooling water	0.00	-25.63	-48.10
LP Steam	0.00	-18.84	-41.64
HP Steam	0.00	-27.57	-52.00
Utilities	0.00	-27.00	-50.81
Invest	0.00	-14.96	-35.69
Total	0.00	-2.30	-7.51
Savings [$M\$/a$]	0.00	0.87	2.84

In order to first investigate the pure chemical benefit of using an optimal blend, the feedstock price will remain constant for all t/i ratios. To investigate the influence of the feedstock price depending on the t/i ratio, the following price correlations are used.

$$P_{\text{blend},1} = \frac{P_{\text{nC12en}}}{2} \cdot \exp\left(\ln 2 \cdot \left(\frac{\dot{n}_{nC12en}}{\dot{n}_{iC12en}}\right)\right) \tag{4.65}$$

$$P_{\text{blend},2} = \frac{P_{\text{nC12en}}}{2} \cdot \exp\left(\ln 2 \cdot \left(\frac{\dot{n}_{nC12en}}{\dot{n}_{iC12en}}\right)^2\right) \tag{4.66}$$

There are two assumptions behind the price correlations. First, the price for pure 1-dodecene is as usual and the price of pure internal dodecene is assumed to be half the price of 1-dodecene. The exponent of the t/i ratio determines the slope of the correlation as illustrated in Fig. 4.24.

From Fig. 4.25 it can be seen that there is no benefit from a chemical point of view (same price for terminal and internal olefin) to use lower grade dodecene because the production costs increase with decreasing t/i ratio. However, assuming lower price

(a) Fluxes

(b) Temperature and pressure

(c) Reaction Rates

(d) Concentrations in liquid
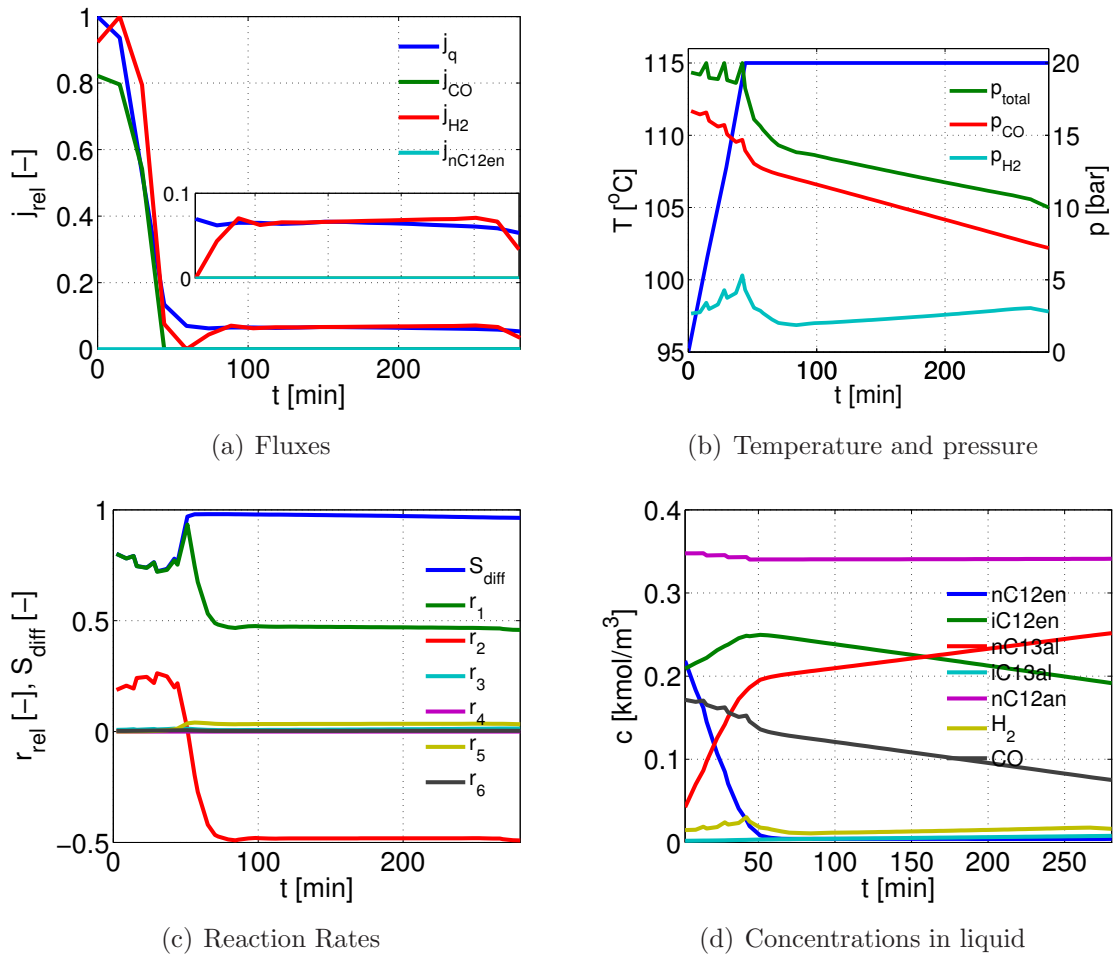
Figure 4.26.: Cost optimal reaction route at optimal olefin blend composition considering olefin blend price correlation 1 (Eq. 4.65) and no liquid dosing $(j_g(t), T(t))$.

(a) Fluxes

(b) Temperature and pressure

(c) Reaction Rates

(d) Concentrations in liquid
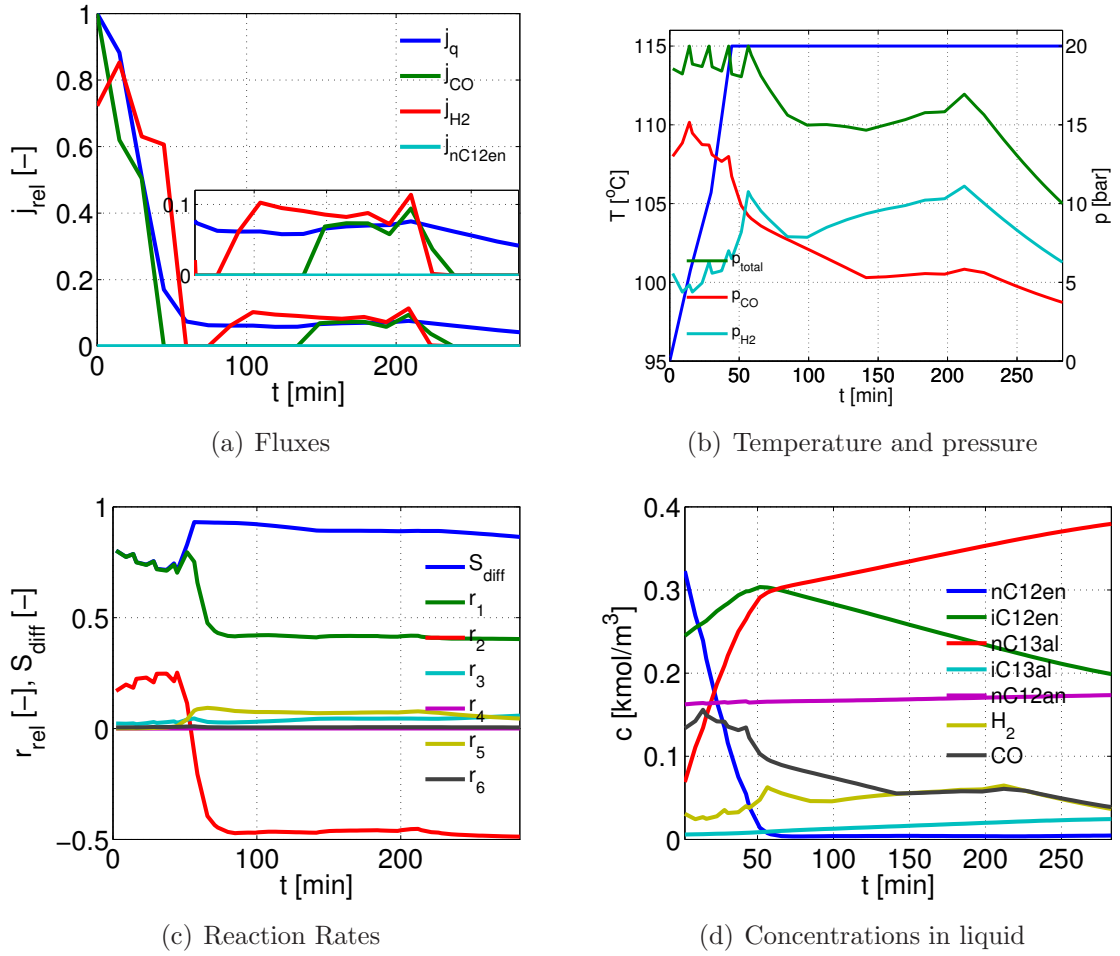
Figure 4.27.: Cost optimal reaction route at optimal olefin blend composition considering olefin blend price correlation 2 (Eq. 4.66) and no liquid dosing $(j_g(t), T(t))$.

with decreasing content of terminal olefin in the feed, yields optimal olefin ratios below 100 %. Assuming the first price correlation (Eq. 4.65) for the olefin blend, the production costs can be reduced about 2.2% at an optimal t/i ratio of 95%. The production costs can be further reduced about 8% if the price of the blend follows the second correlation (Eq. 4.66).

In any case there is no remarkable difference between the various intensification options, they all show approximately the same behavior. Hence, the optimal route with the least degree of freedom can be chosen.

4.4.11. Influence of Catalyst Leaching

In previous chapters the effect of catalyst leaching into the product phase was omitted since there is no reliable mathematical model available that predicts the distribution of the catalyst in organic and aqueous phase. The availability of such a model would actually enable the calculation of a reactor outlet composition which minimizes catalyst leaching if the solvent composition is fixed. If the solvent composition is a degree of freedom a simultaneous optimization of solvent composition, reaction route, and process parameters can be performed. In this section the robustness of the optimal reaction route regarding catalyst leaching is investigated by means of a sensitivity analysis with respect to the catalyst loss ($w_{cat,loss}$). There is still no mechanistic model for the catalyst distribution considered, but $w_{cat,loss}$ is varied as a fixed parameter performing an optimization for each value of $w_{cat,loss}$. The catalyst loss is assumed to be a fraction of the catalyst mass flow in the reactor outlet, which is according to Tab. 4.1 proportional to the molar flow of the solvent. The running expenses for catalyst makeup are calculated based on the price of the rhodium metal and the catalyst loss fraction which is the independent parameter.

$$C_{Rh,loss} = M_{Rh} \cdot \dot{n}_{cat,201} \cdot \omega_{cat,loss} \qquad (4.67)$$

(a) Production Costs

(b) Selectivity

(c) Conversion

(d) n/iso Aldehyde Ratio
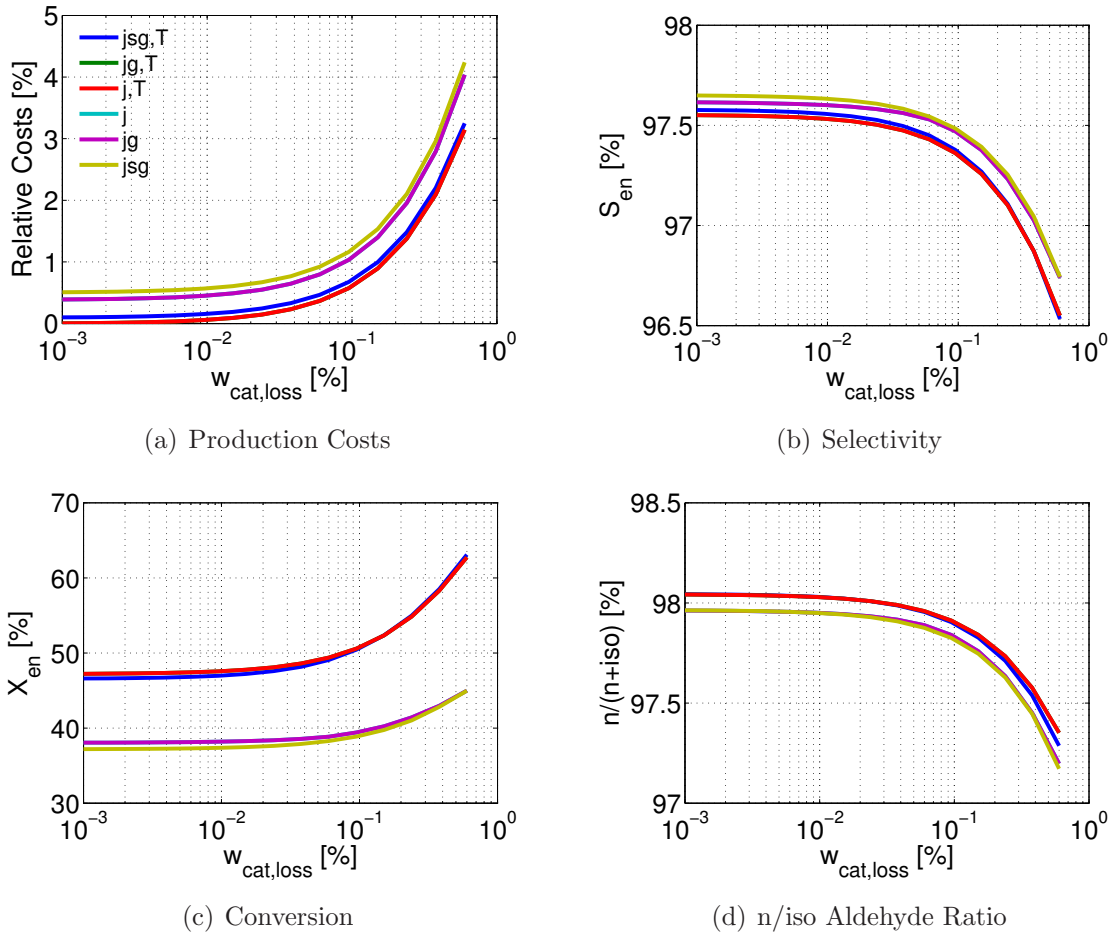
Figure 4.28.: Sensitivity of various performance measures over catalyst loss for different intensification options.

Fig. 4.28 shows a summary of how the catalyst loss affects the various performance measures of process and reactor for different intensification options. The relative production costs increase with increasing catalyst loss exponentially (Fig. 4.28(a)). While this result seems rather trivial, it is interesting that the difference of relative production costs of different intensification options, in particular between options with and without temperature profile increases with increasing catalyst loss. That means that in contrast to a constant optimal temperature, a temperature profile can reduce the production costs at higher catalyst loss, hence the temperature profile enables more robust trajectories. Comparing selectivity, conversion and n/iso ratio, the advantage of the reaction routes with temperature profile is obviously connected to the higher conversion which can be obtained with the temperature profile. As data points related to j and j_g are always overlapped a liquid dosing is not beneficial, hence options

Table 4.11.: Comparison of reactor performance at minimum ($\omega_{cat,loss,min} = 6 \cdot 10^{-4}\%$) and maximum ($\omega_{cat,loss,max} = 0.6\%$) catalyst leaching without liquid dosing $jg(t), T(t)$.

Case	$w_{cat,loss}$	S_{C12en}	X_{C12en}	τ	STY	n/(n+i)	Costs	rel. Costs
	%	%	%	min	$\frac{mol}{m^3 h}$	%	$\frac{\$}{kmol}$	%
CatLossMin	$6 \cdot 10^{-4}$	97.6	47.2	266.6	36.9	98.0	728.7	± 0
CatLossMax	0.6	96.5	62.7	507.9	27.1	97.4	751.6	3.1

$j_g(t), T(t)$ and $j_{sg}(t), T(t)$ should be the best choice.

While the optimal conversion increases with increasing catalyst loss, selectivity and n/iso aldehyde ratio decrease. Thus, it can be concluded that to compensate costs for catalyst makeup it is more beneficial to increase conversion, hence reducing the solvent recycle than increasing product selectivity. Moreover, the conversion is increased on the expense of lower selectivity, hence higher costs for product separation. To get a deeper understanding of the effect of catalyst loss, the optimal reaction routes at minimum ($\omega_{cat,loss} = 6 \cdot 10^{-4}\%$) and maximum ($\omega_{cat,loss} = 0.6\%$) catalyst loss are compared. Tab. 4.11 shows that the higher conversion is also connected to a much higher reaction time, which at 0.6% catalyst loss is about twice as much as at minimum loss. The higher reaction time in combination with a lower selectivity leads to a lower STY. Ultimately increasing the catalyst loss about 0.6% leads to an increase of production costs about 3% which corresponds to an annual loss of $1.2M\$$.

Tab. 4.12 shows the costs in more detail. The lower selectivity and higher conversion at maximum catalyst loss lead to higher feedstock costs. The solvent loss increases about more than an order of magnitude. This indicates a lower separation efficiency of the solvent separation column C1 leading to a higher fraction of solvent in the iso aldehyde stream of C2. All utilities are significantly reduced (about 28%) at maximum catalyst loss. However, at 0.6% catalyst loss the cost for catalyst makeup are about twice as much as utility costs and almost the same as capital investment. The investment costs reduce about 2.6% at high catalyst loss.

Fig. 4.29 illustrates the stream distribution of the process. The higher conversion of the reactor at maximum catalyst loss leads to a significantly lower mass flowrate in the reactor, decanter and solvent column C1 while the aldehyde separation column remains unaffected. In case of high catalyst loss the recycle stream coming from the top of the solvent separation column (stream 401) contains a lower fraction of dode-

Table 4.12.: Comparison of main cost factors for minimum ($\omega_{cat,loss,min} = 6 \cdot 10^{-4}\%$) and maximum ($\omega_{cat,loss,max} = 0.6\%$) catalyst leaching.

Costs	CatLossMin [$/kmol$]	CatLossMax [$/kmol$]	Rel. Change [%]
1-Dodecene	681.68	689.45	1.14
H_2	4.10	4.14	1.04
CO	4.07	4.09	0.63
Feedstock	689.85	697.69	1.14
Decan	$3.50 \cdot 10^{-4}$	$1.59 \cdot 10^{-3}$	353.62
DMF	$1.86 \cdot 10^{-6}$	$1.33 \cdot 10^{-5}$	615.36
Solvent	$3.52 \cdot 10^{-4}$	$1.60 \cdot 10^{-3}$	355.01
Electricity	0.71	0.48	-32.25
Cooling water	5.26	3.88	-26.27
LP Steam	0.26	0.21	-17.59
HP Steam	8.54	6.12	-28.27
Utilities	14.77	10.70	-27.56
Catalyst	0.03	19.80	71515.53
Invest	24.01	23.38	-2.63
Total	728.66	751.57	3.14
Savings [$M\$/a$]	±0	-1.19	
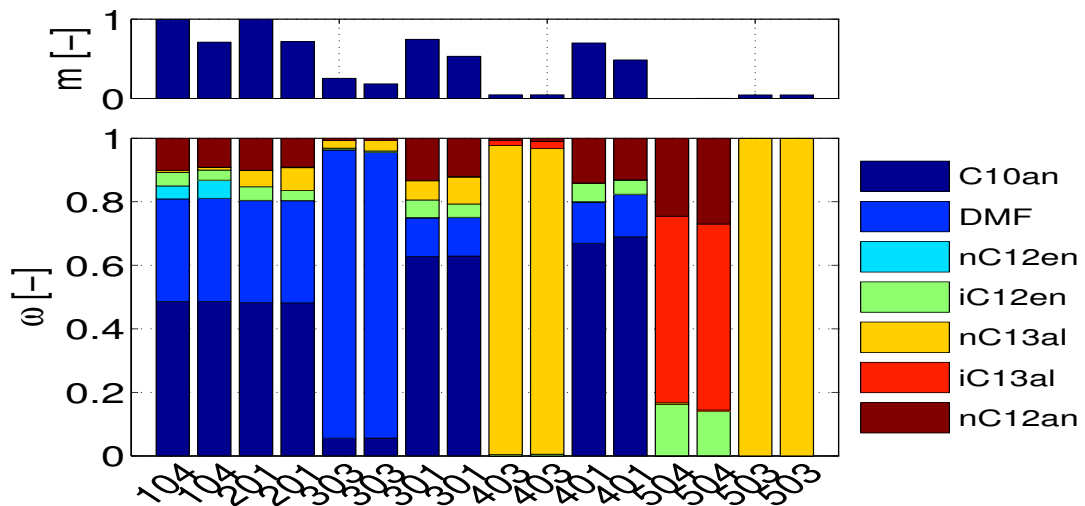
Figure 4.29.: Comparison of stream mass flow distribution at minimum (left stream) and maximum (right stream) catalyst leaching for $jg(t), T(t)$.

(a) Fluxes

(b) Temperature and Pressure

(c) Reaction Rates

(d) Concentrations
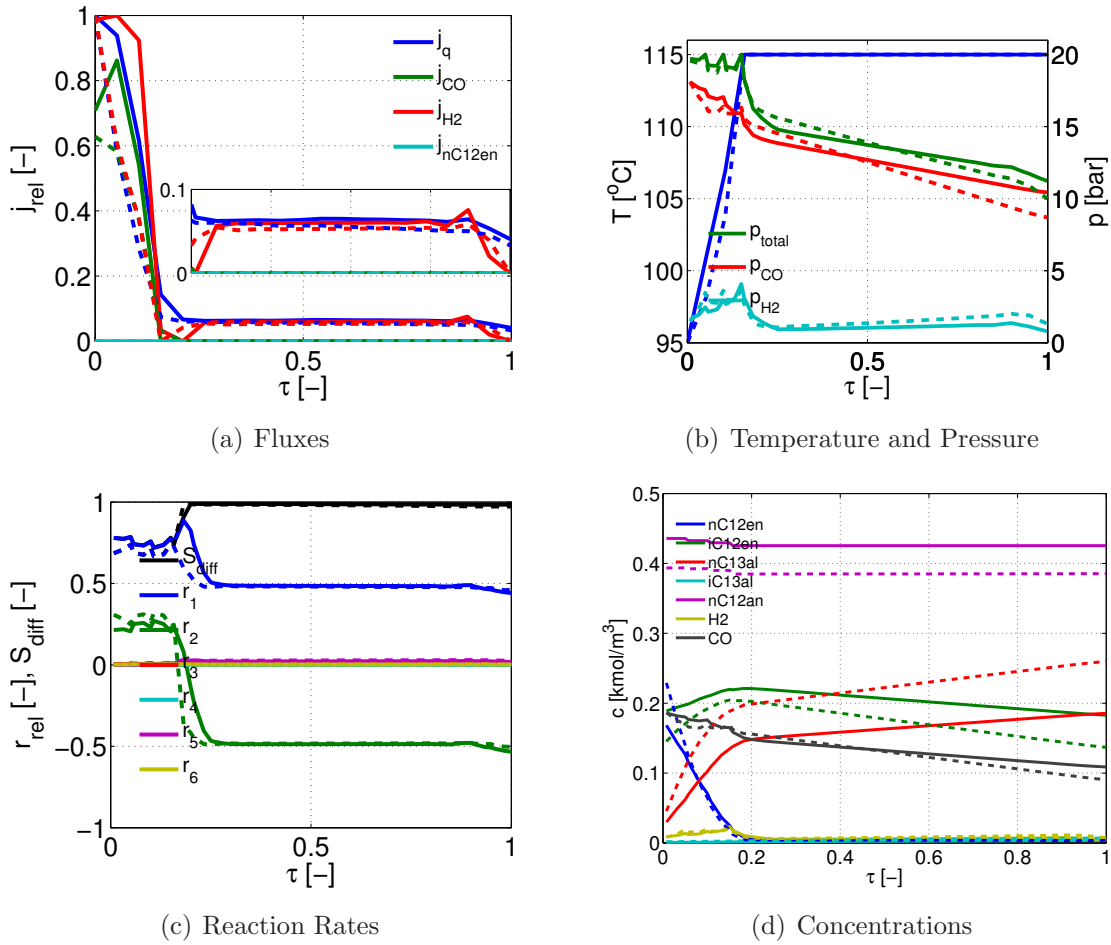
Figure 4.30.: Comparison of optimal reaction routes at minimum (solid) and maximum (dashed) catalyst leaching for $jg(t), T(t)$.

cane and internal dodecene. The higher separation efficiency of the column avoids the buildup of the alkane and dodecene concentration which was previously identified as the reason for a higher selectivity in the reactor. However, a higher recycle leads to a higher mass flow in reactor and decanter. The phase split constraint leads to higher DMF and decane flow, hence higher catalyst flow and catalyst loss.

The control policy in case of high catalyst loss can be summarized as solvent reduction policy. This solvent reduction is achieved by higher conversion to reduce the reactor outlet flow in combination with a lower separation efficiency of the solvent separation column allowing more solvent entering the aldehyde separation column, thus, avoiding the buildup of high alkane and dodecene levels in the solvent loop (refer to Fig. 4.30).

4.4.12. Summary

In this chapter the optimal process concept for the hydroformylation of 1-dodecene in a TMS was derived by simultaneous optimization of reaction concept and process parameters. This approach enables the identification of a distinct cost optimal design for a complex multiphase reaction system.

Supported by the optimal composition of the recycle streams from the stand-alone reactor section a process model embedding the fluid element model as reaction section was derived. For the overall process mathematical models to compute operating and investment costs were set up for each unit. The cost model and the process model were included into the dynamic optimization problem in order to calculate a cost optimal reaction route and optimal process parameters simultaneously.

The cost optimal solution is a trade-off solution of high reactor performance and separation efficiency. There is a high potential for cost reduction when working at high conversion since the solvent separation in column C1 is the most expensive operation.

In order to investigate the influence of backmixing, the costs of the optimal reaction route were compared to the costs of CSTR cascades with varying tank number. It can be shown that a cascade with three CSTRs yields the best approach to the optimal route, while lower tank numbers yield lower selectivity but higher conversion and higher tank numbers yield higher selectivity but also higher reactor costs. Further, CSTR cascades with intermediate dosing of 1-dodecene yield a closer approach to the optimum.

Since the overall production costs are highly dominated by the costs of 1-dodecene sensitivity studies regarding the price and composition of the feedstock were performed. It turned out that a feedstock with higher content of internal dodecene only yields different reaction routes with lower production cost if the price of a olefin blend is much lower than pure 1-dodecene.

Further, the influence of catalyst loss was investigated in a sensitivity study. A higher catalyst loss yields higher conversion and lower separation efficiency in the solvent separation column C1, reducing the solvent circulation rate by avoiding buildup of high alkane and internal dodecene levels.

5. Summary, Conclusion and Outlook

5.1. Summary

In order to explain the different hierarchical levels of a production process and their interactions Freund and Sundmacher [79] proposed the hierarchy pyramid shown in Fig. 5.1. Each of the illustrated levels gives rise for optimization. However, the impact on the total improvement of the production process by manipulating a phenomenon
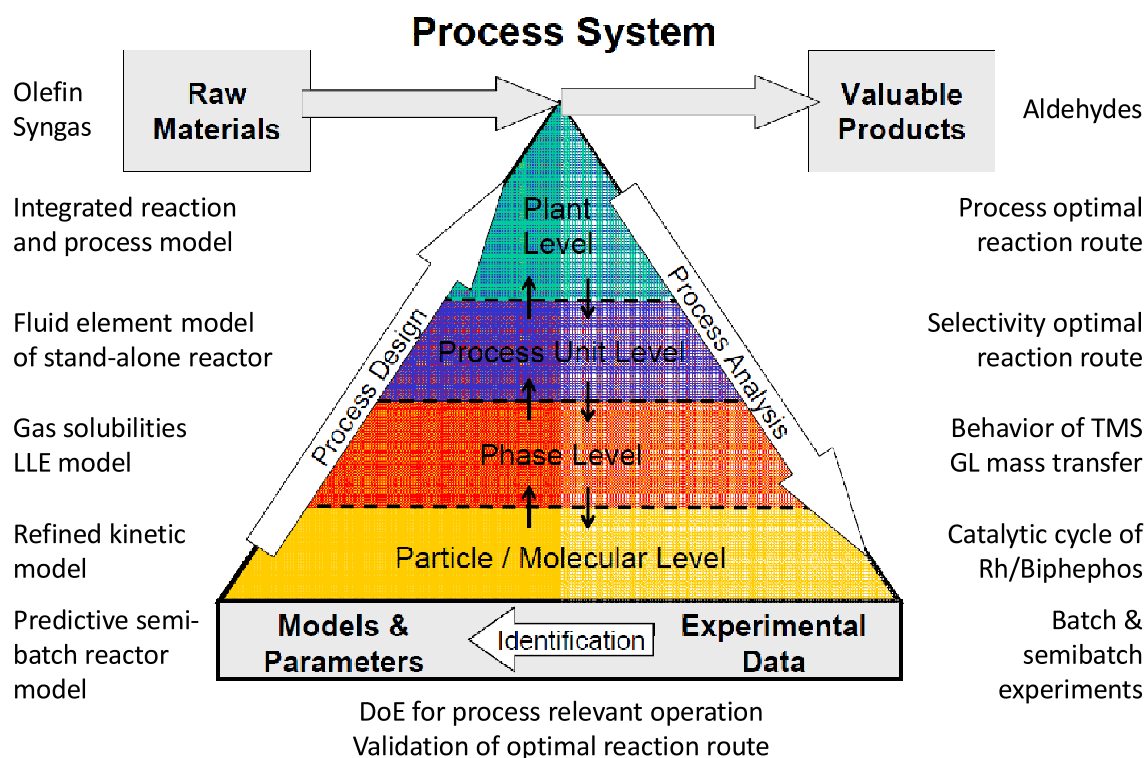
Figure 5.1.: Hierarchical pyramid of chemical production systems related to the hydroformylation system in this thesis. Adapted from [79]. To be read starting from experimental data clockwise.

on a lower level is normally higher than on a higher level. So to say, a bad catalyst performance can barely be compensated by a good process design, but a good catalyst performance normally yields a good process in combination with a suitable process design. That means the lever at the base of the pyramid is more efficient than at the top.

Thus, a good process intensification practice would be to improve each level of the pyramid sequentially beginning at the base upwards. However, the procedure is not strictly towards the top, since feedback is necessary from a higher level, such as in form of an objective that has to be met by the level below.

To summarize the work of this thesis the process pyramid provides a scaffold. The basis of the addressed reaction system was compiled by the choice of the catalyst which was designed to give high activity and selectivity to the desired product to enhance the reaction on the one hand side. On the other hand the ligand was designed to have an affinity to polar solvents, such as DMF. Hence, on the molecular level there is feedback coming from the phase level (catalyst separation task) and from the plant level (product purification task and catalyst recovery task). However, these aspects are not in the scope of this thesis. Concerning this thesis, the catalyst recovery concept and the corresponding choice of catalyst and solvent was defined before and is not subject to optimization here.

Starting with the given catalyst and solvent system and having preliminary reaction kinetics and a reaction mechanism available, the first step of this thesis was the identification of a promising operation window. For that purpose a mathematical model of a semi-batch reactor was formulated and used for dynamic optimization. It turned out, that maximum selectivity to the product is obtained at high conversion of 1-dodecene and the optimal concentration profiles revealed that the re-isomerization reaction is crucial for the overall reaction performance. Hence, validation experiments were planned in order to identify the kinetic parameters of the isomerization reaction. With the proposed validation experiments the kinetic parameters as well as the reaction network could be refined to yield a higher predictability of the model. Based on the predictive model two selectivity optimal trajectories (with and without recycle condition) were calculated and successfully validated in semi-batch experiments. It was found that the reaction performance can be drastically improved by recycling the isomeric olefin back to the reactor. The recycle leads to a high level of isomeric olefin in the reactor and thus, an inhibition of the unwanted isomerization reaction.

The validated dynamic model was then used to calculate apparatus independent optimal reaction routes with and without recycle conditions. Different objectives as

well as various intensification options by means of included control fluxes have been screened. The screening showed that recycling of isomeric olefin is always superior and that different objective functions yield contradictory results, such as inverse correlation of maximum selectivity and maximum n/iso ratio. Since a multitude of relevant objectives exist for the reaction system only a Pareto-optimal solution can be found, but ultimately the optimal reaction route depends on the impact of the reactor output on the downstream processing by means of operational and equipment costs. Hence, in the next step a process model was formulated and the optimal reaction route in combination with the optimal process parameters was calculated simultaneously minimizing the total annualized production costs of tridecanal. With this approach the definition of a local objective function for the reactor becomes unnecessary, but it turned out that, due to the high costs of the olefin feedstock, the selectivity optimal reaction route is a good representation of the process wide objective.

In order to investigate the sensitivity of the results with respect to variations in process parameters sensitivity studies have been performed.

Shortly summarized, the main achievements of this thesis are:

- Identification of kinetic parameters for the hydroformylation of 1-dodecene in a TMS by means of model based design of experiments.

- Calculation of the selectivity optimal reaction route for the hydroformylation of 1-dodecene in TMS for a semi-batch reactor, based on the obtained parameters.

- Experimental validation of predicted optimal reaction routes in semi-batch experiments and thereby proving the practical applicability of the EPF concept.

- Evaluation of different objective functions for the optimization of the reaction route for 1-dodecene hydroformylation in TMS.

- Development of a design strategy for reactor design within an integrated process comprising three stages: reactor without recycle, with ideal (selective) recycle, and with realistic recycle.

- Evaluation of the influence of backmixing on the optimal reaction route by comparison with a CSTR cascade model.

- Assessment of the relation of mass transfer and catalyst concentration.

- Development of an integrated reaction and process model for the hydroformylation of 1-dodecene in TMS including short cut models for a three phase decanter

and vacuum columns to evaluate equipment sizes and equipment costs.

- Development of an economic model to evaluate operational and investment costs as basis for the minimization of total production costs of the desired linear aldehyde.

- Identification of the process wide optimal reaction route of the hydroformylation of 1-dodecene in a TMS.

5.2. Conclusion

Based on the results summarized above it can be concluded that the EPF concept cannot only be applied for reactor design purposes, but it also facilitates the design of experiments by means of calculating reaction routes which are suitable to estimate the kinetic parameters in a practically important operation window. By analyzing the optimal reaction route based on preliminary parameters the experimental conditions for the parameter refinement can be calculated.

Further it was shown that for the application of the EPF concept possible recycling of intermediates should always be considered, which is not intuitive in the first place since the intermediates and reversible reactions are not an explicit feed stream. Especially concerning complex reaction networks with many intermediates the model should contain the possibility of recycling to evaluate the possibility of selective recycles.

By evaluating several possible objective functions it was found that the definition of a single objective function based on chemical engineering measures, such as selectivity or space-time yield, does not necessarily represent process wide optimality. Actually the objective which represents the process in a whole would be a linear combination of several local objectives. This, however, yields two problems:

- The weighting factors of the local objectives depend on the importance of the measure in the process, such as in case of the n/iso ratio, the costs of the n/iso separation.

- The weighting factors are not constant, since there is feedback between reactor and downstream process via the recycles.

Thus, the only reasonable objective is the total production costs of the process, which can be called a generalized objective function for the whole process. In analogy to the

famous sentence of Aristoteles: "The whole is more than the sum of its parts" [80], a process of locally optimal units is not necessarily the optimal process. Especially in liquid multiphase systems, which inherently contain more recycles than e.g. single phase systems, the process should be optimized as an integrated system.

5.3. Outlook

Although this work assesses the influence of backmixing on the optimal reaction route by comparison with CSTR cascades, but this aspect is still not rigorously included in the EPF approach. The effect of backmixing is indirectly included in the reactor design approach of Peschel [38] as one way of interpreting constant dosing fluxes. However, this is not totally true, since backmixing is not selective but affects all components of the fluid element. Since backmixing can be approximated by constant dosing fluxes it may not be important to explicitly include it in case of the stand-alone reactor when a chemical engineering objective is used. However, regarding a cost optimal reaction route it may make a difference.

The reactor design method should be extended to comprise back-mixing, thus residence time distribution. In terms of the fluid element concept a residence time distribution results from a population of fluid elements with different residence time through the reactor which are able to exchange matter and energy among each other. The population of fluid elements could be modeled using the method of moments using residence time as the property coordinate. The moment model could then efficiently be solved using the sigma point method.

Further, it would be beneficial to set up a rigorous multiphase model of the reaction system, based on an equation of state model, in order to use a single model to describe the entire process. For that purpose a convenient programming environment should be established which enables external function calls, such as python or gproms. Having such a model implemented would enable the calculation of multifunctional modules, such as simultaneous reaction and phase separation in order to identify innovative reaction routes and to fully exploit the thermodynamic state space, which is not possible with the presented simplified model. However, it seems unlikely at the moment to compile such a model which is predictive over a wide range of operating conditions due to lack of experimental data.

In order to fully exploit the effect of catalyst leaching on the reactor performance a comprehensive thermodynamic model for the catalyst separation section is neces-

sary. In this way the reactor can provide outlet compositions which minimize catalyst loss.

The most important extension of the EPF approach might be the inclusion of uncertainty in order to predict robust optimal reaction routes that can be provide a reliable process performance even if the model parameters slightly change due to model uncertainty or process parameter uncertainty.

List of Figures

List of Tables

A. Appendix

A.1. Parameters of Reaction Kinetics

Table A.1.: Gas solubility parameters (Eq. (4.2)).

Component	$a_{H,0} \left[\frac{MPam^3}{kmol} \right]$	$E_{A,H} \left[\frac{kJ}{mol} \right]$
H_2	$9.10 \cdot 10^2$	10.173
CO	$3.55 \cdot 10^4$	22.975

Table A.2.: Original parameters for reaction kinetics (Eqs. (4.3) and (4.7)) from Kiedorf et al. [13].

Variable	Eq.	E_A	k_0	K_1	K_2	K_3
r_1	(4.3)	113.08	$5.00 \cdot 10^7$	$5.75 \cdot 10^2$	$3.02 \cdot 10^3$	$1.17 \cdot 10^4$
r_2	(4.4)	136.89	$6.96 \cdot 10^2$	$3.86 \cdot 10^1$	$2.26 \cdot 10^2$	-
r_3	(4.5)	76.11	$1.40 \cdot 10^2$	2.66	7.1	1.28
r_4	(4.6)	102.26	$7.00 \cdot 10^{-1}$	-	-	-
r_5	(4.7)	120.84	$6.00 \cdot 10^2$	-	-	-
C_{cat}	(4.9)	-	-	10	1	-

Table A.3.: Equilibrium constants (Eq. (4.11)).

Variable	$a_0[kJ/mol]$	$a_1[kJ/mol/K]$	$a_2[kJ/mol/K^2]$
$k_{p,3}$	-11.00	0	0
$k_{p,4}$	-126.28	$1.27 \cdot 10^{-1}$	$6.80 \cdot 10^{-6}$

Table A.4.: Parameters of reaction kinetics (Eqs. (4.3)–(4.21)) from Kiedorf et al. [13]. Reaction r_6 was added and frequency factors $k_{0,j}$ and catalyst parameters $K_{cat,1/2/3}$ were adjusted to semibatch experiments in this work. The refined parameters are emphasized in bold numbers.

Variable	Eq.	$E_A \left[\frac{kJ}{mol}\right]$	k_0	Unit	$K_1 \left[\frac{ml}{mol}\right]$	$K_2 \left[\frac{ml}{mol}\right]$	$K_3 \left[\frac{ml}{mol}\right]$
r_1	(4.3)	113.08	$\mathbf{4.904 \cdot 10^{16}}$	$\frac{ml^3}{gminmol^2}$	574876	3020413	11732838
r_2	(4.4)	136.89	$\mathbf{4.878 \cdot 10^6}$	$\frac{ml}{gmin}$	38632	226214	-
r_3	(4.5)	76.11	$\mathbf{2.724 \cdot 10^8}$	$\frac{ml^2}{gminmol}$	2661.2	7100	1280
r_4	(4.6)	102.26	$\mathbf{2.958 \cdot 10^4}$	$\frac{ml^2}{gminmol}$	-	-	-
r_5	(4.7)	120.84	$\mathbf{3.702 \cdot 10^{10}}$	$\frac{ml^3}{gminmol^2}$	-	-	-
r_6	(4.21)	113.08	$\mathbf{3.951 \cdot 10^{11}}$	$\frac{ml^3}{gminmol^2}$	-	-	-
C_{cat}	(4.9)	-	-	-	$\mathbf{3.041 \cdot 10^4}$	$\mathbf{0}$	$\mathbf{0.644}$

Table A.5.: Relative confidence intervals of kinetic parameters given in Tab. A.4. Values of refined parameters are emphasized in bold. Values of original parameters before refinement are given in brackets.

Variable	Eq.	E_A	k_0	K_1	K_2	K_3
r_1	(4.3)	±33.0%	$\mathbf{\pm13.9}$% (±34.0%)	±355.0%	±270.0%	±1.0%
r_2	(4.4)	±29.0%	$\mathbf{\pm9.7}$% (±10.0%)	±252.1%	±21.0%	-
r_3	(4.5)	±26.0%	$\mathbf{\pm8.5}$% (±95.0%)	±139.1%	±97.2%	±117.2%
r_4	(4.6)	±13.0%	$\mathbf{\pm6832.3}$% (±1842.9%)	-	-	-
r_5	(4.7)	±408.0%	$\mathbf{\pm5.1}$% (±144.0%)	-	-	-
r_6	(4.21)	-	$\mathbf{\pm10.9}$%	-	-	-
C_{cat}	(4.9)	-	-	$\mathbf{\pm84.1}$% (±205.0%)	- (±59.4%)	$\mathbf{\pm12.4}$%

A.2. Parameters for Substance Properties

Table A.6.: Parameters for density correlation (Eq. (4.37)).

Component	a_0	a_1
C10an	981.60	$-8.3536 \cdot 10^{-1}$
DMF	1256.52	-1.0306
nC12en	993.89	$-7.8875 \cdot 10^{-1}$
nC12an	977.04	$-7.6743 \cdot 10^{-1}$
nC13al	1068.12	$-8.0180 \cdot 10^{-1}$
iC12en	993.89	$-7.8875 \cdot 10^{-1}$
iC13al	1068.12	$-8.0180 \cdot 10^{-1}$

Table A.7.: Parameters for heat capacities and enthalpies (Eqs. (4.38)).

Component	$h_{f,0} \cdot 10^{-5}$	$p_{Cp,0}$	$p_{Cp,1} \cdot 10^3$	$p_{Cp,2} \cdot 10^5$	$p_{Cp,3} \cdot 10^8$	$p_{Cp,4} \cdot 10^{12}$
DMF	-1.911874	63.727	607.08	-161.63	185.6	0
C10an	-2.482645	79.741	1692.6	-452.87	497.693	0
H2	0	25.399	20.178	-3.8549	3.188	-8.7588
CO	-1.105300	29.556	-6.5807	2.013	-1.2227	2.2617
nC12en	-1.638537	129.203	1584.2	-404.61	438.51	0
iC12en	-1.638537	129.203	1584.2	-404.61	438.51	0
nC12an	-2.892453	84.485	2035.8	-509.81	521.86	0
nC13al	-3.902267	74.377	2437.9	-567.13	540.89	0
iC13al	-3.902267	74.377	2437.9	-567.13	540.89	0

Table A.8.: Parameters of conversion dependent LLE distribution coefficient in decanter section (Eq. (4.45)).

Component	$a_0 \cdot 10^2$	$a_1 \cdot 10^5$	$a_2 \cdot 10^4$
DMF	922.45	-7393.7	2.4187
C10an	3.5035	16.716	0
nC12en	4.4237	17.022	0
iC12en	4.0267	16.573	0
nC12an	3.8857	-8.6453	0
nC13al	25.422	-28.025	0
iC13al	25.422	-28.025	0

Table A.9.: Parameters for vapor pressure correlations

Correlation 1: $p_{\mathrm{vap},i} = 0.1 \cdot \exp\left(a_0 + \frac{a_1}{T} + a_2 \ln(T) + a_3 T^{a_4}\right)$ from [68]

Correlation 2: $p_{\mathrm{vap},i} = 10^{\left(a_0 + \frac{a_1}{T} + a_2 \log_{10}(T) + a_3 T + a_4 T^2\right)} \cdot 133 \cdot 10^{-6}$ (fitted to ASPEN property data).

Component	Correl.	a_0	a_1	a_2	a_3	a_4
DMF	1	-47.99	-2385	28.80	$-5.86 \cdot 10^{-2}$	$3.139 \cdot 10^{-5}$
C10an	1	26.51	-3358	-6.12	$-3.32 \cdot 10^{-10}$	$4.855 \cdot 10^{-7}$
nC12en	1	-8.59	-3524	10.81	$-2.82 \cdot 10^{-2}$	$1.427 \cdot 10^{-5}$
nC12an	1	-5.65	-3470	9.03	$-2.32 \cdot 10^{-2}$	$1.124 \cdot 10^{-5}$
nC13al	1	161.50	-9766	-55.59	$2.10 \cdot 10^{-2}$	$5.550 \cdot 10^{-13}$
iC12en	2	75.79	-9964	-8.97	$4.94 \cdot 10^{-18}$	6
iC13al	2	10.42	-6149	0.20	$-2 \cdot 10^{-4}$	1

Table A.10.: Parameters for heat of vaporization (Eq. (A.56)) taken from the literature [68].

Component	a_1	a_2	a_3
DMF	59.355	647	0.381
C10an	71.428	618	0.451
nC12en	77.166	658	0.407
nC12an	78.802	657	0.437
nC13al	95.624	700	0.414
iC12en	77.229	663	0.403
iC13al	95.624	700	0.414

A.3. Connectivity Constraints

A.3.1. Solvent Composition

To ensure the feasibility of the reaction kinetics and to guarantee the phase split in the decanter, the mass fractions of the solvents are fixed in the reactor outlet stream.

$$n_{\text{cat,R}} = x_{\text{cat}} \frac{w_{\text{nC12en}}}{w_{\text{DMF}}} \frac{M_{\text{DMF}}}{M_{\text{nC12en}}} n_{\text{liq,DMF}}(t_0) \tag{A.1}$$

$$w_{\text{C10an}} \cdot \sum_{i \in \text{COM}} (\dot{n}_{i,201} \cdot M_i) = \dot{n}_{\text{C10an,201}} \cdot M_{\text{C10an}} \tag{A.2}$$

$$w_{\text{DMF}} \cdot \sum_{i \in \text{COM}} (\dot{n}_{i,201} \cdot M_i) = \dot{n}_{\text{DMF,201}} \cdot M_{\text{DMF}} \tag{A.3}$$

All streams in the flowsheet are connected via connectivity constraints for molar streams, pressure, and temperature.

A.3.2. Composition

The connectivity constraints for molar streams are the following:

$$\dot{n}_{i,001} = 0 \qquad\qquad , i \in \text{COM} \setminus \{\text{nC12en}, \text{C10an}, \text{DMF}\} \qquad \text{(A.4)}$$

$$\dot{n}_{i,101} = \sum_{s \in \{001,304,402\}} \dot{n}_{i,s} \qquad\qquad \text{(A.5)}$$

$$\dot{n}_{i,101} = \dot{n}_{i,s} \qquad\qquad , s \in \{102, 103\} \qquad \text{(A.6)}$$

$$\dot{n}_{i,104} = \sum_{s \in \{103,308\}} \dot{n}_{i,s} \qquad\qquad \text{(A.7)}$$

$$\dot{n}_{i,105} = 0 \qquad\qquad , i \in \text{COM} \setminus \text{FEED} \qquad \text{(A.8)}$$

$$\dot{n}_{\text{C1,in},i} = \dot{n}_{i,s} \qquad\qquad , s \in \{301, 302\} \qquad \text{(A.9)}$$

$$\dot{n}_{i,405} = \dot{n}_{\text{C1,D},i} \qquad\qquad , i \in \text{COM} \setminus \text{GAS} \qquad \text{(A.10)}$$

$$\dot{n}_{i,s} = \dot{n}_{\text{C1,B},i} \qquad\qquad , s \in \{403, 404\} \qquad \text{(A.11)}$$

$$\dot{n}_{\text{C2,in},i} = \dot{n}_{i,404} \qquad\qquad \text{(A.12)}$$

$$\dot{n}_{i,s} = \dot{n}_{\text{C2,D},i} \qquad\qquad , s \in \{504, 505, 507\} \qquad \text{(A.13)}$$

$$\dot{n}_{i,s} = \dot{n}_{\text{C2,B},i} \qquad\qquad , s \in \{503, 506, 508\} \qquad \text{(A.14)}$$

$$\dot{n}_{i,406} = x_{\text{purge},405} \cdot \dot{n}_{i,405} \qquad\qquad \text{(A.15)}$$

$$\dot{n}_{i,s} = (1 - x_{\text{purge},405}) \cdot \dot{n}_{i,405} \qquad\qquad , s \in \{401, 402\} \qquad \text{(A.16)}$$

$$\dot{n}_{i,306} = x_{\text{purge},305} \cdot \dot{n}_{i,305} \qquad\qquad \text{(A.17)}$$

$$\dot{n}_{i,s} = (1 - x_{\text{purge},305}) \cdot \dot{n}_{i,405} \qquad\qquad , s \in \{307, 308\} \qquad \text{(A.18)}$$

A.3.3. Temperature

The connectivity constraints for temperature are the following:

$$T_s = T_{\text{cw}} \qquad\qquad , s \in \{001, 105, 106\} \qquad \text{(A.19)}$$

$$T_{104} = T_{\text{R}}(t_0) \qquad\qquad \text{(A.20)}$$

$$T_{201} = T_{\text{R}}(t_f) \qquad\qquad \text{(A.21)}$$

$$T_{308} = T_{307} \cdot \left(\frac{p_{308}}{p_{307}} \right)^{\frac{(1.4-1)}{1.4 \cdot N_{\text{CPS}}}} \qquad\qquad \text{(A.22)}$$

$$T_{601} = T_{\text{dew,C1,D}} \qquad\qquad \text{(A.23)}$$

$$T_{603} = T_{\text{dew,C2,D}} \qquad\qquad \text{(A.24)}$$

$$T_s = T_{\text{D}} \qquad\qquad , s \in \{202, 301, 303, 304, 305, 306, 307\} \qquad \text{(A.25)}$$

$$p_{\text{reb,C1}} = \sum_{i \in \text{COM} \backslash \text{GAS}} \left(p^{\text{vap}}_{302,i}(T_{302}) \cdot x_{i,302} \right) \tag{A.26}$$

$$T_s = T_{\text{bub,C1,D}} \qquad\qquad\qquad , s \in \{401, 402, 405, 406\} \tag{A.27}$$

$$T_s = T_{\text{bub,C1,B}} \qquad\qquad\qquad\qquad , s \in \{403, 404\} \tag{A.28}$$

$$T_s = T_{\text{bub,C2,D}} \qquad\qquad\qquad\qquad , s \in \{504, 505\} \tag{A.29}$$

$$T_s = T_{\text{bub,C2,B}} \qquad\qquad\qquad\qquad , s \in \{503, 506\} \tag{A.30}$$

$$T_s = T_{\text{B.L.}} \qquad\qquad\qquad\qquad\qquad , s \in \{507, 508\} \tag{A.31}$$

The battery limit temperature is $T_{\text{BL}} = 50^oC$. Temperature T_{101} and T_{103} are calculated from the energy balance of the mixers.

$$\sum_{i \in \text{COM}} \left(\dot{n}_{i,101} \cdot h_{i,101}(T_{101}) \right) = \sum_s \sum_{i \in \text{COM}} \left(\dot{n}_{i,s} \cdot h_{i,s}(T_s) \right) \tag{A.32}$$
$$s \in \{001, 304, 402\}$$

$$\sum_{i \in \text{COM}} \left(\dot{n}_{i,104} \cdot h_{i,104}(T_{101}) \right) = \sum_s \sum_{i \in \text{COM}} \left(\dot{n}_{i,s} \cdot h_{i,s}(T_s) \right) \tag{A.33}$$
$$s \in \{103, 306\}$$

A.3.4. Pressure

The connectivity constraints for pressure are the following:

$$p_s = p_{\text{R,tot}}(t_0) \qquad , s \in \{001, 101, 102, 103, 104, 304, 306, 402\} \tag{A.34}$$

$$p_s = p_{\text{R,tot}}(t_f) \qquad\qquad\qquad\qquad\qquad , s \in \{201, 202\} \tag{A.35}$$

$$p_s = p_{\text{R,min}} \qquad\qquad\qquad\qquad\qquad\qquad , s \in \{105, 106\} \tag{A.36}$$

$$p_s = p_{\text{D}} \qquad\qquad\qquad\qquad , s \in \{301, 302, 303, 305, 306, 307\} \tag{A.37}$$

$$p_s = p_{\text{reb,C1}} - \Delta p_{\text{col,C1}} \qquad\qquad\qquad , s \in \{401, 405, 406, 601\} \tag{A.38}$$

$$p_{403} = p_{\text{reb,C1}} \tag{A.39}$$

$$p_s = p_{\text{reb,C2}} - \Delta p_{\text{col,C2}} \qquad\qquad\qquad\qquad , s \in \{504, 603\} \tag{A.40}$$

$$p_s = p_{\text{reb,C2}} \qquad\qquad\qquad\qquad\qquad , s \in \{404, 503\} \tag{A.41}$$

$$p_s = p_{BL} \qquad\qquad\qquad\qquad , s \in \{505, 506, 507, 508\} \tag{A.42}$$

The battery limit pressure is $p_{BL} = 1$ bar.

A.4. Utilities

Since the operational and investment costs of the plant are estimated based on the specific energy consumption of each device, the heat and work requirements have to be quantified. Utilities are cooling water (cw), steam (st) and electricity (el). Heat exchanger duties are connected to cooling water in case of heat removal and to steam in case of heat supply. Electricity is consumed by pumps and compressors. It has not been taken care of heat integration here, since this is not the focus of this work. Heat integration, of course, could further reduce the production costs.

A.4.1. Pumps

Pump and compressor duties are derived from the pressure difference that has to be overcome between the two sides of the respective devices. There are pumps in the liquid recycles (A.44) as well as in the dosing stream of the reactor (A.43). The pump duties are calculated as follows:

$$P_{104} = \frac{1}{\epsilon_m \epsilon_p} \sum_{e \in \mathrm{FE}} \frac{j_{\mathrm{nC12en},e} \cdot M_i}{\rho_{i,104}} \cdot \left(\sum_{i \in \mathrm{GAS}} (p_{R,i,e}) - p_{104} \right) \cdot 10^3/60 \tag{A.43}$$

$$P_s = \frac{1}{\epsilon_m \epsilon_p} \sum_{i \in \mathrm{COM \backslash GAS}} \frac{\dot{n}_{i,s} M_i}{\rho_{i,s}} \cdot (p_{s+1} - p_s) \cdot 10^3/60 \tag{A.44}$$

$$s \in \{303, 401, 403, 503, 504\}$$

Motor and pump efficiency are assumed to be $\epsilon_m = 0.9$ and $\epsilon_p = 0.5$ [69].

A.4.2. Compressors

The dosing of gaseous components into the liquid phase is modeled as isentropic compression. A fixed temperature and a constant pressure difference is assumed (Eq. (A.45)). For the compression of the gas stream which is recycled from the decanter to the reactor a cascade of $N_{CPS} = 4$ isentropic compressors with intermediate cooling is assumed. The required equations are the following:

$$P_{104} = \sum_{e \in \mathrm{FE}} \sum_{i \in \mathrm{GAS}} j_{i,e} \cdot \frac{1.4}{1.4 - 1} R \cdot 378.15 \cdot \left(1.5^{\frac{1.4-1}{1.4}} - 1 \right) \cdot 10^3/60 \tag{A.45}$$

$$P_{305} = \frac{N_{\mathrm{CPS}}}{\epsilon_m \epsilon_c} \cdot \dot{n}_{305} \frac{1.4}{1.4 - 1} RT_{305} \left(\left(\frac{p_{306}}{p_{305}} \right)^{\frac{1.4-1}{1.4 N_{\mathrm{CPS}}}} - 1 \right) \cdot 10^3/60 \tag{A.46}$$

Motor and compression efficiency are assumed to be $\epsilon_m = 0.9$ and $\epsilon_c = 0.8$ [69].

A.4.3. Distillation Columns

In order to quantify the condenser and reboiler duties, the reflux ratio of the columns has to be known. With the Underwood correlation the minimum reflux ratio is estimated as follows:

$$1 - q = \sum_{i \in \text{COM}} \left(\frac{\bar{\alpha}_{i,\text{HK}} \cdot x_{\text{in},i}}{\bar{\alpha}_{i,\text{HK}} - \Theta} \right) \tag{A.47}$$

$$1 \leq \Theta \leq \bar{\alpha}_{\text{LK,HK}} \tag{A.48}$$

$$R_{\min} = \sum_{i \in \text{COM}} \left(\frac{\bar{\alpha}_{i,\text{HK}} \cdot x_{\text{D},i}}{\bar{\alpha}_{i,\text{HK}} - \Theta} \right) - 1 \tag{A.49}$$

As it is assumed that the feed of the columns is in a state of satured liquid, hence $q = 1$. The minimum reflux ratio gives the lower bound of the real reflux ratio R which is a degree of freedom in the optimization. Since no rigorous distillation model is used, it is assumed that the optimal reflux ratio R is about 1.2 times of the minimum reflux $R_{\min}$, which is a common rule of thumb [69]. With the optimal reflux ratio the theoretical number of stages N_{th} is estimated via the Gilliland correlation.

$$R > R_{\min} \tag{A.50}$$

$$X = \frac{R - R_{\min}}{R + 1} \tag{A.51}$$

$$X_1 = 1 - \exp\left(\frac{1 + 54.4X}{11 + 117.2X} \cdot \frac{X - 1}{X^{0.5}} \right) \tag{A.52}$$

$$N_{\text{th}} = \frac{N_{\min} + X_1}{1 - X_1} \tag{A.53}$$

With the reflux R the molar flow rate to be condensed and reboiled can be calculated. Assuming a total condenser the vapor $\dot{n}_V$ in the top of the column is totally liquified. Hence the heat duty equals the heat of vaporization of the vapor stream at dew point temperature T_{dew}. The dew point temperature is calculated via the dew point condition (A.55). The parameters for the correlation of the heat of vaporization are

taken from the literature [68] and are given in Tab. A.10.

$$\dot{Q}_{\text{con}} = (R+1) \cdot \dot{n}_D \cdot \sum_{i \in \text{COM}} (x_{\text{D},i} \cdot h_{\text{vap},i}(T_{\text{dew}})) \tag{A.54}$$

$$p_{\text{vap,LK}}(T_{\text{dew}}) = p_{\text{con}} \cdot \sum_{i \in \text{COM}} \left(\frac{x_{\text{D},i}}{\alpha_{i,\text{LK}}} \right) \tag{A.55}$$

$$h_{\text{vap},i}(T) = a_{1,i} \cdot \left(1 - \frac{T}{a_{2,i}} \right)^{a_{3,i}} \tag{A.56}$$

The reboiler duty is calculated in the same way, again a total reboiler is assumed. It is assumed that reflux and boilup ratio are equal. The reboiler temperature is at bubble point conditions and is calculated according to (A.58).

$$\dot{Q}_{\text{reb}} = (R+1) \cdot \dot{n}_D \cdot \sum_{i \in \text{COM}} (x_{\text{B},i} \cdot h_{\text{vap},i}(T_{\text{bub}})) \tag{A.57}$$

$$p_{\text{vap,HK}}(T_{\text{bub}}) = p_{\text{reb}} \cdot \sum_{i \in \text{COM}} \left(\frac{x_{\text{B},i}}{\alpha_{i,\text{HK}}} \right) \tag{A.58}$$

The column pressure drop is calculated from the pressure drop per height of packing, which is set to $1 \frac{mbar}{m}$ [81].

$$\Delta p_{\text{col}} = \Delta p_{\text{h}} \cdot H_{\text{packing}} \tag{A.59}$$

A.4.4. Heat Exchangers

The heat duty of the heat exchangers is calculated from the enthalpy difference of outlet and inlet of each heat exchanger. In order to keep the convention that a negative sign represents cooling, the definitions of different heat exchangers may differ. Hence, normal heat exchangers used for heating or cooling a certain stream are calculated via Eq. (A.60), whereas Eq. (A.61) represents the heat duty of compression with intermediate cooling.

$$\dot{Q}_s = \sum_{i \in \text{COM}} (n_{i,s+1} h_{i,s+1} - n_{i,s} h_{i,s}) \qquad s \in \{101, 102, 201, 301, 505, 506\} \tag{A.60}$$

$$\dot{Q}_s = - \sum_{i \in \text{COM}} (n_{i,s+1} h_{i,s+1} - n_{i,s} h_{i,s}) \qquad s \in \{307\} \tag{A.61}$$

Condensers in distillation columns depend on the reflux ratio as well as on the composition of the distillate stream. Since the condensers remove heat, a negative sign has to be added (Eqs. (A.62)-(A.63)). The equations of the reboilers (Eqs. (A.64)-(A.65))

yield a positive heat flux.

$$\dot{Q}_{405} = -\dot{n}_{405}(R_{\text{c1}} + 1) \sum_{i \in \text{COM}} (x_{i,405} h_{\text{vap},i,405}) \tag{A.62}$$

$$\dot{Q}_{504} = -\dot{n}_{504}(R_{\text{c2}} + 1) \sum_{i \in \text{COM}} (x_{i,504} h_{\text{vap},i,504}) \tag{A.63}$$

$$\dot{Q}_{403} = \dot{n}_{405}(R_{\text{c1}} + 1) \sum_{i \in \text{COM}} (x_{i,403} h_{\text{vap},i,403}) \tag{A.64}$$

$$\dot{Q}_{503} = \dot{n}_{504}(R_{\text{c2}} + 1) \sum_{i \in \text{COM}} (x_{i,503} h_{\text{vap},i,503}) \tag{A.65}$$

A.5. Sizing

For the estimation of the investment costs the characteristic sizes of the respective devices have to be calculated. According to the method of Guthrie [82] characteristic dimensions are correlated to the costs of the equipment.

A.5.1. Reactor

The reactor volume is calculated from the outlet molar flow rate and the residence time t_f of the fluid element. The effective volume is twice the liquid volume in order to account for the gas phase. It is sized as vertical vessel with a length to diameter ratio of four, which is a common rule of thumb [69].

$$V_{\text{R,liq}} = t_{\text{f}} \cdot \sum_{i \in \text{COM} \backslash \text{GAS}} \frac{\dot{n}_{i,201} M_i}{\rho_i(T_{201})} \tag{A.66}$$

$$D_{\text{R}} = \sqrt[3]{\frac{2V_{\text{R,liq}}}{\pi}} \tag{A.67}$$

$$L_{\text{R}} = 4D_{\text{R}} \tag{A.68}$$

A.5.2. Decanter

The size dimensions of the decanter are estimated in the same way as the reactor. Whereas the residence time of the reactor results from the optimal route, the residence

Table A.11.: Heat transfer coefficients of heat exchangers (Eq. (A.72)).

Unit	$U[W/m^2/K]$	Assumption
H 101	283.9	organic solvents (shell)/water (tube)
H 102	1135.4	propane, butane, etc. (shell)/ steam condensing (tube)
H 201	283.9	organic solvents (shell)/water (tube)
H 301	1135.4	propane, butane, etc. (shell)/ steam condensing (tube)
H 307	113.54	water (shell)/ compressed air (tube)
H 403	1135.4	propane, butane, etc. (shell)/ steam condensing (tube)
H 405	283.9	organic solvents low NC vacuum (shell)/ water (tube)
H 503	1135.4	propane, butane, etc. (shell)/ steam condensing (tube)
H 504	283.9	organic solvents low NC vacuum (shell)/ water (tube)
H 505	283.9	organic solvents (shell)/water (tube)
H 506	283.9	organic solvents (shell)/water (tube)

time of the decanter was set to a fixed value of $\tau_D = 20\ min$. This value is in good agreement with the experimental observations.

$$V_{\mathrm{D,liq}} = \tau_{\mathrm{D}} \cdot \sum_{i \in \mathrm{COM \backslash GAS}} \frac{\dot{n}_{i,202} M_i}{\rho_i(T_{\mathrm{D}})} \tag{A.69}$$

$$D_{\mathrm{D}} = \sqrt[3]{\frac{2V_{\mathrm{D,liq}}}{\pi}} \tag{A.70}$$

$$L_{\mathrm{D}} = 4D_{\mathrm{D}} \tag{A.71}$$

A.5.3. Heat Exchangers

The characteristic size of heat exchangers is the heat transfer area A_{hex} which depends on the transfered heat, the mean temperature difference between the hot and cold medium, and the heat transfer coefficient.

$$A_{\mathrm{hex},s} = \left| \frac{\dot{Q}_s}{U_s \Delta T_{\mathrm{m},s}} \right| \tag{A.72}$$

The transferred heat results from the energy balance and can be obtained from the previous section. The mean temperature difference depends on the relative flow direction of hot and cold medium. In counter current flow the log mean temperature difference gives accurate estimates.

The log mean temperature difference in counter current heat exchangers is defined

depending on the temperature level of the external medium. Eq. (A.73) defines the log mean temperature differences using cooling water, denoting T_h as the high temperature and T_c as the low temperature of the stream.

$$\Delta T_{\mathrm{lm}}(T_{\mathrm{h}}, T_{\mathrm{c}}) = \frac{(T_{\mathrm{h}} - T_{\mathrm{cw}}) - (T_{\mathrm{c}} - (T_{\mathrm{cw}} + \Delta T_{\mathrm{cw}}))}{log(\frac{T_{\mathrm{h}} - T_{\mathrm{cw}}}{T_{\mathrm{c}} - (T_{\mathrm{cw}} + \Delta T_{\mathrm{cw}})})} \tag{A.73}$$

The index cw denotes the temperature of the cooling medium and ΔT_{cw} is the temperature rise of the cooling medium due to heat exchange. All coolers, except H201 use normal cooling water as cooling medium. The temperature of normal cooling water is $T_{\mathrm{cw}} = 25^o C$. Cooler H201 uses chilled cooling water with a lower temperature of $T_{\mathrm{ccw}} = 5^o C$ The temperature rise is $\Delta T_{\mathrm{cw}} = 10K$.

Since in case of condensing steam the temperature of the hot medium does not change, the arithmetic mean temperature is used for reboilers.

$$\Delta T_{\mathrm{m,st}}(T_{\mathrm{h}}, T_{\mathrm{c}}) = T_{\mathrm{st}} - 0.5 \cdot (T_{\mathrm{h}} + T_{\mathrm{c}}) \tag{A.74}$$

For convenience the mean temperature differences of the different heat exchangers are expressed as function-argument relations in the following.

$$\Delta T_{\mathrm{m},101} = \Delta T_{\mathrm{lm,cw}}(T_{101}, T_{102}) \tag{A.75}$$

$$\Delta T_{\mathrm{m},102} = \Delta T_{\mathrm{m,st}}(T_{103}, T_{102}) \tag{A.76}$$

$$\Delta T_{\mathrm{m},201} = \Delta T_{\mathrm{lm,ccw}}(T_{201}, T_{202}) \tag{A.77}$$

$$\Delta T_{\mathrm{m},301} = \Delta T_{\mathrm{m,st}}(T_{302}, T_{301}) \tag{A.78}$$

$$\Delta T_{\mathrm{m},307} = \Delta T_{\mathrm{lm,cw}}(T_{308}, T_{307}) \tag{A.79}$$

$$\Delta T_{\mathrm{m},403} = \Delta T_{\mathrm{m,st}}(T_{\mathrm{bub},403}, T_{403}) \tag{A.80}$$

$$\Delta T_{\mathrm{m},405} = \Delta T_{\mathrm{lm,cw}}(T_{601}, T_{405}) \tag{A.81}$$

$$\Delta T_{\mathrm{m},503} = \Delta T_{\mathrm{m,st}}(T_{\mathrm{bub},503}, T_{503}) \tag{A.82}$$

$$\Delta T_{\mathrm{m},504} = \Delta T_{\mathrm{lm,cw}}(T_{603}, T_{504}) \tag{A.83}$$

$$\Delta T_{\mathrm{m},505} = \Delta T_{\mathrm{lm,cw}}(T_{505}, T_{507}) \tag{A.84}$$

$$\Delta T_{\mathrm{m},506} = \Delta T_{\mathrm{lm,cw}}(T_{506}, T_{508}) \tag{A.85}$$

Besides transfered heat and temperature difference, the heat transfer coefficient needs to be defined in order to calculate the heat transfer area. This coefficient represents the overall heat transfer resistance of conductive heat transfer over the wall and convective heat transfer on both sides of the wall. Actually it is hard to find a mechanistic correlation to determine U, but its value was tabulated for various combinations of shell and tube medium. Hence, assumption were made for each heat exchanger on the type of medium on both sides and the value for U could be obtained from the literature [82]. The values of the heat transfer coefficients together with the specific assumptions are given in Tab. A.11.

A.5.4. Distillation Columns

In order to estimate the capital investment for the distillation columns, the column height, diameter, and packing volume have to be calculated. The total column height is the sum of heights of packing, feed space, top and bottom space, and skirt height (in m).

$$H_{\text{col}} = H_{\text{packing}} + 1.5 + 1.5 + 1.5 + 1.5 \tag{A.86}$$

The height of the packing results from the height equivalent to a theoretical plate HETP, which represents the height of packing in which a theoretical stage may be accomplished [74].

$$H_{\text{packing}} = N_{\text{th}} \cdot HETP \tag{A.87}$$

The value of HETP is different for each kind of packing material. It depends on its shape and size, which essentially determines its specific surface area. In this example it is assumed that the packing consists of 1-inch carbon steel Rasching rings, which provide a HETP of 0.6 meters per theoretical stage.

The column diameter depends on the flooding velocity of the packing which is different in the distillation (D) and bottom (B) section. Hence, two diameters are calculated and the overall diameter is the mean value of both sections. Although usually the larger diameter is chosen for the cost estimation, but for convergence reasons the mean value approach is used since it gives more convex solutions.

$$D_{\text{col}} = 0.5 \sum_{s \in \{\text{B,D}\}} D_{col,s} \tag{A.88}$$

$$D_{\text{col},s} = \sqrt{\frac{4\dot{m}_{\text{V},s}}{\pi w_{\text{gas,max}} \epsilon_{\text{vap}} \hat{\rho}_{\text{gas},s}}} \tag{A.89}$$

$$s \in \{\text{B, D}\}$$

The fraction of flooding of random packing is commonly set to $\epsilon_{\text{fl}} = 0.6$. In order to estimate the maximum flooding gas velocity a correlation of Leva [83] is used.

$$w_{\text{gas,max}} = \sqrt{\frac{Y \cdot g \cdot \rho_{\text{H}_2\text{O}}}{F_p \cdot \hat{\rho}_{\text{gas,B}} \cdot F_\rho \cdot F_\eta}} \tag{A.90}$$

$$\ln Y = -3.7121 - 1.0371 \ln F_{LG} - 0.1501 \left(\ln F_{LG}\right)^2 - 0.007544 \left(\ln F_{LG}\right)^3 \tag{A.91}$$

$$0.01 \leq Y \leq 10 \tag{A.92}$$

The reference state of the correlation is liquid water, hence the functions F_ρ and F_η represent the deviation from the properties of water.

$$F_\rho = -0.8787 + 2.6776\frac{\rho_{\text{H}_2\text{O}}}{\hat{\rho}_{\text{liq},s}} - 0.6313\left(\frac{\rho_{\text{H}_2\text{O}}}{\hat{\rho}_{\text{liq},s}}\right)^2 \tag{A.93}$$

$$0.65 \leq \frac{\rho_{\text{H}_2\text{O}}}{\hat{\rho}_{\text{liq},s}} \leq 1.4 \tag{A.94}$$

$$F_\eta = 0.96\eta_{liq}^{0.19} \tag{A.95}$$

$$0.3 \leq \eta_{liq} \leq 20\text{cP} \tag{A.96}$$

The density of water is set to $1000\frac{kg}{m^3}$. The packing factor F_p has a value special for the packing material used. For the used 1-inch carbon steel Rasching rings the value is $F_p = 165 ft^{-1}$ [84] and the gravity is $g = 32.174\frac{ft}{s^2}$.

$$\rho_{\text{liq},i,s} = a_{0,i} + a_{1,i}T_s \tag{A.97}$$

$$\omega_{\text{liq},i,s} = \frac{\dot{n}_{i,s}M_i}{\sum_{i\in\text{COM}}(\dot{n}_{i,s}M_i)} \tag{A.98}$$

$$\hat{\rho}_{\text{liq},s} = \sum_{i\in\text{COM}}(\omega_{\text{liq},i,s}\rho_{\text{liq},i,s}) \tag{A.99}$$

$$\hat{\rho}_{\text{gas},\text{D}} = p_{\text{con}}\sum_{i\in\text{COM}}\left(\frac{x_{i,\text{D}}M_i}{RT_{\text{dew}}}\right) \tag{A.100}$$

$$\hat{\rho}_{\text{gas},\text{B}} = p_{\text{reb}}\sum_{i\in\text{COM}}\left(\frac{x_{i,\text{B}}M_i}{RT_{\text{bub}}}\right) \tag{A.101}$$

$$\dot{m}_{\text{vap},s} = (R+1)\cdot\dot{n}_{\text{D}}\sum_{i\in\text{COM}}(x_{i,s}M_i) \tag{A.102}$$

$$\dot{m}_{\text{liq},\text{B}} = \sum_{i\in\text{COM}}(\dot{n}_{\text{in},i}M_i) + R\cdot\dot{n}_{\text{D}}\sum_{i\in\text{COM}}(x_{i,\text{B}}M_i) \tag{A.103}$$

$$\dot{m}_{\text{liq},\text{D}} = R\cdot\dot{n}_{\text{D}}\sum_{i\in\text{COM}}(x_{i,\text{D}}M_i) \tag{A.104}$$

$$F_{\text{fl},s} = \frac{\dot{m}_{\text{liq},s}}{\dot{m}_{\text{vap},s}}\cdot\sqrt{\frac{\hat{\rho}_{\text{gas},s}}{\hat{\rho}_{\text{liq},s}}} \tag{A.105}$$

$$s \in \{\text{B},\text{D}\}$$

Finally, for the total column investment costs the volume of the packing needs to be calculated.

$$V_{\text{packing}} = \frac{\pi}{4}D_{\text{col}}^2\left(H_{\text{packing}}\right) \tag{A.106}$$

$$V_{\text{col}} = \frac{\pi}{4}D_{\text{col}}^2\left(H_{\text{col}} - 1.5\right) \tag{A.107}$$

The total volume of the column is required for the calculation of the air leakage flow into the column which determines the vacuum duty of the steam ejectors.

A.6. Costs Model

The costs of the process are divided into capital investment, utility, and raw material costs. Capital investment are the fixed costs for the units including setup and installation. Utility costs are the costs for cooling water, steam, and electricity. Costs for reactants and solvents count as raw material costs. The objective function of the optimization is the minimization of the total production costs as defined in Eq. (OP3). In order to account for the investment costs in the optimization of the process, their contribution to the total production costs is measured in form of depreciation on a three year basis (see Eq. (OP3)).

A.6.1. Capital Investment

The costs for capital investment are calculated from the bare module costs (BMC) of each device and the costs of the catalyst inside the reactor. According to the method of Guthrie [82] the bare module costs of each device after installation depend on the bare costs (BC) scaled by a material and pressure factor (MPF), which accounts for non-standard conditions, and a module factor (MF), which accounts for the installation equipment. The update factor (UF) correlates the historic data source to the present cost level. The bare costs represent a standard price of the equipment based on up to two main characteristic dimensions (S_1 and S_2). The update factor is based on the "Chemical Engineering Index" which is published monthly by Chemical Engineering. The CE index used in this work is based on the year 2011 with a value of $CE = 585$. For simplicity the location aspect was omitted in this work.

$$C_{\mathrm{invest}} = \sum_u BMC_u + \Psi_{\mathrm{cat}} \dot{n}_{\mathrm{cat}} M_{\mathrm{cat}} \tau_R \tag{A.108}$$

$$BMC_u = UF_u \cdot (MPF_u + MF_u - 1) \cdot BC_u \tag{A.109}$$

$$BC_u = a_{0,u} \left(\frac{S_1}{a_{1,u}} \right)^{a_{2,u}} \left(\frac{S_2}{a_{3,u}} \right)^{a_{4,u}} \tag{A.110}$$

$$UF_u = \frac{CE}{CE_{\mathrm{base}}} \tag{A.111}$$

The parameters for BC, MPF, MF, and CE_{base} are given in Tab. A.13.
Usually cost models for capital investment have a rather high uncertainty. The errors of the cost models used in this work are in the range of $30 - 40\%$ as reported in the literature [69]. Due to this high uncertainty the absolute costs values might not be very accurate, but, since the cost comparison is on the same basis, the relative trends and relative qualitative performance are comparable. Usually in the first stage of

Table A.12.: Prices of raw materials and utilities.

Utility	Price Ψ	Unit	Source
DMF	73.1	$/kmol$	[85]
n-Decane	71.4	$/kmol$	[85]
1-Dodecene	661.5	$/kmol$	[85]
H_2	4.0	$/kmol$	assumed
CO	4.0	$/kmol$	assumed
Catalyst	85150.0	$/kg$	assumed
Cooling water	2.54e-6	$/kJ$	[20]
Steam	1.41e-5	$/kJ$	[20]
Electricity	2.22e-5	$/kJ$	[20]

process development cost models of this level of uncertainty are used, however, the more the final design is approached the accuracy of the cost models increases.

A.6.2. Utility and Raw Material Costs

Utility costs are proportional to the molar flows of raw material feed, solvent make-ups, heat duty, and compression or pump work, respectively. The specific prices Ψ are given in Tab. A.12 and are with respect to molar amount or energy. The price of cooling water is based on a constant heat capacity of $c_p = 75.3 J/mol/K$ and a constant cooling temperature increase of $\Delta T_{\mathrm{cw}} = 10K$. The price of steam is based on a constant heat of vaporization of $h_{\mathrm{vap,st}} = 1888 kJ/kg$ and a steam temperature of 600 K. The prices for raw material correspond to spot market prices.

$$C_{\mathrm{util}} = \sum_i \Psi_i \dot{n}_{i,s} \qquad s \in \{001, 104\} \tag{A.112}$$

$$C_i = \Psi_i \cdot (\dot{n}_{001,i} + \dot{n}_{103,i}) \qquad i \in \{\mathrm{nC12en, H_2, CO}\} \tag{A.113}$$

$$C_i = \Psi_i \cdot \dot{n}_{001,i} \qquad i \in \{\mathrm{C10an, DMF}\} \tag{A.114}$$

$$C_{\mathrm{cw}} = -\Psi_{\mathrm{cw}} \cdot \sum_s (Q_s + Q_{\mathrm{R}}) \qquad s \in \{101, 201, 306, 405, 504, 601, 603\} \tag{A.115}$$

$$C_{\mathrm{st}} = \Psi_{\mathrm{st}} \cdot \sum_s Q_s \qquad s \in \{301, 403, 503\} \tag{A.116}$$

$$C_{\mathrm{el}} = \Psi_{\mathrm{el}} \cdot \sum_s P_s \qquad s \in \mathrm{PUMP} \wedge \mathrm{COMP} \tag{A.117}$$

Table A.13.: Parameters for bare costs (BC), material and pressure factors (MPF), module factors (MF), and CE-cost index (CE_{base}) of the cost data (Eqs. (A.110) and (A.109)).

Unit	a_0	a_1	a_2	a_3	a_4	MPF	MF	CE_{base}
VES R	1e3	1.2192	0.81	0.9144	1.05	1.45	4.23	115
VES D	690	1.2192	0.78	0.9144	0.98	1	3.18	115
VES C1	1e3	1.2192	0.81	0.9144	1.05	1	4.23	115
VES C2	1e3	1.2192	0.81	0.9144	1.05	1	4.23	115
STA C1	180	3.048	0.97	0.6096	1.45	1.87	3.29	115
STA C2	180	3.048	0.97	0.6096	1.45	1.87	3.29	115
H 101	5e3	37.1612	0.65	1	0	1.35	3.29	115
H 201	5e3	37.1612	0.65	1	0	1.87	3.29	115
H 301	5e3	37.1612	0.65	1	0	1.35	3.29	115
H 305	5e3	37.1612	0.65	1	0	1	3.29	115
H 403	5e3	37.1612	0.65	1	0	1.35	3.29	115
H 405	5e3	37.1612	0.65	1	0	1	3.29	115
H 503	5e3	37.1612	0.65	1	0	1	3.11	115
H 504	5e3	37.1612	0.65	1	0	1	3.11	115
H 601	5e3	37.1612	0.65	1	0	1	3.11	115
H 603	5e3	37.1612	0.65	1	0	1	3.11	115
CP 104	23e3	74.6	0.77	1	0	2.8	1	115
CP 305	23e3	74.6	0.77	1	0	2.8	1	115
CP 601	23e3	74.6	0.77	1	0	2.8	1	115
CP 603	23e3	74.6	0.77	1	0	2.8	1	115
P 104	1800	7.5	0.3	1	0	1.5	3.38	402
P 303	1800	7.5	0.3	1	0	1.5	3.38	402
P 401	1800	7.5	0.3	1	0	1.5	3.38	402
P 403	1800	7.5	0.3	1	0	1.5	3.38	402

A.7. Numerical Solution Method

To solve the dynamic optimization problems the differential algebraic equation system is discretized with the method of orthogonal collocation on finite elements [86, 87] and thereby converted into a large scale system of nonlinear algebraic equations. All optimization problems are solved using CONOPT 3.14 G under AMPL on a PC with two Intel(R) Xeon(R) with 3.0 GHz (calculation on a single CPU), a memory of 3.8 GB, and a Linux operating system. CONOPT is a generalized reduced-gradient solver based on sequential quadratic programming designed for large scale NLP problems [88, 89].

Since the mathematical model is non-convex, global optimality cannot be assured. However, the control problem was solved repeatedly for many different initial parameter values. During the conversion study at conversions above $X = 95\%$ two distinct local solutions can be identified, which differ significantly in the required reaction time, hence leading to a bi-stable behavior. The short reaction time solution corresponds to the reaction route with dominant forward-isomerization, whereas the long reaction time solution is dominated by the re-isomerization. In the figures the solution with the greater objective function value was illustrated as optimal solution.

Bibliography

[1] H.-W. Schütt. *Der Chemiker im Wandel der Zeiten*. Verlag Chemie, 1973.

[2] H.-B. Amecke. *Chemiewirtschaft im Überblick*. Verlag Chemie, 1987.

[3] H. Freund and K. Sundmacher. Towards a methodology for the systematic analysis and design of efficient chemical processes part 1. from unit operations to elementary process functions. *Chem. Eng. Process.*, 47(12):2051–2060, 2008.

[4] A. Peschel, H. Freund, and K. Sundmacher. Methodology for the design of optimal chemical reactors based on the concept of elementary process functions. *Ind. Eng. Chem. Res.*, 49(21):10535–10548, 2010.

[5] E. Müller, R. Berger, E. Blass, D. Sluyts, and A. Pfennig. Liquid-liquid extraction. *Ullmann's Encyclopedia of Industrial Chemistry*, 2008.

[6] H.-W. Bohnen and B. Cornils. Hydroformylation of alkenes: An industrial view of status and importance. *Adv. Catal.*, 47:1–64, 2002.

[7] P. W. N. M. van Leeuwen. *Rhodium catalyzed hydroformylation*, volume 22 of *Catalysis by metal complexes*. Kluwer Academic Publ., 2000.

[8] R. Dittmeyer, W. Keim, G. Kreysa, and A. Oberholz. *Winnacker - Küchler: Chemische Technik - Prozesse und Produckte. Band 4: Energieträger, Organische Grundstoffe*. Weinheim : Wiley-VCH, 2005.

[9] http://heraeus-recycling.com/de/services/pricing_chart/chart_tool.aspx. 29.10.2015.

[10] A. Behr, G. Henze, L. Johnen, and C. Awungacha. Advances in thermomorphic liquid/liquid recycling of homogeneous transition metal catalysts. *J. Mol. Catal. A: Chem.*, 285(1-2):20–28, 2008.

[11] A. Behr. *Angewandte homogene Katalyse*. Wiley-VCH, 2008.

[12] A Behr and P. Neubert. *Applied Homogeneous Catalysis*. Wiley-VCH, 2012.

[13] G. Kiedorf, M. H. Duc, A. Müller, A. Jörke, J. Markert, H. Arellano-Garcia, A. Seidel-Morgenstern, and C. Hamel. Kinetics of 1-dodecene hydroformylation in a thermomorphic solvent system using a rhodium-biphephos catalyst. *Chem. Eng. Sci.*, 115:31–48, 2014.

[14] J. Hibbel, E. Wiebus, and B. Cornils. 75 jahre hydroformylierung - oxoreaktoren und oxoanlagen der ruhrchemie ag und der oxea gmbh von 1938 bis 2013. *Chem. Ing. Tech.*, 85:1853 – 1871, 2013.

[15] A. Behr, G. Henze, and R. Schomaecker. Thermoregulated liquid/liquid catalyst separation and recycling. *Adv. Synth. Catal.*, 348(12-13):1485–1495, 2006.

[16] H. Bahrmann, H. Bach, and D. G. Frey. Oxo synthesis. *Ullmann's Encyclopedia of Industrial Chemistry*, 2013.

[17] R. Tudor and M. Ashley. Enhancement of industrial hydroformylation processes by the adoption of rhodium-based catalyst: Part i. *Platinum Metals Rev.*, 51(3):116–126, 2007.

[18] R. Tudor and M. Ashley. Enhancement of industrial hydroformylation processes by the adoption of rhodium-based catalyst: Part ii. *Platinum Metals Rev.*, 51(4):164–171, 2007.

[19] O. Wachsen, K. Himmler, and B. Cornils. Aqueous biphasic catalysis: Where the reaction takes place. *Catal. Today*, 42:373–379, 1998.

[20] M. Baerns, A. Behr, A. Brehm, J. Gmehling, H. Hofmann, U. Onken, and A. Renken. *Technische Chemie*. Weinheim : Wiley-VCH, 2006.

[21] J. Haggin. New hydroformylation process developed. *Chem. Eng. News*, 73(16):25 – 26, 1995.

[22] C. M. Hansen. *Hansen Solubility Parameters: A Users̀ Handbook*. CRC Press, 2000.

[23] K. McBride and K. Sundmacher. Data driven conceptual process design for the hydroformylation of 1-dodecene in a thermomorphic solvent system. *Ind. Eng. Chem. Res.*, 54:6761–6771, 2015.

[24] K. McBride, T. Gaide, A. Vorholt, A Behr, and K. Sundmacher. Thermomorphic solvent selection for homogeneous catalyst recovery based on cosmo-rs. *Chem. Eng. Process.: PI*, 99:97–106, 2016.

[25] Y. Q. Zhang, Z. S. Mao, and T. Y. Chen. Interfacial kinetics of biphasic hydroformylation of 1-dodecene catalyzed by water -soluble rhodium complex by a combined numerical and experimental approach. *Ind. Eng. Chem. Res.*, 40(21):4496 – 4505, 2001.

[26] M. Haumann, H. Koch, P. Hugo, and R. Schomacker. Hydroformylation of 1-dodecene using rh-tppts in a microemulsion. *Appl. Catal., A*, 225(1-2):239–249, 2002.

[27] T. Hamerla, N. Paul, M. Kraume, and R. Schomäcker. Aufklärung der stofftransportwege in mizellaren mehrphasenreaktionen am beispiel der hydroformylierung. *Chem. Ing. Tech.*, 85(10):1530 – 1539, 2013.

[28] D. Müller, D. Hoang Minh, V. A. Merchan, H. Arellano-Garcia, Y. Kasaka, M. Müller, R. Schomäcker, and G. Wozny. Towards a novel process concept for the hydroformylation of higher alkenes: Mini-plant operation strategies via model development and optimal experimental design. *Chem. Eng. Sci.*, 115:127 – 138, 2014.

[29] I. T. Horvath, G. Kiss, R. A. Cook, J. E. Bond, P. A. Stefens, J. Rabai, and E. J. Mozeleski. Molecular engineering in homogeneous catalysis: One-phase catalysis coupled with biphase catalyst separation. the fluorous-soluble hrh(co)P[CH2CH2(CF2)5CF3]33 hydroformylation system. *J. Am. Chem. Soc.*, 120:3133 – 3143, 1998.

[30] C. Liu, X. Li, and Z. Jin. Progress in thermoregulated liquid/liquid biphasic catalysis. *Catal. Today*, 247:82–89, 2015.

[31] F. Favre, H. Olivier-Bourbigou, D. Commereuc, and L. Saussine. Hydroformylation of 1-hexene with rhodium in non-aqueous ionic liquids: How to design the solvent and the ligand to the reaction. *Chem. Commun.*, page 1360, 2001.

[32] J. Dupont, S. M. Silva, and R. F. de Souza. Mobile phase effects in rh/sulfonated phosphine/molten salts catalysed the biphasic hydroformylation of heavy olefins. *Catal. Lett.*, 77:131, 2001.

[33] C.C. Brasse, U. Englert, A. Salzer, H. Waffenschmidt, and P. Wasserscheid. *Organometallics*, 19:3818, 2000.

[34] R. P. J. Bronger, S. M. Silva, P. C. J. Kamer, and P. W. N. M. van Leeuwen. *Chem. Commun.*, 2002:3044, 2002.

[35] D. A. Cole-Hamilton. Homogeneous catalysis - new approaches to catalyst separation, recovery, and recycling. *Science*, 299:1702 – 1706, 2003.

[36] H.-P. Steinrück and P. Wasserscheid. Ionic liquids in catalysis. *Catal. Lett.*, 145(1):380–397, 2015.

[37] A. Sharma, C. J. Lebigue, R. M. Deshpande, A. A. Kelkar, and H. Delmas. Hydroformylation of 1-octene using [bmim][pf6]-decane biphasic media and rhodium complex catalyst: Thermodynamic properties and kinetic study. *Ind. Eng. Chem. Res.*, 49(21):10698–10706, 2010.

[38] A. Peschel, B. Hentschel, H. Freund, and K. Sundmacher. Optimal reactor design for the hydroformylation of long chain alkenes in biphasic liquid systems. In *21st European Symposium on Computer Aided Process Engineering*, volume 29, pages 1246–1250, 2011.

[39] A. Peschel, B. Hentschel, H. Freund, and K. Sundmacher. Design of optimal multiphase reactors exemplified on the hydroformylation of long chain alkenes. *Chem. Eng. J.*, 188:126–141, 2012.

[40] B. G. Rong, E. Kolehmainen, and I Turunen. Methodology of conceptual process synthesis for process intensification. *Comp. Aid. Ch.*, 25:283–288, 2008.

[41] M. Jakuttis, A. Schönweiz, S. Werner, R. Franke, K.-D. Wiese, M. Haumann, and P Wasserscheid. Rhodium-phosphite silp catalysis for the highly selective hydroformylation of mixed c 4 feedstocks. *Angewandte Chemie - International Edition*, 50(19):4492–4495, 2011.

[42] M. Haumann, M. Jakuttis, R. Franke, A. Schönweiz, and P. Wasserscheid. Continuous gas-phase hydroformylation of a highly diluted technical c4 feed using supported ionic liquid phase catalysts. *Chem. Cat. Chem.*, 3(11):1822–1827, 2011.

[43] U. Hintermair, T. Gong, A. Serbanovic, M. J. Muldoon, C. C. Santini, and D. J. Cole-Hamilton. Continuous flow hydroformylation using supported ionic liquid phase catalysts with carbon dioxide as a carrier. *Dalton Trans.*, 39:8501–8510, 2010.

[44] J. P. Arhancet, M. E. Davis, J. S. Merola, and B. E. Hanson. Hydroformylation by supported aqueous-phase catalysis: a new class of heterogeneous catalysts. *Nature*, 339:454, 1989.

[45] L. C. Matsinha, P. Malatji, A. T. Hutton, G. A. Venter, S. F. Mapolie, and G. S. Smith. Water-soluble half-sandwich ru^{II} -arene complexes: Synthesis, structure, electrochemistry, dft studies, and aqueous phase hydroformylation of 1-octene. *Eur. J. Inorg. Chem.*, (24):4318–4328, 2013.

[46] G. Ertl, H. Knözinger, and J. Weitkamp. *Handbook of heterogeneous catalysis*, volume 5. Wiley-VCH, Weinheim, 1997.

[47] D. I. Enache, W. Thiam, D. Dumas, S. Ellwood, G. J. Hutchings, S. H. Taylor, S. Hawker, and E. H. Stitt. Intensification of the solvent-free catalytic hydro-formylation of cyclododecatriene: Comparison of a stirred batch reactor and a heat-exchange reactor. *Catal. Today*, 128(1-2):18–25, 2007.

[48] D. Koch and W. Leitner. Rhodium-catalyzed hydroformylation in supercritical carbon dioxide. *J. Am. Chem. Soc.*, 120:13398–13404, 1998.

[49] H. Jin and B. Subramaniam. Homogeneous catalytic hydroformylation of 1-octene in co2-expanded solvent media. *Chem. Eng. Sci.*, 59:4887–4893, 2004.

[50] K. Ye. *Process Design Based on CO_2-Expanded Liquid as Solvents*. PhD thesis, Otto-von-Guericke University Magdeburg, 2014.

[51] H.J. Beckers, J.M. De Rijke, and R.D. Garton. Hydroformylation process employing loop reactors, June 9 1998. US Patent 5,763,678.

[52] R.D. Garton, M. Findlay, K. Sankaranarayanan, and A. van Vliet. Internal loop reactor and oxo process using same, January 25 2011. US Patent 7,875,254.

[53] K.C. Nadler, T.R. Broussard, and J.K. Pitre. Stripper-reactor for volatile cobalt recovery, August 10 1993. US Patent 5,235,112.

[54] W.H. Summerlin. Method for removing hydroformylation catalyst, August 17 1993. US Patent 5,237,105.

[55] K. D. Wiese, O. Möller, G. Protzmann, and M. Trocha. A new reactor design for catalytic fluid-fluid multiphase reactions. *Catal. Today*, 79-80:97–103, 2003.

[56] K. Sundmacher and H. Freund. Chemical process design: Moving matter elements along optimal travel routes in the thermodynamic state space. In *The 5th International Symposium on Design, Operation and Control of Chemical Processes, PSE Asia 2010, July 25-28, Singapore*, 2010.

[57] A. Peschel. *Model-based design of optimal chemical reactors*. PhD thesis, Otto-von-Guericke-University Magdeburg, 2012.

[58] A. Peschel, F. Karst, H. Freund, and K. Sundmacher. Analysis and optimal design of an ethylene oxide reactor. *Chem. Eng. Sci.*, 66(24):6453–6469, 2011.

[59] A. Peschel, A. Jörke, K. Sundmacher, and H. Freund. Optimal reaction concept and plant wide optimization of the ethylene oxide process. *Chem. Eng. J.*, 207:656–674, 2012.

[60] R. Krishna and S. T. Sie. Strategies for multiphase reactor selection. *Chem. Eng. Sci.*, 49(24):4029–4065, 1994.

[61] R. Krishna. A systems approach to multiphase reactor selection. *Advances in Chemical Engineering*, 19:201–249, 1994.

[62] V. L. Mehta and A .C. Kokossis. Nonisothermal synthesis of homogeneous and multiphase reactor networks. *AIChE J.*, 46(11):2256–2273, 2000.

[63] V. V. Kelkar and K. M. Ng. Screening multiphase reactors for nonisothermal multiple reactions. *AIChE J.*, 46(2):389–406, 2000.

[64] B. Hentschel, H. Freund, and K. Sundmacher. Modellbasierte ermittlung der optimalen reaktionsführung für integrierte mehrphasenprozesse. *Chem. Ing. Tech.*, 86(7):1080–1087, 2014.

[65] E. Schäfer, Y. Brunsch, G. Sadowski, and A. Behr. Hydroformylation of 1-dodecene in the thermomorphic solvent system dimethylformamide/decane. phase behavior-reaction performance-catalyst recycling. *Ind. Eng. Chem. Res.*, 51(31):10296–10306, 2012.

[66] C. Vogelpohl, C. Brandenbusch, and G. Sadowski. High-pressure gas solubility in multicomponent solvent systems for hydroformylation. part i: Carbon monoxide solubility. *J. Supercrit. Fluids*, 81:23 – 32, 2013.

[67] J. Markert, Y. Brunsch, T. Munkelt, G. Kiedorf, A Behr, C. Hamel, and A. Seidel-Morgenstern. Analysis of the reaction network for the rh-catalyzed hydroformylation of 1-dodecene in a thermomorphic multicomponent solvent system. *Appl. Catal., A*, 462 - 463:287 – 295, 2013.

[68] C. Yaws. *Chemical Properties Handbook: Physical, Thermodynamics, Engironmental Transport, Safety & Health Related Properties for Organic & Inorganic Chemical.* McGraw-Hill Professional, 1 edition, 1998.

[69] L. T. Biegler, I. E. Grossmann, and A. W. Westerberg. *Systematic methods of chemical process design.* Prentice Hall, Upper Saddle River, 1997.

[70] T. Beierling and F. Ruether. Separation of the isomeric long-chain aldehydes dodecanal/2-methylundecanal via layer melt crystallization. *Chem. Eng. Sci.*, 77:71–77, 2012.

[71] J. Micovic, T. Beierling, P. Lutze, G. Sadowski, and A. Gorak. Design of hybrid distillation/melt crystallization processes for separation of close-boiling mixtures. *Chem. Ing. Tech.*, 84(11):2035–2047, 2012.

[72] J. Micovic, T. Beierling, P. Lutze, G. Sadowski, and A. Gorak. Design of hybrid distillation/melt crystallisation processes for separation of close boiling mixtures. *Chem. Eng. Process.*, 67:16–24, 2013.

[73] J. Steimel, M. Harrmann, G. Schembecker, and S. Engell. Model-based conceptual design and optimization tool support for the early stage development of chemical processes under uncertainty. *Comput. Chem. Eng.*, 59:63 – 73, 2013.

[74] J.R. Couper, W.R. Penney, J.R. Fair, and S.M. Walas. *Chemical Process Equipment.* Elsevier, 2 edition, 2010.

[75] A. Pikulik and H. E. Diaz. Cost estimating for major process equipment. *Chem. Eng.*, 84(21):106–122, 1977.

[76] R. McGraw. Description of aerosol dynamics by the quadrature method of moments. *Aerosol Sci. Technol.*, 27:255–265, 1997.

[77] W. Heineken, D. Flockerzi, A. Voigt, and K. Sundmacher. Dimension reduction of bivariate population balances using the quadrature method of moments. *Comput. Chem. Eng.*, 35:50–62, 2011.

[78] R. Dürr, T. Müller, S. Duvigneau, and Kienle A. An efficient approximate moment method for multi-dimensional population balance models - application to virus replication in multi-cellular systems. *Chem. Eng. Sci.*, 160:321–334, 2017.

[79] H. Freund and K. Sundmacher. Process intensification: 1. fundamentals and molecular level. *Ullmann's Encyclopedia of Industrial Chemistry. Online Edition.*, Wiley-VCH, Weinheim, 2011.

[80] Aristoteles. *Metaphysik, Buch VII.* 322 AD.

[81] Woods. *Rules of Thumb in Engineering Practice.* Wiley, 2007.

[82] K. M. Guthrie. Data and techniques for preliminary capital cost estimating. *Chem. Eng.*, 76(6):114ff, 1969.

[83] M. Leva. Flow through irrigated dumped packings. *Chem. Eng. Progress Symp. Ser.*, 50(10):51–59, 1954.

[84] W. D. Seider. *Product and Process Design Principles*, volume 3. John Wiley, 2010.

[85] www.alibaba.com. 19.01.2013.

[86] J. S. Logsdon and L. T. Biegler. Accurate solution of differential algebraic optimization problems. *Ind. Eng. Chem. Res.*, 28(11):1628–1639, 1989.

[87] J. E. Cuthrell and L. T. Biegler. Simultaneous-optimization and solution methods for batch reactor control profiles. *Comput. Chem. Eng.*, 13(1-2):49–62, 1989.

[88] A. S. Drud. Conopt - a grg code for large sparse dynamic nonlinear optimization problems. *Math. Program.*, 31(2):153–191, 1985.

[89] A. S. Drud. Conopt - a large-scale grg code. *ORSA Journal on Computing*, 6(2):207–16, 1994.